Vortices in quantum droplets: Analogies between boson and fermion systems

H. Saarikoski* and S. M. Reimann†

Mathematical Physics, LTH, Lund University, SE-22100 Lund, Sweden

A. Harju

Department of Applied Physics and Helsinki Institute of Physics, Aalto University, FI-02150 Espoo, Finland

M. Manninen

Nanoscience Center, Department of Physics, University of Jyväskylä, FI-40014 Jyväskylä, Finland

(Published 29 September 2010)

The main theme of this review is the many-body physics of vortices in quantum droplets of bosons or fermions in the limit of small particle numbers. Systems of interest include cold atoms in traps as well as electrons confined in quantum dots. When set to rotate, these in principle different quantum systems show remarkable analogies. The topics reviewed include the structure of the finite rotating many-body state, universality of vortex formation and localization of vortices in both bosonic and fermionic systems, and the emergence of particle-vortex composites in the quantum Hall regime. An overview of the computational many-body techniques sets focus on the configuration-interaction and density-functional methods. Studies of quantum droplets with one or several particle components, where vortices as well as coreless vortices may occur, are reviewed, and theoretical as well as experimental challenges are discussed.

DOI: 10.1103/RevModPhys.82.2785 PACS number(s): 03.75.Lm, 67.85.−d, 71.10.−w, 73.21.La

CONTENTS

I. Introduction 2786
A. Finite quantum liquids in traps 2786
1. Atoms in traps 2786
2. Electrons in low-dimensional quantum dots 2787
B. Vortex formation in rotating quantum liquids 2787
1. Vortices in Bose-Einstein condensates 2788
2. Vortices in quantum Hall droplets 2788
3. Quantum Hall regime in bosonic condensates 2788
4. Self-bound droplets 2789
C. About this review 2789
II. Many-Body Wave Function 2789
A. Model Hamiltonian 2789
1. Rotating quantum droplets of bosons 2789
2. Electron droplet in a magnetic field 2790
3. Role of symmetry breaking 2791
B. Vortices in the exact many-body wave function 2791
1. Pauli vortices 2791
2. Off-particle vortices 2791
3. Particle-vortex composites 2791
C. Internal structure of the many-body states 2792
1. Conditional probability densities 2792
2. One-body density matrix 2792
3. Reduced wave functions 2792
D. Particle-hole duality in electron systems 2793
E. Quantum Hall states 2794
1. Maximum density droplet state and its excitations 2795
2. Laughlin wave function 2795
3. Jain construction and composite particles 2796
F. Mapping between fermions and bosons 2796
III. Computational Many-Body Methods 2797
A. The Gross-Pitaevskii approach for trapped bosons 2798
1. Gross-Pitaevskii equation for simple condensates 2798
2. Gross-Pitaevskii approach for multicomponent systems 2799
B. Density-functional approach 2799
1. Spin-density-functional theory for electrons 2799
2. Density-functional theory for bosons 2800
C. Exact diagonalization method 2800
IV. Single-Component Quantum Droplets 2801
A. Vortex formation at moderate angular momenta 2801
1. Vortex formation in trapped bosonic systems 2801
2. Weakly interacting bosons under rotation 2802
3. Single-vortex states in electron droplets 2804
B. Vortex clusters and lattices 2806
1. Vortex lattices in bosonic condensates 2806
2. Vortex molecules and lattices in quantum dots 2808
3. Signatures of vortices in electron transport 2810

*Present address: Institut für Theoretische Physik, Universität Regensburg, D-93040 Regensburg, Germany.
†Corresponding author. reimann@matfys.lth.se

C. Localization of particles and vortices 2811
1. Particle localization and Wigner molecules 2811
2. Rotational spectrum of localized particles 2812
3. Localization of bosons 2813
4. Vortex localization in fermion droplets 2813
5. Vortex molecules 2815
D. Melting of the vortex lattice 2817
1. Lindemann melting criterion 2817
2. Transition to vortex liquid state 2817
3. Breakdown of small vortex molecules 2818
E. Giant vortices 2818
1. Bose-Einstein condensates in anharmonic potentials 2819
2. Giant vortices in quantum dots 2819
F. Formation of composite particles at rapid rotation 2820
V. Multicomponent Quantum Droplets 2821
A. Pseudospin description of multicomponent condensates 2822
B. Two-component bosonic condensates 2822
1. Asymmetric component sizes 2823
2. Condensates with symmetric components 2825
3. Vortex lattices and vortex sheets 2825
C. Two-component fermion droplets 2826
1. Coreless vortices with electrons 2826
2. Quantum dots with weak Zeeman coupling 2827
3. Nonpolarized quantum Hall states 2828
D. Bose gases with higher spins 2828
VI. Summary and Outlook 2829
Acknowledgments 2829
References 2830

I. INTRODUCTION

In recent years, advances in experimental methods in quantum optics as well as semiconductor physics have made it possible to create confined quantum droplets of particles and to manipulate them with unprecedented control. Bose-Einstein condensates of ultracold atomic gases, for example, may be set rotating either by rotating the trap or by "stirring" the cold atoms with lasers. These clouds of bosons are large in present day experiments, but the regime of few-particle bosonic droplets ultimately may be reached. Confined electron droplets, on the other hand, are nowadays routinely realized as low-dimensional nanostructured quantum dots in semiconductors, where the droplet size and its angular momentum can be accurately fixed by an external voltage bias and a magnetic field, respectively. A bosonic atom cloud in a trap and electrons confined in quantum dots are different systems by nature. However, when set to rotate, their microscopic properties show remarkable analogies. While quantum dots are usually quasi-two-dimensional due to the semiconductor heterostructure, the dimensionality is reduced also in a trapped rapidly rotating atom gas due to the centrifugal force, which flattens the cloud of atoms.

The structure of a quantum state describing a rotating droplet fundamentally reflects how the system carries angular momentum. Intriguingly, some of the underlying mechanisms appear universal in two-dimensional (2D) systems regardless of the particle statistics, wave-function symmetries, and the form of the interparticle interaction. For example, both bosonic and fermionic droplets show formation of vortices in the droplet with increasing angular momentum. Eventually, in the regime of rapid rotation, finite-size precursors of fractional quantum Hall states with particle-vortex composites are predicted to emerge similarly in both bosonic and fermionic systems. Due to these universalities in the structure of the quasi-two-dimensional many-body state, rotating quantum droplets can often be described theoretically by similar concepts and analogous vocabulary. These analogies are the main theme of this review, where boson and fermion systems are treated in parallel and similarities and differences between these systems are extensively discussed.

Despite the close connection between rotating cold atom gases and electrons in nanostructured quantum systems in solids, research efforts in these fields have advanced mostly independently of each other. In this review we highlight the similarities between these fields, with the hope that it may inspire further studies on rotating quantum systems where complex and sometimes unexpected phenomena emerge.

A. Finite quantum liquids in traps

Confining elementary particles or indistinguishable composite particles, such as atoms, by cavities or external potentials at low temperatures, one may create finite-size quantum systems with particle numbers ranging from just a few to millions. Cold atomic quantum gases in traps and lattices, photons in cavities, and electrons confined in low-dimensional semiconductor nanostructures are well-known examples.

1. Atoms in traps

Bose and Einstein predicted already in the 1920s the condensation of an ideal gas of bosonic particles into a single coherent quantum state (Bose, 1924; Einstein, 1924, 1925). Apart from strongly interacting systems such as liquid helium, the experimental discovery of this phenomenon had to wait many decades, until advances in cooling and trapping techniques for dilute atomic gases finally made possible the observation of Bose-Einstein condensation (BEC) in a cloud of cold bosonic alkali atoms (Anderson *et al.*, 1995; Davis, Mewes, Andrews, *et al.*, 1995; Davis, Mewes, Joffe, *et al.*, 1995; Ensher *et al.*, 1996; Cornell and Wieman, 2002; Ketterle, 2002). These celebrated experiments clearly marked a new era in quantum physics combining the fields of quantum optics, condensed matter physics, and atomic physics. For the physics of BEC, see the review article by Leggett (2001) as well as Dalfovo *et al.* (1999), Inguscio *et al.* (1999), Pethick and Smith (2002), Pitaevskii and Stringari (2003), and Leggett (2006).

A BEC can be set rotating not only by rotating the trap but also by stirring the bosonic droplet with lasers (Chevy *et al.*, 2000; Madison *et al.*, 2000, 2001;

Abo-Shaeer *et al.*, 2001) or by evaporating atoms (Haljan *et al.*, 2001; Engels *et al.*, 2002, 2003) [see the discussion in the recent review by Fetter (2009)]. A weakly interacting dilute system becomes effectively two dimensional when set rotating, making a description in the lowest Landau level possible. We mainly restrict our analysis of BECs in this review to this limit of quasi-two-dimensional droplets of atoms.

Recently superfluid states have also been realized for trapped fermionic atoms, where fermion pairing or molecule formation can occur in two distinct regimes depending on the atomic interaction strength. Pairing can take place in real space via molecule formation and these composite bosons may then show Bose-Einstein condensation (Greiner *et al.*, 2003; Jochim *et al.*, 2003; Regal *et al.*, 2004; Zwierlein *et al.*, 2004). Pairing can also occur in momentum space via formation of correlated Cooper pairs and the superfluid state would be analogous to the Bardeen-Cooper-Schrieffer (BCS) type of a superconducting state (Zwierlein *et al.*, 2005; Chin *et al.*, 2006). This is a relatively novel field and not treated here; part of it has been reviewed by Bloch *et al.* (2008) and Giorgini *et al.* (2008).

2. Electrons in low-dimensional quantum dots

Quantum dots are man-made nanoscale droplets of electrons trapped in all spatial directions. As they show typical properties of atomic systems, such as shell structure and discrete energy levels, they are often referred to as artificial atoms (Ashoori, 1996). Electron numbers in quantum dots may reach thousands. Quantum dots are often fabricated in semiconductor materials, but the use of graphene has also been proposed (Trauzettel *et al.*, 2007; Wunsch *et al.*, 2008). These nanostructured finite fermion systems have been studied extensively for two decades. Several reviews discussing the quantum transport through quantum dots (van der Wiel *et al.*, 2003), electronic structure (Reimann and Manninen, 2002), the role of symmetry breaking and correlation (Yannouleas and Landman, 2007), as well as spin in connection with quantum computing (Cerletti *et al.*, 2005; Coish and Loss, 2007; Hanson *et al.*, 2007) were published.

The semiconductor quantum dots discussed here are of either lateral or vertical type. In a lateral device the electrons in a two-dimensional electron gas are trapped by external electrodes, while vertical dots are formed by, e.g., etching out a pillar from a wafer containing a heterostructure. In both cases the motion of electrons is restricted into a thin disk, with a typical radius of few tens up to hundred nanometers, and a thickness that is often an order of magnitude smaller. Electrons in quantum dots can be set rotating by external magnetic fields perpendicular to the plane of motion. Other stirring mechanisms have also been proposed, e.g., rotation in the electric field of laser pulses (Räsänen *et al.*, 2007). Due to the band structure of the underlying semiconductor material, magnetic field strengths giving rise to transitions in the electronic structure of quantum dots are orders of magnitude lower than in real atomic systems and attainable in laboratories. Much of the information about the electronic structure must be extracted from electron transport measurements (Oosterkamp *et al.*, 1999). Direct imaging methods of electron densities in quantum dots have also been attempted, see, for example, Fallahi *et al.* (2005) and Dial *et al.* (2007) but not yet proven equally useful in this context.

Quantum dots in external magnetic fields have a close connection to quantum Hall systems, the main difference being that the quantum Hall effect is measured in a sample of the two-dimensional electron gas (2DEG), which is often modeled as an infinite system. Quantum dots, however, are finite-size many-body systems. At strong magnetic fields, where electrons occupy only the lowest Landau level, they are thus often referred to as "quantum Hall droplets" (Oaknin *et al.*, 1995; Yang and MacDonald, 2002). Many concepts familiar from the theory of the quantum Hall effect, such as the Landau level filling factor, can be generalized for these finite-size droplets (Kinaret *et al.*, 1992; Reimann and Manninen, 2002). However, due to the presence of the external confining potential in quantum dots, the analogy to quantum Hall states in the infinite 2DEG is not exact and edge effects play an important role (Cooper, 2008; Viefers, 2008).

B. Vortex formation in rotating quantum liquids

The formation of vortices in a liquid that is set to rotate is often a result of turbulent flow. In the epic poem "The Odyssey," Homer described Ulysses' encounter with Charybdis, a monster-goddess who sucked sea water and created a giant whirlpool (Homer, 8th century B.C.). This early account of vortex dynamics is strikingly accurate in identifying the characteristics of vortices, namely, the rotating current of the whirlpool and the cavity at the center of the vortex which engulfed the ships sailing nearby. Homer's description may well be illustrated by other examples of more harmless vortices, such as whirlpools in bathtubs where water is draining out (Andersen *et al.*, 2003). Other well-known examples of vortices in air include tornadoes or wake vortices created by an airplane wing [Figs. 1(a) and 1(b)].

Vortices are also ubiquitous in quantum-mechanical systems under rotation [see Figs. 1(c)–1(e)]. It is well known that the magnetic field in type-II superconductors penetrates through vortex lines (Tinkham, 2004); see Fig. 1(c). Superfluid ^{4}He is another example where vortices may form in a strongly interacting bosonic quantum fluid (Williams and Packard, 1974; Yarmchuk *et al.*, 1979; Yarmchuk and Packard, 1982). [See also the early work by Onsager (1949), London (1954), and Feynman (1955) and, for example, Donnelly (1991).] Vortices appear as a general phenomenon in Bose as well as in Fermi systems with high as well as low particle density. They may emerge for short-range interactions between the particles, as in condensates of neutral atoms [as shown in Fig. 1(d) for a rotating Bose-Einstein condensate of ^{87}Rb atoms] or, perhaps more surprisingly, even

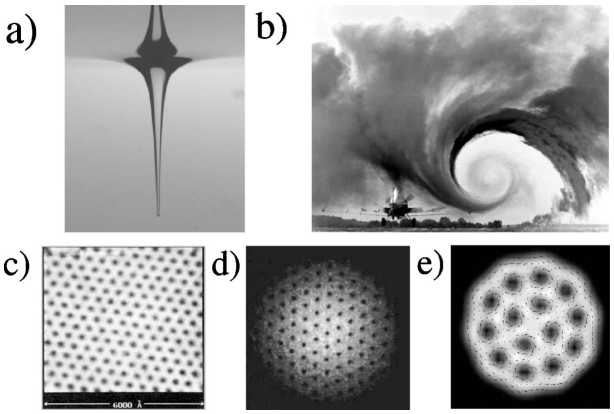

FIG. 1. Examples of vortices and vortex lattices. Vortices are ubiquitous in both classical and quantum systems: (a) classical whirlpool vortex (Andersen *et al.*, 2003), (b) wake vortex of a passing airplane wing, revealed by colored smoke (NASA Langley Research Center, Figure ID: EL-1996-00130), (c) STM image of an Abrikosov vortex lattice (Abrikosov, 1957) in a type-II superconductor (Hess *et al.*, 1989), (d) vortex lattice in a rotating Bose-Einstein condensate of ^{87}Rb atoms [adapted from Coddington *et al.* (2004)], (e) cluster of vortices in the calculated electron density of a 24-electron quantum dot, after Saarikoski *et al.* (2004). In (c)–(e), the vortices appear as "holes" in the particle density.

in electron systems with long-range Coulomb repulsion, see Fig. 1(e) showing the vortices in a quantum dot at a strong magnetic field.

1. Vortices in Bose-Einstein condensates

For vortices in rotating Bose-Einstein condensates, early theoretical descriptions have focused on the Thomas-Fermi regime of strong interactions, see, for example, Rokhsar (1997), Feder *et al.* (1999a, 1999b), García-Ripoll and Pérez-García (1999), and Svidzinsky and Fetter (2000), as well as weak interactions (Butts and Rokhsar, 1999; Mottelson, 1999; Kavoulakis *et al.*, 2000). Baym and Pethick (1996) treated vortex lines in terms of the Gross-Pitaevskii approach and later on also discussed the transition to the lowest Landau level when the rotation frequency was increased (Baym and Pethick, 2004).

Intense experimental research efforts were made to observe vortices in rotating clouds of bosonic atoms, see, e.g., the early experimental work by Matthews *et al.* (1999), as well as Madison *et al.* (2000), Abo-Shaeer *et al.* (2001), Engels *et al.* (2002, 2003), and Schweikhard *et al.* (2004). For recent reviews, see Bloch *et al.* (2008) as well as Fetter (2009).

In weakly interacting and dilute systems, an effective reduction of dimensionality can, for example, be caused by rotation as a simple consequence of the increase in angular momentum. Due to the reduction in dimensionality, phase singularities, i.e., nodes in the wave functions, become important.

With increasing angular momentum, one finds successive transitions between patterns of singly quantized vortices arranged in regular arrays. In finite-size systems, so-called "vortex molecules" are formed, in much analogy to finite-size superconductors (Milošević and Peeters, 2003).

There exist many analogies of a rotating cloud of bosonic atoms with (fractional) quantum Hall physics (Wilkin *et al.*, 1998; Cooper and Wilkin, 1999; Viefers *et al.*, 2000; Ho, 2001). This in fact may also give important theoretical insights into the regime of extreme rotation which has not yet been achieved experimentally. [For related reviews, see Cooper (2008), Viefers (2008), and Fetter (2009).]

2. Vortices in quantum Hall droplets

Vortices have been an integral part of the theory of quantum Hall states in the 2D electron gas since the proposal of the Laughlin state (Laughlin, 1983). They also emerge in quantum dots (Saarikoski *et al.*, 2004; Toreblad *et al.*, 2004) at strong magnetic fields, and close connections of these vortices to those that can be found in rotating bosonic systems have been established (Toreblad *et al.*, 2004, 2006; Manninen *et al.*, 2005; Borgh *et al.*, 2008). The vortex patterns in quantum dots depend on the strength of the external magnetic field and on intricate details of particle interactions (Saarikoski *et al.*, 2004; Tavernier *et al.*, 2004).

In the regime of slow rotation, vortices (except those originating from the Pauli principle) are not bound to particles and form charge deficiencies in the density distribution, which may localize to structures in the particle and current densities that resemble the aforementioned vortex molecules or regular vortex arrays in rotating Bose-Einstein condensates (Saarikoski *et al.*, 2004; Saarikoski, Reimann, *et al.*, 2005; Manninen *et al.*, 2005). The emergence of vortices that carry the angular momentum of the droplet is manifest in the structure of the many-body states. For fermions they may be described as hole-like quasiparticles (Manninen *et al.*, 2005). When the number of vortices increases with the angular momentum, the electrons and vortices may form composites well known from the theory of the fractional quantum Hall effect, see, for example, Jain (1989) or Viefers (2008).

3. Quantum Hall regime in bosonic condensates

In quantum dots, the fractional quantum Hall regime with a high vortex density can be readily attained at high magnetic fields. For the case of rotating cold atom condensates, despite extensive experimental studies (Coddington *et al.*, 2003; Schweikhard *et al.*, 2004), this regime of extreme rotation is not yet within easy reach. Recently, however, it was suggested to exploit the equivalence of the Lorentz and the Coriolis force to realize "synthetic" magnetic fields in rotating neutral systems, which could be an important step forward in the efforts to realize BECs at extreme rotation (Lin *et al.*, 2009). To date experiments with rotating BECs are only able to access states where the number of vortices is relatively small compared to the number of particles (Matthews *et al.*, 1999; Madison *et al.*, 2000; Abo-Shaeer *et al.*, 2001;

Engels *et al.*, 2002, 2003; Schweikhard *et al.*, 2004; Fetter, 2009). A high vortex density creates a highly correlated state. Counterparts of typical quantum Hall states, such as the bosonic Laughlin state and other incompressible states, as well as states having non-Abelian particle excitations, are predicted to emerge (Wilkin *et al.*, 1998; Cooper and Wilkin, 1999; Viefers, 2008; Lin *et al.*, 2009). Compared to the quantum Hall systems in the 2D electron gas, rotating cold-atom condensates offer a high level of tunability since particle interactions and trap geometries can be modified. This makes bosonic quantum Hall states an extremely interesting field of research (Cooper, 2008; Viefers, 2008).

4. Self-bound droplets

A common feature of all the systems discussed above is that the particles are bound by an external confinement, which often can be approximated to be harmonic. Nuclei, helium droplets, and atomic clusters provide other interesting finite quantum systems where rotational states have been studied. These systems are self-bound due to attractive interactions between (at least some of) the components.

Rotational states, shape deformations, and fission of self-bound droplets are interesting topics in their own right. However, while in a harmonic confinement the fast rotation causes the droplet to flatten into a quasi-two-dimensional circular disk, this is usually not the case in self-bound clusters, where the rotation can be accompanied with a noncircular deformation, often a two-lobed or even more complicated shape (Hill and Eaves, 2008). Eventually this can lead to a fission of the droplet to smaller fragments, preventing the occurrence of very large angular momenta and vortex formation. In the case of nuclei, the rotational spectrum is usually related to deformation (Bohr and Mottelson, 1975). In fact, the possibility of vortexlike excitations has also been discussed, see Fowler *et al.* (1985) and Brink and Broglia (2005), and nuclear matter is expected to carry vortices in neutron stars (Baym *et al.*, 1969; Link, 2003; Avogadro *et al.*, 2007).

The only small self-bound system where vortices are likely to occur is a helium droplet. Grisenti and Toennies (2003) indicated that anomalies in their cluster beam experiments could be caused by vortex formation. However, no clear experimental evidence of vortex formation in small helium droplets has yet emerged, while theoretical studies suggest that vortices form in ^{4}He nanodroplets (Mayol *et al.*, 2001; Lehmann and Schmied, 2003; Sola *et al.*, 2007). The properties of helium nanodroplets were reviewed by Barranco *et al.* (2006).

C. About this review

The main concern of this review are the structural properties of the many-body states of small two-dimensional quantum droplets, where rotation induces strong correlations and vortex formation. The direct connections between bosonic and fermionic systems as well as finite-size quantum droplets and infinite quantum Hall systems are recurrent themes. Other reviews complement our work by taking different approaches: we refer to Fetter (2009) for a review of rotating BECs especially in the regime which is accessible with present day experimental setups and to Viefers (2008) for a review which focuses on the quantum Hall physics in rotating BECs. Another review by Cooper (2008) describes rotating atomic gases in both the mean-field and strongly correlated regimes. A review on the many-body phenomena and correlations in dilute ultracold gases that also discusses rotation was given by Bloch *et al.* (2008).

Quantum dot physics is a versatile field. We refer to Reimann and Manninen (2002) and Yannouleas and Landman (2007) as well as van der Wiel *et al.* (2003) and Hanson *et al.* (2007) for reviews on the electronic structure and spin-related phenomena. Vortices in superconducting quantum dots have also been much discussed but are not treated here. We instead refer the interested reader to recent articles by Baelus *et al.* (2001, 2004), Baelus and Peeters (2002), and Grigorieva *et al.* (2006).

We begin this review in Sec. II by introducing basic concepts to characterize the many-body states of rotating systems. Section III discusses some of the computational many-body methods used. Section IV discusses vortex formation in rotating quantum liquids which are composed of one type of particles (or one spin component), while Sec. V is concerned with coreless vortices in multicomponent systems. We conclude the review and discuss possible future challenges in Sec. VI.

Unless stated otherwise, equations are presented in SI units, whereas most results of calculations are in atomic units.

II. MANY-BODY WAVE FUNCTION

In the following, we describe concepts and methods to analyze the internal structure of the many-body states, such as pair-correlation functions and conditional probabilities. We then proceed to show the connections between boson and fermion states, and particle-hole duality that treats vortices as holelike quasiparticles. We finally give an overview of the connections to the quantum Hall physics in the (infinite) two-dimensional electron gas.

A. Model Hamiltonian

1. Rotating quantum droplets of bosons

Clouds of bosonic condensates are usually confined by a harmonic trap that extends in all three spatial dimensions. An axisymmetric rotation with frequency Ω leads to centrifugal forces which flatten the density by extending the radial size of the system, while the cloud contracts in the axial direction. The ratio between the axial thickness R_z and radial thickness $R_\perp$ of the rotating cloud, i.e., the aspect ratio, can be calculated within the Thomas-Fermi approximation (Fetter, 2009)

$$\frac{R_z}{R_\perp} = \frac{\sqrt{\omega_\perp^2 - \Omega^2}}{\omega_z}, \tag{1}$$

where ω_z and $\omega_\perp$ are the radial and axial trapping frequencies, respectively. Imaging of the condensate (Raman *et al.*, 2001; Schweikhard *et al.*, 2004) confirms that the rotation reduces the aspect ratio effectively.

One conveniently introduces a rotating frame at the angular velocity Ω, in which the Hamiltonian contains an extra inertial term $-\Omega\mathbf{L}$, where $\mathbf{L}$ is the total angular momentum operator. In the case of circular symmetry of the 2D system, for its rotation around the z axis, the angular momentum operator $L=L_z$ commutes with the Hamiltonian. We may write

$$H_\Omega = H - \Omega L_z, \tag{2}$$

where the many-body Hamiltonian is

$$H = \sum_{i=1}^{N} \left(\frac{\mathbf{p}_i^2}{2m} + V_{\text{ext}}(\mathbf{r}_i) \right) + \sum_{i<j} V^{(2)}(\mathbf{r}_i - \mathbf{r}_j). \tag{3}$$

Here V_{ext} is the trapping potential that is usually harmonic with oscillator frequency ω,

$$V_{\text{ext}} = \tfrac{1}{2} m\omega^2 r^2, \tag{4}$$

and $V^{(2)}$ is the two-body interaction between the trapped atoms.

The ground states of the Hamiltonian (2) are then angular momentum eigenstates of the Hamiltonian (3) which have the lowest energy at some finite frequency of rotation Ω.

The effective interaction between the bosons is often assumed to be a contact interaction of zero range,

$$V^{(2)}(\mathbf{r}_i - \mathbf{r}_j) = \frac{1}{2} g \sum_{i \neq j} \delta(\mathbf{r}_i - \mathbf{r}_j), \tag{5}$$

where $g = 4\pi\hbar^2 a/M$, with atom mass M and a being the scattering length for elastic s-wave collisions between the atoms. In the regime of weak interactions, $gn \ll \hbar\omega$, where n is the particle density and $\hbar\omega$ is the quantum energy of the confining potential. In a rotating system, the problem becomes effectively two dimensional when gn is much smaller than the energy difference between the ground and first excited states for motion along the z axis.

The single-particle energies of the two-dimensional harmonic oscillator are $\epsilon = \hbar\omega(2n + |m| + 1)$, where n is the radial quantum number and m is the single-particle angular momentum. In a noninteracting rotating many-particle system, consequently, the lowest-energy configuration is characterized by quantum numbers $n=0$ and $0 \leqslant m \leqslant L$, where m has the same sign as the angular momentum L. This single-particle basis is identical to the lowest Landau level (LLL) at strong magnetic fields. In this subspace, a configuration can be denoted by the Fock state $|n_0 n_1 n_2 \cdots n_m \cdots n_L\rangle$, where n_i is the (here bosonic) occupation number for the single-particle state with angular momentum m, and $m=L$ is the largest single-particle angular momentum that can be included in the basis. As the angular momentum L is a good quantum number, we have the restriction $\Sigma_m m n_m = L$.

For a harmonic trap, there is a large degeneracy in the absence of interactions, which originates from the many different ways to distribute the N bosons on the basis states with $0 \leqslant m \leqslant L$ (Wilkin *et al.*, 1998; Mottelson, 1999). Interactions break this degeneracy, and a particular state can be selected at a given L that minimizes the interaction energy. With reference back to the nuclear physics terminology, the highest angular momentum state at a given energy is called the *yrast* state (Grover, 1967; Bohr and Mottelson, 1975), the name originating from the Swedish word for "*the most dizzy.*" The line connecting the lowest energy states in the energy-angular momentum diagram is consequently called the *yrast line*.

For interacting particles, the yrast line is a nonmonotonic function of the angular momentum. At angular momenta corresponding to the ground states at a certain trap rotation frequency Ω, it shows pronounced cusps reflecting the vortex structures of the system, as it will become clear later on.

2. Electron droplet in a magnetic field

We focus here on droplets of electrons trapped in a quasi-two-dimensional quantum dot (Reimann and Manninen, 2002). The spatial thickness of the confined electron droplet is of the order of nanometers for typical quantum dot samples. Electrons in quantum dots are set rotating, not by mechanical stirring but instead by applying an external magnetic field perpendicular to the dot surface (i.e., along the z axis) quite analogously to the circular motion in a cyclotron.

A droplet of electrons in a quantum dot can be modeled using an effective-mass Hamiltonian in the x-y plane,

$$H = \left(\sum_{i=1}^{N} \frac{(-i\hbar\nabla_i + e\mathbf{A})^2}{2m^*} + V_{\text{ext}}(r_i) \right) + \frac{e^2}{4\pi\epsilon} \sum_{i<j} \frac{1}{r_{ij}}, \tag{6}$$

where N is the number of electrons, m^* and ϵ are the effective mass and dielectric constant of the semiconductor material, $\mathbf{A}$ is the vector potential of the magnetic field, $\mathbf{B} = \nabla \times \mathbf{A}$, and the Zeeman term has been omitted. The external confining potential V_{ext} is usually parabolic to a good accuracy (Matagne *et al.*, 2002). The single-particle states in the external harmonic potential Eq. (4) are known as Fock-Darwin states (Fock, 1928; Darwin, 1931). At strong magnetic fields the magnetic confinement dominates over the electric confinement, and the Fock-Darwin states bunch to Landau levels, as described above for the case of rotation. The LLL is then the most important subspace for ground-state properties of the system.

Using a symmetric gauge $\mathbf{A} = B(y\hat{\mathbf{e}}_x - x\hat{\mathbf{e}}_y)/2$ the first term in the Hamiltonian (6) can be expanded to give two terms that are proportional to the magnetic field. The diamagnetic term is scalar, $(e^2B^2/8m^*)(x^2+y^2)$, and the other, the paramagnetic term, is proportional to the z

component of the angular momentum $(e\hbar/2m^*i)B\mathbf{r}\times\nabla = (e/2m^*)BL_z$. The scalar term depends on the square radius from the center of the droplet and describes the squeezing effect of the magnetic field. The latter term lowers the energy of the states that circulate in the direction of the cyclotron motion and favors alignment of the magnetic moment parallel to the external magnetic field. By combining the diamagnetic term in the Hamiltonian (6) with the external confining potential and writing the paramagnetic term as $(e/2m^*)BL_z = \Omega L_z$, we see directly that, except for the Zeeman term and the type of interparticle interactions, the Hamiltonian is exactly the same as that for a rotating bosonic system (2). The rotation corresponds to a magnetic field strength of $\mathbf{B} = (2m^*\Omega/e)\hat{\mathbf{e}}_z$ in a weaker confinement $V'_{\text{ext}} = \frac{1}{2}m^*(\omega_0^2 - \Omega^2)\mathbf{r}^2$. This constitutes a close analogy between systems in mechanical rotation and systems of charged particles in a perpendicular magnetic field.

3. Role of symmetry breaking

In the thermodynamic limit, mean-field theories incorporating order parameters can describe states with broken symmetries. However, the exact wave function of the many-body system must always preserve the underlying symmetry of the Hamiltonian.

Construction of a symmetry-broken state and a subsequent restoration of symmetry has been proposed to construct wave functions in rotating, correlated many-particle systems (Yannouleas and Landman, 2007). By construction, this approach focuses on the role of particle ordering in the confining trap potential. On the other hand, small perturbations in the symmetric potentials can be used to probe the internal structure of the many-body states. For vortices in small quantum droplets, this may be achieved effectively using point perturbations, or deforming the external field slightly (Saarikoski, Reimann, *et al.*, 2005; Christensson, Borgh, *et al.*, 2008; Parke *et al.*, 2008; Dagnino, Barberán, and Lewenstein, 2009; Dagnino *et al.*, 2009).

B. Vortices in the exact many-body wave function

Vortices in a complex-valued wave function are associated with phase singularities. They are manifested through a phase change of a multiple of 2π in every path encircling the singularity. The phase is not defined at the singularity, which means that the wave function must vanish at this point. The particle deficiency in the vicinity of the singularity gives rise to the vortex core. Different types of phase singularities can be recognized: (i) those which are related to the antisymmetry of the fermion wave function, (ii) those which are largely independent of particle positions and may be called isolated or free vortices (and occur for bosonic as well as fermionic systems in a rather similar way), and (iii) those which are attached to particles to form a bound system, i.e., a "composite" particle.

1. Pauli vortices

Exchange of two identical, indistinguishable bosons or fermions can change the wave function of the system at most by a factor $C=\pm 1$ so that $\Psi(\ldots,\mathbf{r}_i,\ldots,\mathbf{r}_j,\ldots) = C\Psi(\ldots,\mathbf{r}_j,\ldots,\mathbf{r}_i,\ldots)$. In the 2D plane, making two exchanges (with a total phase change of 2π) is equivalent to rotating the particles in plane with respect to each other. In the LLL this phase change implies that there is a vortex attached to the electron [see Fig. 3(b)]. This vortex (related to the fermion antisymmetry) is called a "Pauli vortex" (or, as in quantum chemistry, the "exchange hole"). As a trivial consequence, a delta-function-type interparticle interaction does not have any effect on fermions with the same spin.

2. Off-particle vortices

Vortices that are not attached to any particles are called "off-particle" vortices. These elementary excitations may occur in boson as well as in fermion systems.

For the two-dimensional electron gas, off-particle vortices have been studied in connection with the quantum Hall effect, both for the bulk and in finite-size quantum dots. The connection between the wave-function phase and the vorticity in such systems can most easily be seen by using the vector potential $\mathbf{A}(\mathbf{r})$ of the magnetic field that couples to the momentum operator in the Hamiltonian [Eq. (6)]. A finite magnetic field leads to an extra phase change of $\Delta\theta = (e/\hbar)\int_A^B \mathbf{A}(\mathbf{r})\cdot d\mathbf{r}$ when the electron moves from A to B. In a closed path in the 2D plane the phase shift must be $2\pi l$, where l is an integer, which causes the magnetic field to penetrate the 2D plane as vortices carrying magnetic flux quanta $\Phi_0 = h/e$. The integer l is called the winding number or vortex multiplicity ($l=0$ means no vortex).

3. Particle-vortex composites

When the total angular momentum and thus also the number of vortices increases, the correlations favor the attachment of additional vortices to the particles. This is well established in the 2DEG, where it leads to Laughlin-type quantum Hall states at high magnetic fields. These states are discussed in Sec. II.E. Analogous Laughlin states are predicted to also form in rotating bosonic systems (Wilkin *et al.*, 1998; Cooper and Wilkin, 1999; Wilkin and Gunn, 2000; Cooper *et al.*, 2001). In general, the wave-function antisymmetry requires that fermions must have an odd number of vortices attached to them, while bosons have an even number of vortices.

In multicomponent systems particle deficiency associated with off-particle vortices in one component may attract particles of other components. In finite-size quantum droplets this is usually energetically favorable. The structures that form are called "coreless vortices" since vortex cores are filled by another particle component, but the singularities in the phase structure remain. Coreless vortices will be analyzed further in Sec. V.

C. Internal structure of the many-body states

The *exact* many-particle wave function is in many cases known only as a numerical approximation, with the complexity growing exponentially with the particle number N. Its dimensionality must be reduced to allow visualization of the correlations and phase structures since symmetries of the underlying Hamiltonian often hide the internal structures in the exact many-body state. Thus, pair-correlation functions and reduced wave functions are often applied. The former has been a standard tool in many-body physics for many years. The latter, on the other hand, is more suitable to visualize the phase structure of the wave function and its singularities.

1. Conditional probability densities

The pair-correlation function is a conditional probability density describing the probability of finding a particle at a position $\mathbf{r}$ when another particle is at a position $\mathbf{r}'$. For systems with only one kind of indistinguishable particles, one may write

$$P(\mathbf{r},\mathbf{r}') = \langle\Psi|\hat{n}(\mathbf{r})\hat{n}(\mathbf{r}')|\Psi\rangle = \int |\psi(\mathbf{r},\mathbf{r}',\mathbf{r}_3,\ldots,\mathbf{r}_N)|^2 d\mathbf{r}_3\cdots d\mathbf{r}_N, \tag{7}$$

where $|\Psi\rangle$ is the many-body state, $\hat{n}$ is the density operator, and ψ is the many-body wave function. For particles with spin (or another internal degree of freedom as, for example, in the case of different particle components), labeled by an index σ, the pair-correlation function is correspondingly defined as

$$P_{\sigma,\sigma'}(\mathbf{r},\mathbf{r}') = \langle\Psi|\hat{n}_\sigma(\mathbf{r})\hat{n}_{\sigma'}(\mathbf{r}')|\Psi\rangle, \tag{8}$$

where $\hat{n}_\sigma$ and $\hat{n}_{\sigma'}$ are the density operators for the components.

In a homogeneous system P depends only on the distance $|\mathbf{r}-\mathbf{r}'|$ while in a finite system this is not the case. Instead, one has to choose a reference point $\mathbf{r}'$ around which the pair-correlation function may then be plotted as a function of $\mathbf{r}$. The details of the pair correlation in finite systems are sensitive to the selection of this reference point. The inherent arbitrariness in choosing the off-centered fixed point must be taken care of by sampling over a range of values for $\mathbf{r}'$ to allow any reasonable interpretation. Usually, a position that does not coincide with any symmetry point and where the density of the system is at a maximum gives the most informative plot. Note, however, that in fermion systems the pair correlations at short distances are strongly dominated by the exchange-correlation hole of the probe particle, which may complicate the analysis.

2. One-body density matrix

The one-body reduced density matrix is defined as

$$n^{(1)}(\mathbf{r},\mathbf{r}') = \langle\Psi|\hat{\psi}^\dagger(\mathbf{r})\hat{\psi}(\mathbf{r}')|\Psi\rangle, \tag{9}$$

where $\hat{\psi}^\dagger$ and $\hat{\psi}$ are field operators (with given statistics), creating and annihilating a particle. The eigenfunctions ψ_i and eigenvalues n_i of the density matrix are solutions of

$$\int d\mathbf{r}' n^{(1)}(\mathbf{r},\mathbf{r}')\psi_i^*(\mathbf{r}') = n_i\psi_i^*(\mathbf{r}). \tag{10}$$

For a noninteracting system, the eigenfunctions are simply the single-particle wave functions, while the eigenvalues give the occupation numbers. For interacting bosons, it is suggestive that the exact eigenstate corresponding to the highest eigenvalue (n_1) of the density matrix plays the role of a "macroscopic wave function" (order parameter) of the Bose condensate. This connection was established many decades ago in the context of off-diagonal long-range order (Ginzburg and Landau, 1950; Landau and Lifshitz, 1951; Penrose, 1951; Penrose and Onsager, 1956; Yang, 1962; Pethick and Smith, 2002; Pitaevskii and Stringari, 2003). For a discussion of fragmentation (Leggett, 2001) in this context, see, for example, Baym (2001), Mueller *et al.* (2006), and Jackson *et al.* (2008).

Since the eigenstates of the density matrix can be complex, their phase can show singularities as they are characteristic for vortices. However, the density matrix bears the same symmetry as the Hamiltonian and, consequently, so do its so-called "natural orbitals" $\psi_i^*(\mathbf{r})$. In a circular confinement, the eigenfunctions of the density matrix can thus only show an overall phase singularity at the origin but not at the off-centered vortex positions.

In a study of vortex formation in boson droplets this problem has been circumvented by adding a quadrupole perturbation to the confining potential (Dagnino *et al.*, 2007; Dagnino, Barberán, and Lewenstein, 2009; Dagnino *et al.*, 2009). Indeed, the positions of all vortices are then seen as phase singularities of the complex "order parameter" $\psi_1^*(\mathbf{r})$. With a related symmetry breaking of the external confinement, the vortices may also be seen as minima in the total particle density (Toreblad *et al.*, 2004; Saarikoski, Harju, *et al.*, 2005; Dagnino *et al.*, 2007), and as circulating currents as shown, for example, in Fig. 29.

3. Reduced wave functions

Pair-correlation functions smoothen out the finer details of the many-particle wave function. As real-valued functions, they are not suited to probe the phase structure, and zeros (nodes) at the center of the vortex cores cannot be directly identified either since integrations over particle coordinates blur their effect. The concept of a reduced (or conditional) wave function has thus been introduced to map out the nodal structure of the wave function as a "snapshot" around the most probable particle configuration. For fermions, reduced wave functions were introduced in the context of two-electron atoms (Ezra and Berry, 1983) and coupled quantum dots

(Yannouleas and Landman, 2000), and then generalized to many-particle systems (Harju *et al.*, 2002; Saarikoski *et al.*, 2004; Tavernier *et al.*, 2004). The basic idea is simple: Instead of calculating average values, the wave function is calculated in a subspace by fixing $N-1$ particles to positions given by their most probable configuration $\mathbf{r}_2^*,\ldots,\mathbf{r}_N^*$. The reduced wave function for the remaining (probing) particle is then calculated at $\mathbf{r}$,

$$\psi_c(\mathbf{r}) = \frac{\Psi(\mathbf{r},\mathbf{r}_2^*,\ldots,\mathbf{r}_N^*)}{\Psi(\mathbf{r}_1^*,\mathbf{r}_2^*,\ldots,\mathbf{r}_N^*)}, \tag{11}$$

where $\mathbf{r}_1^*$ is the most probable position of the probe particle and the denominator is used to normalize the maximum value of ψ_c to unity. The most probable configuration for fixed particles $(\mathbf{r}_1^*,\mathbf{r}_2^*,\ldots,\mathbf{r}_N^*)$ is obtained by maximizing the absolute square of Ψ.

It is often convenient to visualize $\psi_c(\mathbf{r})$ by plotting its absolute value using contours, usually in a logarithmic scale, together with its phase as a density plot. The resulting diagram represents a single-particle wave function in a selected "particle's-eye-view" reference frame. Nodes in the wave function can be identified as zeros in $\psi_c(\mathbf{r})$ associated with a phase change of integer multiple of 2π for each path that encloses the zero. Figure 2 shows the reduced wave function in the simple case of a two-electron quantum dot in the spin singlet and triplet states, respectively. One electron position is fixed, as marked by the cross. In the singlet state, the electrons have opposite spins and there is no vortex. In the triplet state, a vortex is attached to the fixed electron in accordance with the Pauli principle.

In the case of larger particle numbers, interpretation of the reduced wave function requires a careful analysis since nodes for different reference frames of fixed particles may not coincide (Graham *et al.*, 2003). However, localized nodes can be readily identified as vortices. These include off-particle vortices, which are associated with holes in the particle density. Also particle-vortex composites can be identified as nodes attached to the immediate vicinity of particles.

The reduced wave function as defined for single-component systems in Eq. (11) can be readily generalized also for multicomponent systems with two or more particle species distinguishable from each other. The wave function is then a direct product of the wave functions of different particle species. As a consequence, the reduced wave function can still be written as in Eq. (11) although different particle species have to be distinguished. The reduced wave function depends on the species of the probe particle, unless the number of particles of each species is equal. The fact that phase singularities of one species coincide with particles of another species [see Fig. 3(c)] may indicate formation of coreless vortices. This is discussed further in Sec. V. As an example, Fig. 3 exemplifies the appearance of the reduced wave functions for different nodal structures, as here for fermions with spin-1/2. Correlations in the many-body state can be further studied by analyzing the reduced wave function in the vicinity of the most probable configuration(s).

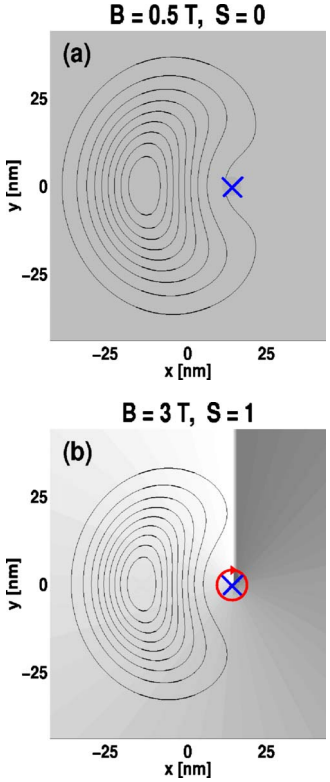

FIG. 2. (Color online) Reduced wave function of a two-electron quantum dot in (a) the singlet and (b) the triplet state. The fixed electron is marked by the cross to the right. The contours give the logarithmic electron density of the probing electron and the gray scale illustrates the phase of the wave function. The phase jumps from 0 to 2π on the line where the scale changes from white to darkest gray. In the singlet state, the electrons have opposite spins and there is no vortex. In the triplet state, the electrons have same spin and a vortex (circle with an arrow in the direction of phase gradient) is attached on top of the fixed electron in accordance with the Pauli principle. Due to fermion antisymmetry the phase changes by 2π if the probe electron is moved around the fixed electron in this case. From Harju, 2005.

D. Particle-hole duality in electron systems

In infinite quantum Hall liquids, particle-hole duality can be used to study vortex formation by interpreting holes as vortices (Girvin, 1996; Shahar *et al.*, 1996; Burgess and Dolan, 2001). Similar arguments for the symmetry of particle and hole states can be used in finite-size systems to gain insight into issues such as vortex localization and fluctuations. We here consider polarized electrons or, more generally, fermions of only one kind (i.e., spinless fermions). However, much of the considerations can be generalized to systems with more degrees of freedom, such as, for example, spinor gases.

In the occupation number representation, the Hamiltonian for interacting electrons in the lowest Landau level can be written as

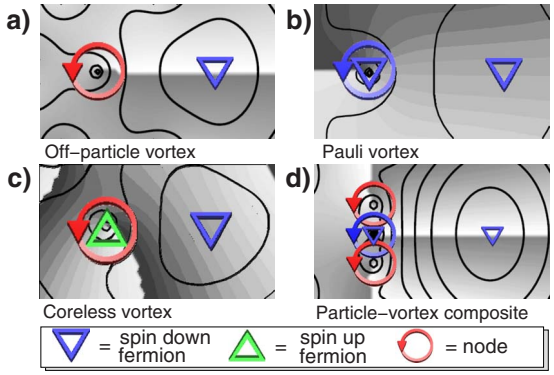

FIG. 3. (Color online) Appearance of vortex structures in the reduced wave function. The details of reduced wave functions for spin-1/2 fermions are shown. The most probable position of the probing particle is to the right; the contours show the magnitude (on a logarithmic scale), and the gray scale shows the phase (darkest gray=0, lightest gray=2π). (a) An isolated localized vortex which is not attached to any particle. (b) A Pauli vortex (exchange hole) which is mandated by the wave-function antisymby metry between interchange of indistinguishable fermions. (c) A coreless vortex where the vortex core of spin-down component is filled by a spin-up fermion. (d) A composite of a fermion (with a Pauli vortex) and two additional nodes which are bound to the particle, reminiscent of the Laughlin $\nu=\frac{1}{3}$ state. From Saarikoski *et al.*, 2009.

$$H_p = \sum_i \epsilon_i c_i^\dagger c_i + \sum_{ijkl} v_{ijkl} c_i^\dagger c_j^\dagger c_l c_k, \tag{12}$$

with annihilation and creation operators c_i and $c_i^\dagger$ acting on determinants of states constructed from a given single-particle basis. Here we use the property that the occupation of each state for fermions can only be zero or one. We note that the annihilation operator c_i can be viewed as an operator creating a hole in the Fermi sea. Formally we can define new operators $d_i=c_i^\dagger$ and $d_i^\dagger=c_i$ as creation and annihilation operators of the holes. Equation (12) can then be written as a Hamiltonian of the holes. For the lowest Landau level, considering only states with good total angular momentum, it reduces to

$$H_h = \sum_i \tilde{\epsilon}_i d_i^\dagger d_i + \sum_{ijkl} v_{ijkl} d_k^\dagger d_l^\dagger d_j d_i + \text{const}, \tag{13}$$

where

$$\tilde{\epsilon}_i = 2\sum_j (v_{ijji} - v_{ijij}) - \epsilon_i. \tag{14}$$

It is important to note that the interaction between the holes is equal to the interaction between the particles (assuming normal symmetry $v_{ijkl}=v_{klij}$), but the single-particle energies of the holes are affected by the inter-particle interactions. We can thus solve the many-particle problem either for the particles or for the holes. The use of the holes, however, does not reduce the complexity of the problem: The same accuracy of the solution requires diagonalization of a matrix which has the same size for particles or holes. However, considering holes instead of particles provides an alternative way to understand the localization of vortices in fermion systems (Jeon *et al.*, 2005; Manninen *et al.*, 2005).

Using the above particle-hole duality picture we can treat the off-particle vortices as holelike quasiparticles (Kinaret *et al.*, 1992; Ashoori, 1996; Yang and MacDonald, 2002; Saarikoski *et al.*, 2004; Manninen *et al.*, 2005). In electron systems, these vortices carry a charge deficiency of an elementary charge e. In the particle-hole duality picture the particles and holes (vortices) can be treated on equal footing. They form a quantum liquid of interacting electrons and vortices, where correlations play an important role.

For a correct description of the internal structure of the many-body system, we need to analyze all correlations between the constituents of the system, i.e., particle-particle, vortex-vortex, and particle-vortex correlations. The relative strength of these correlations determines the physics of the ground state. To give an example, clustering of electrons to a Wigner-crystal-like "molecule" of localized electrons is a signature of particularly strong particle-particle correlations. Analogously, the formation of a cluster or "molecule" of localized vortices shows the correlations between the vortex positions. Since the vortex dynamics is not independent of the electron dynamics, strong correlations between electrons and vortices may emerge, leading to the formation of particle-vortex composites.

E. Quantum Hall states

Vorticity increases with angular momentum, leading to the formation of particle-vortex composites at high magnetic fields. In the theory of the quantum Hall effect they were introduced to explain formation of incompressible electron liquids at fractional filling (Laughlin, 1983; Jain, 1989). However, the phenomenon is more general, and similar in both fermion and boson systems where vorticity is sufficiently high (Wilkin *et al.*, 1998; Cooper and Wilkin, 1999; Viefers, 2008).

It should be noted that the analogy between quantum Hall states in finite-size droplets and corresponding states in the infinite 2D electron gas is only approximate since the particle density inside the trapping potentials is often inhomogeneous, and edge effects play an important role. Nevertheless, in order to (at least approximatively) relate the states in finite-size electron droplets to those in the infinite gas, the Landau level filling factor concept has been generalized to finite-size systems. There is obviously no unique way to do such a generalization. However, a definition

$$\nu = \hbar \frac{N(N-1)}{2L}, \tag{15}$$

which is based on the structure of Jastrow states, has been used in the $\nu<1$ regime (Girvin and Jach, 1983; Laughlin, 1983). In large fermion systems, the filling factor becomes equal to the particle-to-vortex ratio, being a useful quantity also to classify rapidly rotating bosonic systems. Its relation to the fermion filling factor defined

above is modified by the absence of Pauli vortices in the bosonic wave function.

The quantum Hall liquid is theoretically described by the Laughlin wave function (Laughlin, 1983) with its extensions, or by the related Jain construction (Jain, 1989; Jeon *et al.*, 2004). These trial wave functions can be constructed using symmetry arguments without any detailed knowledge of the interparticle interactions. It has been shown that similar trial wave functions work for bosons and fermions (Regnault and Jolicoeur, 2003, 2004). Below we discuss the vortex structures of these trial wave functions and demonstrate that one can map the boson wave function onto the fermion wave function, allowing a direct comparison of the vortex structures in these different systems.

1. Maximum density droplet state and its excitations

When an electron droplet is placed in a sufficiently strong magnetic field, it may polarize and the single-particle orbitals in the lowest Landau level become singly occupied. [We remark that at some angular momenta the electrons may polarize even if the Zeeman effect is ignored[1] (Reimann and Manninen, 2002; Koskinen *et al.*, 2007).] The spin-polarized compact droplet of electrons in the LLL, with total angular momentum $L=N(N-1)/2$, is called the maximum density droplet (MDD) state (MacDonald *et al.*, 1993). The MDD has the lowest possible angular momentum which is compatible with the Pauli principle. In the MDD, each electron carries a Pauli vortex and the wave function can be written as

$$\Psi_{\mathrm{MDD}} = \prod_{i<j}^{N} (z_i - z_j) \exp\left[-\sum_{i=1}^{N} r_i^2/2 \right], \tag{16}$$

where $z_j = x_j + iy_j$, $r^2 = x^2 + y^2$, and x and y are coordinates in the 2D plane. The MDD can be written as a single-determinantal wave function; for example, for seven particles it is $|11111110000\cdots\rangle$, where a 1 at position i denotes an occupied state in the LLL with single-particle angular momentum $i-1$. Clearly, the MDD is the finite-size counterpart of the integer quantum Hall state with $\nu=1$.

Removing the Jastrow factor $\Pi(z_i - z_j)$ (i.e., the Pauli vortices) from the MDD in Eq. (16) leaves a product of Gaussians which form the nonrotating bosonic ground state. The MDD state can therefore be interpreted as a fermionic "condensatelike" state of particles that engulf the flux quanta and, in effect, move in a zero magnetic field. In this way, the MDD state with $L_{\mathrm{MDD}} = N(N-1)/2$ is closely related to the nonrotating $L=0$ state of a bosonic system. We discuss this relation further in Sec. II.F, where we show conceptually that by removing the Pauli vortices from each fermion the wave function of a fermion system at L is often a good approximation for a bosonic state with angular momentum $L' = L - L_{\mathrm{MDD}}$.

[1]Nonpolarized states will be discussed in Sec. V.

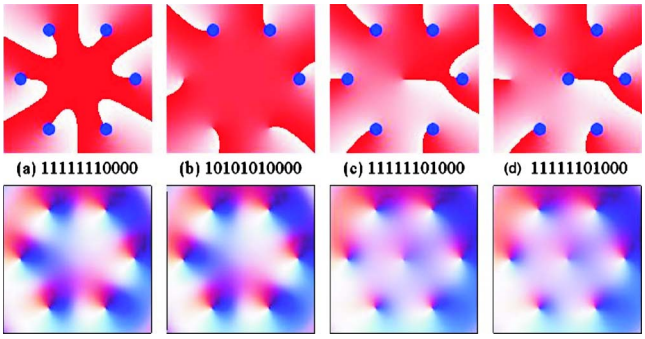

FIG. 4. (Color online) Reduced wave functions. (a) A seven-particle MDD state, (b) the MDD state with three holes, and (c) and (d) MDD state with a center-of-mass excitation. The upper panels show the phase and the lower panels the magnitude of the reduced wave function. The bullets mark the fixed particle positions.

The first excitation of the MDD in the LLL can be approximated as a single determinant where one of the single-particle states is excited to a higher angular momentum. This state can be understood in two different ways. It is definitely a center-of-mass excitation since

$$|11\cdots 110100\cdots\rangle = \sum_{i=1}^{N} z_i |\mathrm{MDD}\rangle. \tag{17}$$

On the other hand, this state is also a simple single-particle excitation where a hole enters the droplet from the surface. This hole is associated with a phase singularity in the reduced wave function.

To illustrate the nodal structure of a MDD, we show in Fig. 4(a), with seven particles as an example, the reduced wave function for this state. Figure 4(b) shows the reduced wave function of the four-particle state $|1010101000\rangle$ with three holes in the MDD, demonstrating that the holes localize on the sites of the "missing" electrons, each of them carrying a vortex that is characterized by zero density at the core, and the corresponding phase change.

It is important to note that in the reduced wave function only the positions of the particles are fixed, while the vortices are free to choose their optimal positions. This is shown in Figs. 4(c) and 4(d) for a center-of-mass excitation: When one of the atoms (here fixed at the vertices of a hexagon) is moved to the center, the free vortex correspondingly moves from the center to the hexagon.

2. Laughlin wave function

The angular momentum of a quantum Hall state increases with the formation of additional vortices. When there are three times more vortices than electrons ($\nu=1/3$), fermion antisymmetry is preserved if two additional vortices (on top of Pauli vortices) are attached to each fermion. The corresponding wave function is the celebrated Laughlin state

$$\Psi_{\mathrm{m}} = \prod_{i<j}^{N} (z_i - z_j)^m \exp\left[-\sum_{i=1}^{N} r_i^2/2 \right], \tag{18}$$

where the antisymmetry of fermion wave functions requires that the exponent m is an odd integer (Laughlin, 1983). The analogous wave function for a boson system in a trap is given by even values of m. The exponent m is related to the filling factor $\nu=1/m$ and to the angular momentum $L=mN(N-1)/2$. According to computational studies that apply diagonalization schemes to the many-body Hamiltonian (see Sec. III), the Laughlin wave function with $\nu=1/3$ gives a good approximation of the ground state at the corresponding filling factors in finite-size quantum Hall droplets. We discuss this regime of strong correlations in the context of rapidly rotating quantum droplets in Sec. IV.F.

3. Jain construction and composite particles

The composite-fermion (CF) theory (Jain, 1989, 2007) generalizes the Laughlin wave function to a larger set of possible filling fractions. The basic idea is that when an even number of vortices or flux quanta is bound to electrons, these interact less as the vortices keep them apart, i.e., the exchange hole is widened by the cores of bound vortices. In addition, the composites move in an effective magnetic field that is weaker than the original one.

Formally, the composite fermion wave function can be written as (Jain, 2007)

$$\Psi_{\mathrm{CF}} = \mathcal{P}_{\mathrm{LLL}} \psi_S \prod_{i>j} (z_i - z_j)^m, \tag{19}$$

where ψ_S is a single Slater determinant of single-particle states, the product $\Pi(z_i-z_j)^m$ adds m vortices at each electron, and the operator $\mathcal{P}_{\mathrm{LLL}}$ projects the wave function to the lowest Landau level. If ψ_S is taken to be the MDD, Eqs. (16) and (19) lead to the Laughlin wave function for the fractional Hall effect with filling factor $\nu=1/(m+1)$ and no projection to the LLL is needed. However, ψ_S is not restricted to the LLL, which allows constructing the states along the whole yrast line. For example, in order to get the MDD of composite particles, we have to take for ψ_S a MDD of states with negative angular momenta, which means replacing z_i and z_j with their complex conjugates z_i^* and z_j^* in Eq. (16). Note that the states with negative angular momenta are at higher Landau levels. Multiplying this by $\Pi(z_i-z_j)^2$ and projecting to the LLL gives the normal MDD wave function of Eq. (16). Wave functions between $\nu=1$ and $1/3$ can be obtained by starting from properly chosen Slater determinants for ψ_S (Jain, 2007). The projection to the LLL, however, is the most difficult part of the Jain construction. In practice, it can be done by replacing z_i^*'s by partial derivatives (Girvin and Jach, 1984).

The composite fermion picture accurately describes states at high angular momentum ($L \gg L_{\mathrm{MDD}}$) where two vortices (in addition to the Pauli vortex) are attached to each electron. However, for the states immediately above the MDD ($L \approx L_{\mathrm{MDD}}$) the CF theory still requires the attachment of two vortices to each electron. This means that the composite particle (electron and two vortices) has to move in an effective magnetic field which is *opposite* to the true magnetic field. In this case the projection operator $\mathcal{P}_{\mathrm{LLL}}$ will remove the two vortices [attached by the product $\Pi(z_i-z_j)^2$] and leads to the physically correct result that only one (Pauli) vortex is attached to each electron. The true number of vortices attached to each electron can thus be determined only after the projection to the lowest Landau level.

Comparison with exact numerical calculations have shown that the CF theory in the mean-field approximation does not predict all ground states correctly (Harju *et al.*, 1999; Yannouleas and Landman, 2007). It is possible to go beyond mean-field theory, but the price to pay is that the beauty of not having variational parameters in the wave function is lost (Jeon *et al.*, 2007).

The CF theory has also been used for bosons (Cooper and Wilkin, 1999; Viefers *et al.*, 2000; Cooper, 2008; Viefers, 2008). In this case an odd number of vortices are attached to each particle, i.e., the exponent m in Eq. (19) is odd. Interestingly, the boson wave function is constructed as a product of two antisymmetric fermionic wave functions. The composite fermion picture naturally predicts a close relation between the bosonic and fermionic states along the yrast line, discussed in the next section.

F. Mapping between fermions and bosons

In the Laughlin state, the difference in angular momentum between the boson and fermion states equals that of the maximum density droplet since, trivially,

$$\prod_{i<j}^{N} (z_i - z_j)^m = \prod_{i<j}^{N} (z_i - z_j) \prod_{i<j}^{N} (z_i - z_j)^{m-1}. \tag{20}$$

As long as the single-particle basis is restricted to the lowest Landau level, a similar transformation can be used to add a Pauli vortex to each bosonic particle, i.e., by multiplying the boson wave function with the determinant of the MDD,

$$\Psi_{\mathrm{fermion}} = \prod_{i<j}^{N} (z_i - z_j) \Psi_{\mathrm{boson}}. \tag{21}$$

This transformation is also valid, in addition to the Laughlin states, for the Jain construction. It is expected that the same mapping is a good approximation for any many-particle state in the lowest Landau level (Ruuska and Manninen, 2005).

The accuracy of the boson-fermion mapping has been studied in detail by computing the overlaps between the exact fermion wave function and the wave function obtained by transforming the exact boson state to a fermion state using Eq. (21) (Borgh *et al.*, 2008). At high angular momenta where the particles localize, the mapping becomes exact, while at small angular momenta the mapping is justified by the small number of possible con-

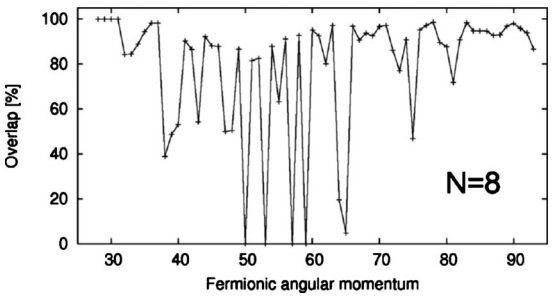

FIG. 5. Overlap between the fermion ground state and the transformed boson ground state as a function of the total angular momentum, for eight particles. From Borgh *et al.*, 2008.

figurations in the LLL. It is important to note that the free vortices of the bosonic system stay as free vortices also in the fermionic state. Only the Pauli vortices which localize at the particle positions are added. After transforming the bosons to fermions, particle-hole duality allows a detailed study of the vortex structure of the bosonic many-body wave function.

Figure 5 shows the calculated overlap between the transformed boson state and the exact fermion state as a function of the total angular momentum for eight particles. The transformation described by Eq. (21) does not always result in the ground state of the fermion system at given angular momentum. Instead, it may be one of the low-lying excitations and, consequently, the overlap drops to zero in these cases, as shown in Fig. 5. Moreover, the complexity of the wave function increases, while overlaps of the transformed wave function with the true fermion ground states tend to decrease with the number of particles N.

Figure 6 shows the effect of the mapping for a droplet with $N=20$ particles in a harmonic trap at angular momenta where three free vortices form. The radial density profile of the bosonic state shows a minimum at the expected radial distance. When the bosonic state is transformed to a fermionic one, its radial density expands and becomes nearly identical to the exact density of the corresponding fermion system. The mapping allows us to study the internal structure of the vortex lattice in the particle-hole duality picture: Fig. 6 also shows the particle-particle and vortex-vortex correlation functions, indicating similar localization of three vortices in both cases.

The simple mapping of Eq. (21) is computationally demanding when the particle number increases. This is due to the fact that every configuration of the boson wave function fragments to numerous fermion configurations. A simpler mapping was suggested by Toreblad *et al.* (2004) with a one-to-one correspondence between each boson and fermion configuration in the few-body limit. This mapping captures the most important configurations but could not give as good overlaps.

The above transformation [Eq. (21)] can be generalized to two-component quantum droplets. The transformation $L_{\text{boson}}=L_{\text{fermion}}-L_{\text{MDD}}$ would attach a Pauli vortex to each boson. It is apparent that fermion states with

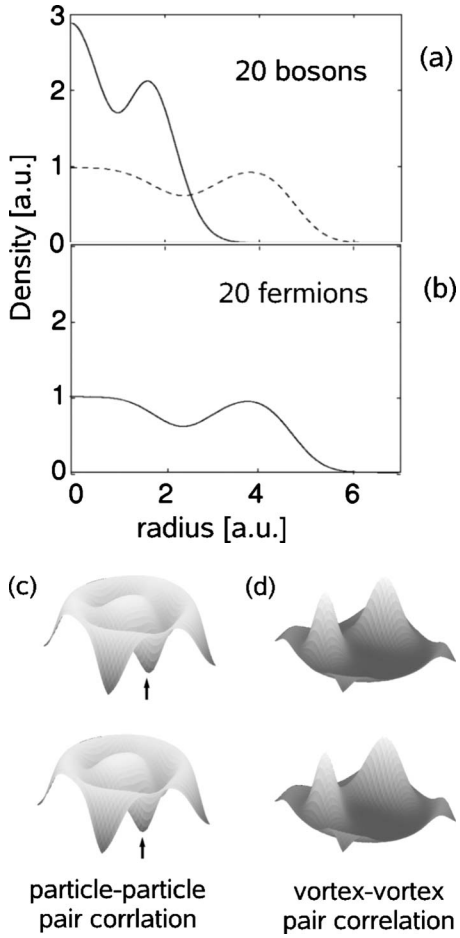

FIG. 6. Mapping between boson and fermion states. The upper panels show the particle density of 20 (a) bosons and (b) fermions with Coulomb interactions, in the region of three vortices as a function of the radial distance of the droplet center. For bosons, the density of the mapped fermion system is shown as a dashed line. The lower panels show in column (c) the particle-particle pair-correlations determined from the fermion wave functions. The position of the reference point is marked by the arrow at the bottom of the exchange-correlation hole. In column (d) the corresponding vortex-vortex pair correlations are shown.

$L_{\text{fermion}}<L_{\text{MDD}}$ cannot have bosonic counterparts in the LLL. Nevertheless, suggestive analogies in the (coreless) vortex structures between bosonic and fermionic states have been obtained in the few-particle limit (Koskinen *et al.*, 2007; Saarikoski *et al.*, 2009).

III. COMPUTATIONAL MANY-BODY METHODS

The complexity of the many-body wave function grows exponentially with the particle number N, which makes computational studies indispensable. We give here an overview of the central methods used in the computational approaches to physics of rotation in both bosonic and fermionic systems, and their applicability to small droplets. As it is often the case for approximate approaches, the methods presented have their limits of usability—no "universal" method exists which is supe-

rior to the others in capturing the essential physics in all parameter regimes.

The exact diagonalization or so-called configuration-interaction (CI) method does not introduce any approximations to the solution of the Schrödinger equation apart from a cutoff in the used basis set. Therefore it is ideally suited to analyze correlations in the system. This method is, however, limited to relatively small particle numbers. Mean-field and density-functional methods are often needed to complement data for larger systems. In the density-functional approach, correlation effects are usually incorporated using local functionals of the spin densities. The method is able to reveal some of the underlying correlations in the system, but local approximations may fail to describe properly the complex particle-vortex correlations and formation of particle-vortex composites (Saarikoski, Reimann, *et al.*, 2005). In the following, we draw upon the analogies between (a conventionally fermionic) density-functional theory and the Gross-Pitaevskii approach for bosons. We finally summarize the configuration-interaction method for the direct numerical diagonalization of the many-body Hamiltonian.

Rather generally, the ground-state energy of an interacting many-body system trapped by an external potential $V_{\rm ext}(\mathbf{r})$ can be written as a functional of the particle density $n(\mathbf{r})$, summing up the kinetic, potential, and interaction energy contributions,

$$E[n(\mathbf{r})] = T_0[n(\mathbf{r})] + \int d\mathbf{r} n(\mathbf{r}) V_{\rm ext}(\mathbf{r}) + \frac{1}{2}\int d\mathbf{r}\int d\mathbf{r}' n(\mathbf{r}) n(\mathbf{r}') V^{(2)}(\mathbf{r},\mathbf{r}') + E_{\rm xc}, \tag{22}$$

where $T_0[n(\mathbf{r})]$ is assumed to be the *noninteracting* kinetic-energy functional, the second term accounts for the trap potential, the third term is the Hartree term for a two-particle potential $V^{(2)}$, and the exchange-correlation energy $E_{\rm xc}$ is defined to include all other many-body effects.

Introducing a set of single-particle orbitals $\psi_i(\mathbf{r})$, the density may be expressed as

$$n(\mathbf{r}) = \sum_{i=0}^{\infty} f_i |\psi_i(\mathbf{r})|^2, \tag{23}$$

with occupancies $\Sigma_i f_i = N$, following either bosonic or fermionic statistics. One can then write the noninteracting kinetic-energy functional for the orbitals ψ_i in the form

$$T_0[n(\mathbf{r})] = \sum_i f_i \int d\mathbf{r} \psi_i^*(\mathbf{r}) \left(-\frac{\hbar^2\nabla^2}{2m}\right)\psi_i(\mathbf{r}). \tag{24}$$

The crux of the matter is that Eq. (24) not necessarily holds for the *exact* kinetic-energy functional $T[n(\mathbf{r})]$. In many cases there will be a substantial correlation part in the kinetic-energy functional that is not accounted for by the expressions above. In the spirit of density-functional theory,[2] the last term in Eq. (22), $E_{\rm xc}$, thus has the task to collect what was neglected by this assumption, together with the effects of exchange and correlation that originate from the difference between the true interaction energy and the simple Hartree term. It is important to note that the Hohenberg-Kohn theorem guarantees that this quantity is a functional of only the density, $E_{\rm xc} = E_{\rm xc}[n(\mathbf{r})]$.

A. The Gross-Pitaevskii approach for trapped bosons

1. Gross-Pitaevskii equation for simple condensates

In the case of bosons, for a simple condensate all bosons are in the lowest state $\psi_0(\mathbf{r})$ and the particle density is

$$n(\mathbf{r}) = |\psi_0(\mathbf{r})|^2 = N|\phi_0(\mathbf{r})|^2, \tag{25}$$

where the condensate wave function $\psi_0(\mathbf{r})$ is normalized to N, and the corresponding "order parameter" $\phi_0(\mathbf{r})$ to unity.

Using contact interactions and ignoring the correlations in Eq. (22) one obtains the well-known Gross-Pitaevskii energy functional,

$$E[n(\mathbf{r})] = \int d\mathbf{r}\left[-\frac{\hbar^2}{2m}|\nabla\psi_0(\mathbf{r})|^2 + V_{\rm ext}(\mathbf{r})|\psi_0(\mathbf{r})|^2 + \frac{1}{2}g|\psi_0(\mathbf{r})|^4\right]. \tag{26}$$

Finding the ground state usually amounts to a variational procedure, i.e., independent variations in ψ and ψ^* under the condition that the total number of particles in the trap is constant. For the variation with respect to ψ_0^*,

$$\frac{\delta}{\delta\psi_0^*(\mathbf{r})}[E[\psi_0,\psi_0^*] - \mu\int d\mathbf{r}|\psi_0(\mathbf{r})|^2] = 0, \tag{27}$$

where the chemical potential μ plays the role of a Lagrange multiplier to fulfill the constraint. We then arrive at the time-independent Gross-Pitaevskii equation

$$\left[-\frac{\hbar^2}{2m}\nabla^2 + V_{\rm ext}(\mathbf{r}) + g|\psi_0(\mathbf{r})|^2\right]\psi_0(\mathbf{r}) = \mu\psi_0(\mathbf{r}) \tag{28}$$

having the typical form of a self-consistent mean-field equation. The corresponding N-particle bosonic wave function is

$$\psi(\mathbf{r}_1,\mathbf{r}_2,\ldots,\mathbf{r}_N) = \prod_{i=1}^{N}\psi_0(\mathbf{r}_i). \tag{29}$$

The Gross-Pitaevskii approach, already derived in the 1960s independently by Gross (1961) and Pitaevskii (1961), has been applied extensively for the theoretical description of inhomogeneous and dilute Bose gases at

[2]See, for example, the book by Dreizler and Gross (1990) for an extensive discussion of these issues.

low temperatures.[3] It is often convenient to solve the Gross-Pitaevskii equations in the imaginary-time evolution method, using a fourth-order split-step scheme (Chin and Krotscheck, 2005).

2. Gross-Pitaevskii approach for multicomponent systems

The above Gross-Pitaevskii equation for a simple single-component Bose condensate Eq. (28) can also be straightforwardly generalized to multiple components of distinguishable species of particles. Consider as an example a two-component gas of atoms of types A and B that are interacting through the usual s-wave scattering with equal interaction strengths $g=g_{AA}=g_{BB}=g_{AB}$. The order parameters ψ_A and ψ_B of the two components then play an analogous role than the spin "up" and "down" orbitals in the spin-dependent Kohn-Sham formalism (see Sec. III.B). The corresponding Gross-Pitaevskii energy functional in the rest frame is

$$E = \sum_{\sigma=A,B} \int d\mathbf{r}\psi_\sigma^*\left(-\frac{\hbar^2\nabla^2}{2M} + V_{\text{ext}}(\mathbf{r})\right)\psi_\sigma + \frac{g}{2}\int d\mathbf{r}(|\psi_A|^4 + |\psi_B|^4 + 2|\psi_A|^2|\psi_B|^2), \tag{30}$$

where $\sigma=\{A,B\}$ plays the role of a pseudospin 1/2. In analogy to the single-component case described above, we minimize the energy functional with respect to ψ_A^* and ψ_B^*, which results in two coupled Gross-Pitaevskii equations:

$$\left(\frac{\mathbf{p}^2}{2M} + \frac{1}{2}M\omega^2\mathbf{r}^2 + g(|\psi_A|^2 + |\psi_B|^2)\right)\psi_A = \mu_A\psi_A,$$

$$\left(\frac{\mathbf{p}^2}{2M} + \frac{1}{2}M\omega^2\mathbf{r}^2 + g(|\psi_B|^2 + |\psi_A|^2)\right)\psi_B = \mu_B\psi_B.$$

Naturally, it is required that $N_A=\int d\mathbf{r}|\psi_A|^2$ and $N_B=\int d\mathbf{r}|\psi_B|^2$, which determines the chemical potentials μ_A and μ_B. One may choose to normalize the order parameter of one of the components, say, B, to unity. Then, N_A is determined by the ratio N_A/N_B. For the total angular momentum, $L=\int d\mathbf{r}(\psi_A^*\hat{L}_z\psi_A+\psi_B^*\hat{L}_z\psi_B)=L_A+L_B$. The above-mentioned imaginary-time evolution method is also in the multicomponent case the method of choice to numerically solve the Gross-Pitaevskii equations.

B. Density-functional approach

The density-functional theory for the solution of many-body problems in physics and chemistry was proposed by Hohenberg, Kohn, and Sham in the 1960s (Hohenberg and Kohn, 1964; Kohn and Sham, 1965). It is a correlated many-body theory where all the ground-state properties can in principle be calculated from the particle density (Hohenberg and Kohn, 1964; Parr and Yang, 1989; Dreizler and Gross, 1990; Kohn, 1999). The original density-functional theory did not take into account the effects of a nonzero spin polarization and currents induced by an external magnetic field. Since these effects have marked consequences on the ground-state properties of the rotating many-body systems, for a description of quantum dots in strong magnetic fields, extensions such as the spin-density-functional method (Gunnarsson and Lundqvist, 1976; von Barth, 1979) and the current-spin-density-functional method (Vignale and Rasolt, 1987, 1988; Rasolt and Perrot, 1992; Capelle and Gross, 1997) were applied. For a pedagogic review on density-functional theory, see Capelle (2006).

1. Spin-density-functional theory for electrons

In the spin-density-functional formalism one can derive self-consistent Kohn-Sham equations for the Hamiltonian (6) that describes N interacting electrons in an external magnetic field:

$$\nabla^2 V_H = -n/\epsilon, \tag{31}$$

$$n_\sigma(\mathbf{r}) = \sum_i^{N_\sigma} |\psi_{i,\sigma}(\mathbf{r})|^2, \tag{32}$$

$$\left\{\frac{1}{2m^*}[\mathbf{p} + e\mathbf{A}(\mathbf{r})]^2 + V_{\text{eff},\sigma}(\mathbf{r})\right\}\psi_{i,\sigma} = \epsilon_{i,\sigma}\psi_{i,\sigma}. \tag{33}$$

Equation (31) is the Poisson equation for the solution of the Hartree potential V_H, i.e., the Coulomb potential for the electronic charge density n, where ϵ is the dielectric constant of the medium. Equation (32) determines the spin densities, where $\sigma=\{\uparrow,\downarrow\}$ is the spin index, N_σ is the number of electrons with spin σ, $\psi_{i,\sigma}$'s are the one-particle wave functions, and the summation is over the N_σ lowest states (which here have fermionic occupancy). In Eq. (33), the *effective* scalar potential for electrons

$$V_{\text{eff},\sigma}(\mathbf{r}) = V_{\text{ext}}(\mathbf{r}) + V_H(\mathbf{r}) + V_{\text{xc},\sigma}(\mathbf{r}) + V_Z \tag{34}$$

consists of the external scalar potential V_{ext}, the Hartree potential V_H, the exchange-correlation potential V_{xc}, and the Zeeman term $V_Z=g^*\mu_B B s_\sigma$, where μ_B is the Bohr magneton, $s_\sigma=\pm 1/2$, B is the magnetic field, and g^* is the gyromagnetic ratio. All interaction effects beyond the Hartree potential V_H are incorporated in the exchange-correlation potential V_{xc}. A more fundamental generalization of the density-functional method for systems in external magnetic fields is the current-density-functional method (Vignale and Rasolt, 1987, 1988), where the vector potential $\mathbf{A}$ is replaced by an effective vector potential $\mathbf{A}_{\text{eff}}=\mathbf{A}+\mathbf{A}_{\text{xc}}$ accounting for many-particle effects on the current densities. In the above equations, only the conduction electrons of the semiconductor are explicitly included in the theory, while effects of the lattice are incorporated via material parameters such as effective mass, dielectric constant, and effective g factor.

Density-functional approaches are often combined with local approximations for the exchange-correlation

[3]For a more detailed discussion, see, for example, Pethick and Smith (2002) and Pitaevskii and Stringari (2003).

potential where V_{xc} in actual calculations is usually taken as the exchange-correlation potential of the uniform electron gas. In 2D electron systems, approximate parametrizations have been calculated (Tanatar and Ceperley, 1989; Attaccalite *et al.*, 2002) and the approach leads to a set of mean-field-type equations. It should be emphasized that density-functional theory *a priori* is not a mean-field method but a true many-particle theory. Its strength is that it often may provide accurate approximations to the ground-state properties such as the total energy with the computational effort of a mean-field method. It is important to note that single-particle states (Kohn-Sham orbitals) and their eigenenergies are auxiliary parameters in the Kohn-Sham equations. However, as an approximation, the Kohn-Sham orbitals may still be used to construct a single Slater determinant to account for the nodal structure.

The density-functional approach in the local density approximation, as well as the unrestricted Hartree-Fock method, may show broken symmetries in particle and current densities. This is often interpreted as reflections of the internal structure of the exact many-body wave function.[4] However, a caveat is that implications of symmetry-breaking patterns may in some cases yield wrong implications of the actual many-body structure of the exact wave function. This problem is well known in quantum chemistry as "spin contamination," and we refer the interested reader to Szabo and Ostlund (1996) as well as Harju *et al.* (2004), Borgh *et al.* (2005), and Schmidt *et al.* (2008) for a thorough discussion. This conceptual problem of spin-density-functional theory often calls for an analysis by more exact computational methods.

2. Density-functional theory for bosons

The Gross-Pitaevskii mean-field approach discussed above is the most widely used theoretical tool to describe Bose-Einstein condensates and has been extensively applied to investigate vortex structures in rotating systems. Clearly, it is a density-functional method based on the functional Eq. (27) where the density is a square of a single one-particle state Eq. (25). However, there are many situations where correlations determine the many-body states that cannot be captured by the standard Gross-Pitaevskii approach (Bloch *et al.*, 2008).

The exact diagonalization method, which captures all correlation effects, cannot be used for systems which consist of more than just a few particles. A bosonic density-functional theory has been introduced as one possible way to go beyond the mean-field approximation (Griffin, 1995; Braaten and Nieto, 1997; Nunes, 1999; Kim and Zubarev, 2003; Hunter, 2004; Rajagopal, 2007; Capelle, 2008). For ground states this approach is not efficient due to a lack of nodal structure in the wave function. This, however, is different in the case of fragmented or depleted condensates (Mueller *et al.*, 2006; Capelle, 2008).

Following the well-known Hohenberg-Kohn theorem, the energy functional $E[n(\mathbf{r})]$ is minimized by the ground-state density. This in fact is independent of whether the particles are bosons or fermions, and a corresponding density-functional approach to bosonic systems was recently formulated by Capelle (2008). Taking the E_{xc} contributions into account, the variation of Eq. (22) adds the potential (Nunes, 1999)

$$V_{xc} = \frac{1}{\psi(\mathbf{r})} \frac{\delta E_{xc}}{\delta \psi(\mathbf{r})}. \tag{35}$$

However, $\psi(\mathbf{r})$ cannot describe correctly the many-body state if the ground state contains "uncondensed" bosons or requires a macroscopic occupation of more than one single-particle state. Capelle (2008) showed that since the Hohenberg-Kohn theorem still holds in these cases, the Gross-Pitaevskii equation [Eq. (28)] can be more generally expressed as

$$\left[-\frac{\hbar^2}{2m}\nabla^2 + V_{ext}(\mathbf{r}) + \int d\mathbf{r} n(\mathbf{r}) n(\mathbf{r}') V^{(2)}(\mathbf{r}-\mathbf{r}') + \frac{\delta E_{xc}[n]}{\delta n(\mathbf{r})} \right] \psi_i(\mathbf{r}) = \epsilon_i(\mathbf{r}) \psi_i(\mathbf{r}), \tag{36}$$

with the label i now running over all solutions of the equation. The orbitals ψ_i do not have a simple relation to the Gross-Pitaevskii order parameter, but they do provide the correct density via Eq. (23) with (bosonic) occupancies f_i of the states ψ_i. These equations took a form that is indeed familiar from the usual Kohn-Sham equations for fermions discussed above (Capelle, 2008). For an account of viable approximations to E_{xc}, see Capelle (2008), as well as Nunes (1999) and Kim and Zubarev (2003).

C. Exact diagonalization method

The CI method, also called "exact diagonalization," is a systematic scheme to expand the many-particle wave function. It traces back to the early days of quantum mechanics, to the work of Hylleraas (1928) on the helium atom. It has been extensively used in quantum chemistry but nowadays found its use also for quantum nanostructures as well as cold atom systems. In the basic formulation of this approach, one takes the eigenstates of the noninteracting many-body problem (called configuration) as a basis and evaluates the interaction matrix elements between these states. The resulting Hamiltonian matrix is then diagonalized.

Rules to calculate the matrix elements were originally derived by Slater (1929, 1931) and Condon (1930) and developed further by Löwdin (1955). We note that the use of the term exact diagonalization that has been widely adopted by the community, often replacing the quantum-chemistry terminology of "configuration inter-

[4]For a comprehensive discussion of this issue in the context of quantum dots, see Reimann and Manninen (2002).

action," might in some cases be misleading, as truly exact results are obtained only in the limit of an infinite basis.

Consider a Hamiltonian operator split into two parts $H=H_0+H_I$, where the Schrödinger equation of the first part is solvable,

$$H_0|\phi_i\rangle = \varepsilon_i|\phi_i\rangle, \tag{37}$$

and the states $|\phi_i\rangle$ form an orthonormal basis. The solution for the full Schrödinger equation can be expanded in this basis as $|\psi\rangle=\Sigma_i\alpha_i|\phi_i\rangle$. Inserting this into the Schrödinger equation

$$H|\psi\rangle = E|\psi\rangle, \tag{38}$$

results in

$$(H_0 + H_I)\sum_i \alpha_i|\phi_i\rangle = E\sum_i \alpha_i|\phi_i\rangle \tag{39}$$

or a matrix equation

$$(H_0 + H_I)\boldsymbol{\alpha} = E\boldsymbol{\alpha}, \tag{40}$$

where $\mathcal{H}_0$ is a diagonal matrix with $\langle\phi_i|H_0|\phi_i\rangle=\varepsilon_i$ and the elements of H_I are $\langle\phi_j|H_I|\phi_i\rangle$. The vector $\boldsymbol{\alpha}$ contains the values α_i. In principle, the basis $\{|\phi_i\rangle\}$ is infinite, but the actual numerical calculations must be done in a finite basis. The main computational task is to calculate the matrix elements of H_I and to diagonalize the corresponding matrix. The convergence as a function of the size of the basis set depends on the problem at hand and is of course fastest for the cases where H_I is only a small perturbation to H_0.

The basic procedure is straightforward textbook knowledge of quantum mechanics. However, one should bear in mind that much of the state-of-the-art computational knowledge must be employed when it comes to numerical implementations, in order to model large and highly correlated systems.

The usual starting point for the exact diagonalization method is the noninteracting problem. In 2D harmonic potentials, harmonic oscillator states or Fock-Darwin states of noninteracting particles in a magnetic field—can be used to construct a suitable basis, but it can also be optimized using states from, e.g., Hartree-Fock or density-functional methods [for a recent example, see Emperador *et al.* (2005)]. For fermions, the solution is a Slater determinant formed from the eigenstates of the single-particle Hamiltonian. The corresponding symmetric N-boson state is a permanent. In the noninteracting ground state, all bosons occupy the same state. On the other hand, fermions occupy the N lowest states due to the Pauli principle. Due to interactions, other configurations than the one of the noninteracting ground state have a finite weight in the expansion of the many-particle wave function. Often, the increasing complexity of the quantum states with large interaction strengths and large system sizes causes severe convergence problems, where the number of basis states needed for an accurate description of the many-body system increases far beyond computational reach.

In rotating weakly interacting systems confined by harmonic potentials, a natural restriction of the single-particle basis is the LLL. It provides a well-defined truncation of the Hilbert space for the given value of the angular momentum L and particle number N. The LLL approximation in the harmonic confinement implies that the diagonal part of the Hamiltonian is independent of the configuration, and solving the Hamiltonian reduces to the diagonalization of the potential energy of the interparticle interactions. This truncation also eliminates the usual issue of regularization that emerges with the use of contact forces in exact diagonalization schemes, see, for example, Huang (1963): the direct diagonalization of the Hamiltonian with contact interactions on a *complete* space yields unphysical solutions unless the class of allowed basis functions obeys special and often impractical boundary conditions (Esry and Greene, 1999). The Hamiltonian matrix in the LLL is often sparse, and in the limit of large N and L it is usually diagonalized in a Lanczos scheme (Lehoucq *et al.*, 1997).

IV. SINGLE-COMPONENT QUANTUM DROPLETS

In the following, we describe the structure of single-vortex states and the formation of vortex "clusters" or vortex "molecules," as they are also often called, in single-component systems. In the strongly correlated regime of rapid rotation, the increased vortex density leads to finite-size counterparts of fractional quantum Hall states, with both bosons and fermions. The existence of giant or multiple-quantized vortices in anharmonic traps is also discussed.

A. Vortex formation at moderate angular momenta

1. Vortex formation in trapped bosonic systems

Following the achievement of Bose-Einstein condensation in trapped cold atom gases, experimental setups were devised to study their rotational behavior. The first observation of vortex patterns in these systems was made for a two-component Bose condensate consisting of two internal spin states of ^{87}Rb, where the formation of a single vortex was detected (Matthews *et al.*, 1999). Soon after this seminal experiment, evidence for the occurrence of vortices was found by literally "stirring" a one-component gaseous condensate of rubidium by a laser beam (Madison *et al.*, 2000). While the vortex cores are too small to be directly observed optically (the core radius is typically from 200 to 400 nm), vortex imaging is possible if the atomic cloud first is allowed to expand by turning off the trap potential (Madison *et al.*, 2000). In this way, regular patterns of vortices were observed in the transverse absorption images of the rubidium condensate (see Fig. 7). At moderate rotation, above a certain critical frequency Ω_c, first a central "hole" occurred, clearly identified as a pronounced minimum in the cross section of the density distribution, shown to the right in Fig. 7(b).

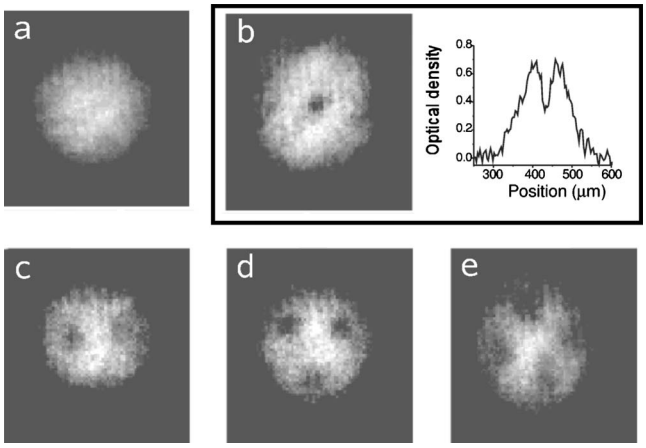

FIG. 7. Transverse absorption images of a Bose-Einstein condensate of ^{87}Rb, stirred with a laser beam. As the rotation of the trap increases from (a) to (e), a clear vortex pattern evolves. The inset to the right of (b) shows the cross section of the optical density which shows a pronounced minimum at the center. After Madison *et al.*, 2000.

As the rotation of the trap increases, the second, third, and fourth vortices penetrate the bosonic cloud. The vortices then arrange in regular geometric patterns. Intriguingly, these patterns coincide with the geometries of Wigner crystals of repulsive *particles*, as they have been found, for example, in quantum dots at low electron densities or strong magnetic fields (Reimann and Manninen, 2002). Vortices with the same sign of the vorticity effectively repel each other [see, for example, Castin and Dum (1999)]. This supports the view of Wigner-crystal-like arrangement of vortices, throwing light on the much debated melting of the vortex lattice at extreme rotation (see also Sec. IV.D). The interplay between vortex and particle localization in a rotating harmonic trap is discussed further in Sec. IV.B.

The theory of vortices in rotating BECs has attracted much attention in recent years, and much work has been published for the Thomas-Fermi regime of strong interactions; see, for example, Rokhsar (1997), Feder *et al.* (1999a, 1999b), García-Ripoll and Pérez-García (1999), and Svidzinsky and Fetter (2000). In this limit, which applies to most experiments on rotating BECs, the coherence length $\xi=(8\pi na)^{1/2}$, where n is the density and a is the scattering length, is much smaller than the extension of the bosonic cloud, and some properties of the system resemble those of a bulk superfluid (Baym and Pethick, 1996). In the case of weakly interacting bosons in a harmonic trap, however, the coherence length becomes larger than the size of the cloud, and the interaction energy plays the dominant role: the mesoscopic limit is reached, where the system becomes like a quantum-mechanical Knudsen gas (Mottelson, 2001). In this mesoscopic limit, the analogies between trapped bosons and quantum dots at strong magnetic fields become apparent. This regime of weak interactions is our primary concern in the following.

2. Weakly interacting bosons under rotation

We now consider a dilute system of N spinless bosons in a harmonic trap, weakly interacting by the usual contact force $g\delta(\mathbf{r}-\mathbf{r}_0)$, where $g=4\pi\hbar^2a/M$ is the strength of the effective two-body interaction with scattering length a and atom mass M. The condition for weak interactions is that the interaction energy is much smaller than the quantum energy of the confining potential, i.e.,

$$ng \ll \hbar\omega, \tag{41}$$

where n is the particle density. As explained in Sec. II.A.1, requiring maximum alignment of the total angular momentum, the relevant single-particle states of the oscillator are those of the LLL. This approach, which has earlier proven successful for the description of the fractional quantum Hall regime for the electron gas, was introduced for bosonic systems by Wilkin *et al.* (1998). As mentioned in Sec. II.A.1, the large degeneracy originating from the many different ways to distribute the N bosons on the single-particle states of the LLL is lifted by the interactions.

Identifying the elementary modes of excitation, Mottelson (1999) showed that besides the usual condensation into the lowest state of the oscillator, the yrast states (i.e., the states maximizing L at a given energy, see Sec. II.A.1) involve additional kinds of condensations that are associated with the many different possibilities for distributing the angular momentum on the degenerate set of basis states in the LLL. For $1\ll L\ll N$, the yrast states and low-energy excitations as a function of L can be constructed by a collective operator

$$Q_\lambda = \frac{1}{\sqrt{2N\lambda!}}\sum_{p=1}^{N} z_p^\lambda, \tag{42}$$

with coordinates of the pth particle $z_p=x_p+iy_p$.

In the case of attractive interactions, the lowest-energy state for fixed angular momentum is the one involving excitations of the center of mass of the cloud. The yrast state is then described by $|\Psi_L\rangle\sim(Q_1)^L|\Psi_{L=0}\rangle$ (Wilkin *et al.*, 1998; Mottelson, 1999).

In the case of repulsive interactions, for bosons in the LLL at $L=0$ the only possible state is the pure condensate in the $m=0$ single-particle orbital, thus maximizing the interaction energy. Increasing the angular momentum by one is possible via a center-of-mass excitation of the nonrotating state. For $L>1$ and $L\ll N$, the excitation energies of the modes $Q_{\lambda\neq1}$ show that the yrast states are predominantly obtained by a condensation into the quadrupole ($\lambda=2$) and octupole ($\lambda=3$) modes, as shown by Mottelson (1999).

Bertsch and Papenbrock (1999) compared these results to a numerical computation of the yrast line. For the harmonic trap in the lowest Landau level, the problem can be solved straightforwardly by numerical diagonalization of the Hamiltonian (3); see the discussion in Sec. III.C. The resulting interaction energy decreases with increasing L for repulsive interactions since centrifugal forces tend to keep the particles further apart

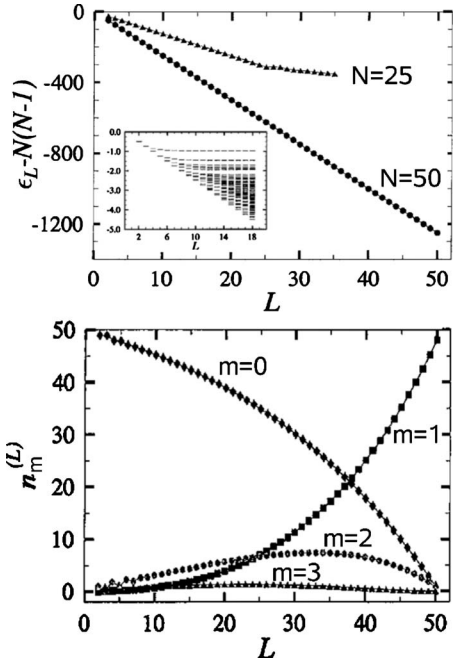

FIG. 8. Yrast lines and occupancies. Upper panel: Many-body yrast lines for $N=25$ and 50 spinless bosons in a harmonic confinement for angular momenta $2 \leqslant L \leqslant 50$. The inset shows the excitation spectrum for $N=50$ and $L \leqslant 18$, excluding the spurious center-of-mass excitations, see text. From Papenbrock and Bertsch, 2001. Lower panel: Occupancies of the lowest single-particle states of the harmonic oscillator in the lowest Landau level, for $m=0$ (diamonds), $m=1$ (squares), $m=2$ (circles), and $m=3$ (triangles). Calculations are within the lowest Landau level. After Bertsch and Papenbrock, 1999.

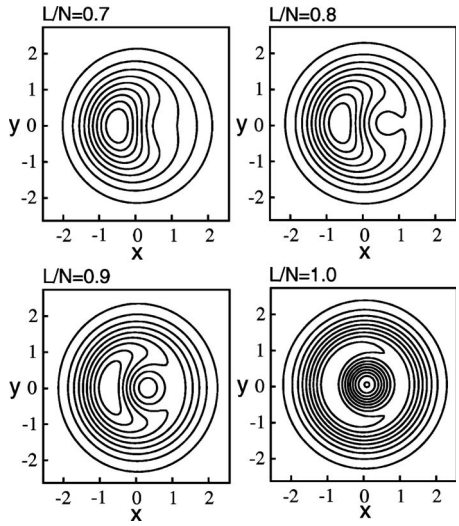

FIG. 9. Equidensity lines of the pair-correlation function $P(\mathbf{r},\mathbf{r}_A)$ for $N=40$ spinless bosons at $L=28$, 32, 36, and 40. For clarity, the reference point was located outside the cloud at $\mathbf{r}_A=(3,0)$. The vortex, which approaches the center from the right with increasing L, gives rise to a pronounced minimum in the pair-correlation plots. From Kavoulakis *et al.*, 2002.

when rotation increases (see Fig. 8 for $N=25$ and 50 bosons). It shows a linear decrease in energy with L, that extends up to $L=N$. This linearity was also found in a study within the Gross-Pitaevskii approach by Kavoulakis *et al.* (2000). The inset to Fig. 8 shows the excitation spectra for $N=50$ bosons at angular momenta $L \leqslant 18$. "Spurious" eigenstates occur that originate from an SO(2,1) symmetry (Pitaevskii and Rosch, 1997) only exciting the center of mass, i.e., the yrast spectrum at $L+1$ includes the full set of states at angular momentum L. (These center-of-mass excitations were excluded in the spectra shown in Fig. 8.) With harmonic confinement the center-of-mass excitations are exactly separated from the internal excitations and they are known to also exist in Fermi systems (Trugman and Kivelson, 1985; Reimann and Manninen, 2002).

The lower panel in Fig. 8 shows the occupancies of the lowest single-particle states for a $N=50$ bosonic state with angular momentum up to $L=N$. In agreement with the aforementioned results of Mottelson (1999), at small L/N the yrast states are mainly built from single-particle states with $m=0$, with small contribution from $m=2$ and $m=3$, where m is the angular momentum of the single-particle state (Bertsch and Papenbrock, 1999). Approaching $L/N=1$, the yrast state takes a much simpler structure, with a dominant occupancy of the $m=1$ single-particle orbital. At $L/N=1$, a single vortex locates at the center of the cloud.

An analytic expression for the exact energies for $2 \leqslant L \leqslant N$ was conjectured by Bertsch and Papenbrock (1999) and subsequently derived by Jackson and Kavoulakis (2000); in atomic units it reads

$$\epsilon_L = \tfrac{1}{2}N(2N - L - 2). \tag{43}$$

Smith and Wilkin (2000) derived analytically the exact eigenstate as an elementary symmetric polynomial of coordinates relative to the center of mass. Later, exact yrast energies for a universality class of interactions were derived (Hussein and Vorov, 2002; Vorov *et al.*, 2003). Generalizing a conjecture by Wilkin *et al.* (1998) for the structure of the unit vortex at $L=N$,

$$|L=N\rangle = \prod_{p=1}^{N} (z_p - z_c)|0\rangle, \tag{44}$$

where $z_c=(z_1+z_2+\cdots+z_N)/N$ is the center-of-mass coordinate, Bertsch and Papenbrock (1999) demonstrated that the exact wave function in the *whole* region $2 \leqslant L \leqslant N$ is given by

$$|L\rangle = \mathcal{N} \sum_{p_1<p_2<\cdots<p_L} (z_{p_1} - z_c) \times (z_{p_2} - z_c) \cdots (z_{p_L} - z_c) \times |0\rangle, \tag{45}$$

where $\mathcal{N}$ is a normalization constant, and the indices run over all particle coordinates, up to the total particle number N.

We now investigate the evolution of the pair-correlated densities, defined in Sec. II.C.3. Figure 9 shows their contours, for $N=40$ bosons with the reference point located at a distance $r_A=3\ell_0$ (chosen outside

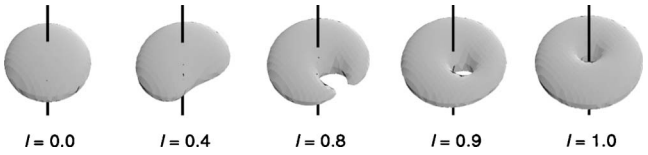

FIG. 10. Vortex entry for a spherical bosonic cloud at angular momenta $l=L/N$. The surfaces of constant density obtained by the Gross-Pitaevskii method are shown. The cloud flattens with increasing angular momentum. From Butts and Rokhsar, 1999.

the bosonic cloud for clarity; ℓ_0 is the oscillator length). Starting from a homogeneous Gaussian density distribution at $L=0$, as L/N increases, the first vortex enters the cloud from its outer parts. At $L=N$, the (azimuthally symmetric) particle density has developed a pronounced central hole that is also apparent from the correlation function shown in the lower right panel of Fig. 9. The nodal pattern of this state, as probed by conditional wave functions, confirms the simple structure of the unit vortex (see the $L=N=5$ state in Fig. 31). For a discussion of the low-energy excitations at and around the unit vortex, see Ueda and Nakajima (2006).

Recently Dagnino, Barberán, and Lewenstein (2009) and Dagnino *et al.* (2009) studied the vortex nucleation process by calculating the density matrix obtained from the CI eigenstates for a trap with a small quadrupole deformation. A related early study was presented by Linn *et al.* (2001), who applied a variational method to investigate the ground-state phase diagram in an axially asymmetric BEC. The analysis by Dagnino, Barberán, and Lewenstein (2009) and Dagnino *et al.* (2009) indicated that when the rotation frequency of the axially deformed trap is increased and the system passes through the first vortex transition, two of the "natural orbitals" of the density matrix have equal weight. Nunnenkamp *et al.* (2009) also studied the noise correlations at criticality for the elliptic trap, while Parke *et al.* (2008) related the transition to vortex tunneling in the process of nucleation.

In light of the above-mentioned findings, however, it is worth noting that the overall picture strongly depends on the symmetry of the chosen trap deformation and is further complicated by finite-size effects—the latter being an inevitable restriction in the CI method that becomes more severe, when the angular momentum no longer commutes with the Hamiltonian.

In the Gross-Pitaevskii approach, the vortices are directly visible in the density as well as the phase of the order parameter, which breaks the rotational symmetry. Butts and Rokhsar (1999) and Kavoulakis *et al.* (2000) were among the first to apply this method to a weakly interacting dilute condensate of bosonic atoms in a rotating harmonic trap. Figure 10 shows the equidensity surfaces for the Gross-Pitaevskii order parameter $\Psi(\mathbf{r})$ for the states along the yrast line between $L=0$ and N (Butts and Rokhsar, 1999), demonstrating how the first vortex enters the cloud. In the nonrotating case, the condensate forms a lump with zero angular momentum at the center of the trap. Beyond a certain critical rotation, however, the ground state becomes a vortex state with one single-quantized vortex that manifests itself as a central hole in the density (see $l=1.0$ in Fig. 10). The phase of the order parameter changes by 2π when encircling this hole (see Fig. 15, upper panel, left). The value of the critical rotation frequency depends on the system parameters, but the angular momentum per particle $l=L/N$ equals unity when the vortex reaches the center. This result is also confirmed by the exact diagonalization calculations in the few-particle regime [see Fig. 12(a)]. The same mechanism of vortex entry was also found in the Gross-Pitaevskii study by Kavoulakis *et al.* (2000). In the limit of large N, Jackson *et al.* (2001) compared the energies obtained in the Gross-Pitaevskii approach to those obtained by the CI method, and found that the mean-field results provided the correct leading-order approximation to the exact energies within the same subspace. For a discussion of the mean-field theory of single-vortex formation in bosonic condensates, see Fetter (2009).

3. Single-vortex states in electron droplets

Two-dimensional electron droplets in quantum dots can be rotated by applying a perpendicular magnetic field. The number of confined electrons and the rotation frequency can be controlled by an external gate voltage and the field strength, respectively.

In symmetric quantum dot devices the confining potential can often be modeled accurately by a 2D harmonic potential (Bruce and Maksym, 2000; Matagne *et al.*, 2002; Nishi *et al.*, 2006). These systems would therefore be ideal testbeds for analysis of vorticity in rotating fermionic systems with repulsive interactions. However, direct experimental detection of signatures of vortex formation in the electron density is difficult due to small charge densities inside the electron droplet that is often buried in a semiconductor heterostructure. Attempts to extract any signatures of vortex formation have usually focused on the analysis of quantum transport measurements (Güçlü *et al.*, 2005; Saarikoski and Harju, 2005).

In weak magnetic fields, electron droplets in quantum dots are composed of electrons which have their spin either parallel or antiparallel to the magnetic field. As the strength of the magnetic field increases, the system gradually spin-polarizes. For details on this process and electronic structure of quantum dots in this regime, see Kouwenhoven *et al.* (2001) and Reimann and Manninen (2002). The first totally spin-polarized state in the LLL is the maximum density droplet (MDD) state (MacDonald *et al.*, 1993) discussed in Sec. II.E.1. The existence of this state was firmly established experimentally (Oosterkamp *et al.*, 1999) using quantum transport measurements. When the angular momentum is further increased with the magnetic field, the MDD state reconstructs, and a vortex may form inside the electron droplet.

The breakdown mechanism of the MDD and its interpretation has been one of the most discussed subjects in the early theoretical studies of quantum dots. Many of

these works were inspired by the theory of excitations of the quantum Hall states. MacDonald *et al.* (1993) and Chamon and Wen (1994) discussed the possibility of edge excitations in large quantum Hall systems. Their studies suggested that the MDD would break up via reconstruction of the MDD edge. This possibility was examined further by Goldmann and Renn (1999) using a set of trial wave functions which described a MDD state surrounded by a ring of localized electrons. In large quantum dots, density-functional studies indicated a charge-density-wave (CDW) solution along the edge of the dot (Reimann *et al.*, 1999) around a rigid MDD-like dot center. These studies showed that for larger dot sizes, a rotating single-component fermion liquid would not develop vortex states but instead the edge of the system would be excited around a rigid MDD-like center. However, Hartree-Fock calculations for small electron droplets predicted that holes are created inside the droplet that would bunch to minimize the exchange energy (Ashoori, 1996). Yang and MacDonald (2002) used the exact diagonalization approach and also found the MDD state unstable toward creation of internal holes in high magnetic fields. A Skyrmion type of excitation above the MDD state was considered by Oaknin *et al.* (1996). This study generalized the theory of Skyrmion type of excitations in the 2D electron gas (2DEG) (Ezawa, 2000) to finite-size quantum Hall droplets, which was motivated by localization of Skyrmions in a Zeeman field. They proposed a wave function whose form for large particle numbers is that of a mean-field type of Skyrmion excitation. Heinonen *et al.* (1999) found also edge spin textures in an ensemble density-functional approach. A Skyrmion-type spin texture can be treated as another manifestation of vorticity, as pointed out in the context of two-component bosonic condensates (see Sec. V). For quantum dots with four and six electrons, a recent study within the CI method showed that meron excitations are dominant for the lowest-lying states in very small quantum dots at strong magnetic fields (in the limit of vanishing Zeeman coupling), see Petković and Milovanović (2007).

Holes in the charge density were identified as vortex cores in the density-functional studies of quantum dots (Saarikoski *et al.*, 2004); see Fig. 11. This work also directly showed with the configuration-interaction method that for the $N=6$ case the nodal structure of the many-body wave function revealed an isolated vortex at the center of the dot.

These results suggested that the first magnetic flux quantum, which penetrates the electron droplet, is a free vortex and not bound to any particle as in the Laughlin wave function. Configuration-interaction calculations for few-electron quantum dots provided further evidence for vortex formation in few-electron systems (Tavernier *et al.*, 2004; Toreblad *et al.*, 2004; Manninen *et al.*, 2005). In the few-electron regime, the unit vortex can be localized at the center of the electron droplet, just as in the bosonic case discussed above. In this respect the vortex in few-electron droplets is a localized holelike quasiparticle (Saarikoski *et al.*, 2004; Manninen *et al.*, 2005).

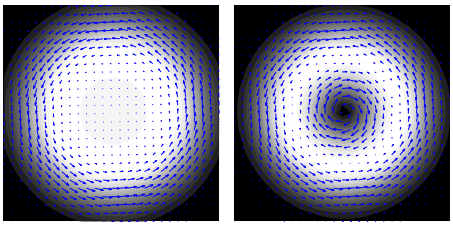

FIG. 11. (Color online) Charge and current densitites. (a) Charge density (grayscale) and current density (arrows) in the maximum density droplet state of a six-electron droplet at magnetic field $B=9$ T calculated with the density-functional method. The angular momentum is $L=15$, and the density inside the droplet is uniform. The solution also shows an edge current reminiscent of those in quantum Hall states. (b) The single-vortex state in the same droplet at slightly increased magnetic field of $B=11$ T with $L=21$. It shows a pronounced vortex hole in the middle with a rotating current around it. Adapted from Saarikoski *et al.*, 2004.

However, in the full quantum-mechanical picture the vortex position in the electron droplet is always subject to fluctuations as shown by the above diagonalization studies.

For bosonic systems, Bertsch and Papenbrock (1999) suggested an ansatz [see Eq. (45)] to describe a single-quantized vortex at the center of the droplet at $L/N=1$. Following Manninen, Viefers, *et al.* (2001) a similar approximation for the corresponding single-vortex state in fermionic droplets can be defined with $L=L_{\mathrm{MDD}}+N$,

$$\Psi_{1v}=\prod_{i=1}^{N}(z_i-z_c)|\mathrm{MDD}\rangle, \tag{46}$$

where z_c is the center-of-mass coordinate, as defined above. When the number of electrons is large, the center of mass is, with a high accuracy, at the center of the trapping potential, and we can approximate $z_c=0$ and $\Psi_{1v}=\Pi z_i|\mathrm{MDD}\rangle=|0111\cdots111000\cdots\rangle$ (for arbitrary N). For a single-vortex state where the hole is not located at the center, the wave function would be composed of single determinants such as $|11011\cdots11000\cdots\rangle$, where the position of the hole determines the average radius where the vortex is most likely to be found. The particle density has a minimum at the distance where the amplitude of the empty single-particle state has a maximum. However, even in the LLL approximation the true many-body state is a mixture of all other determinants in the LLL subspace, and the exact vortex position is then subject to fluctuations. This effect can be captured by different trial wave functions. Oaknin *et al.* (1995) constructed a nearly exact wave function for the single-vortex state. Jeon *et al.* (2005) described the vortices in the composite fermion approach formulated for the hole states. This issue is discussed further in Sec. IV.C which addresses vortex localization and fluctuations.

In a bosonic system, the yrast line has a pronounced cusp at angular momentum $L=N$ (see Fig. 14), corresponding to a state with a single-quantized vortex at the

center of the trap. In a fermion system, however, the first cusp of the yrast line is not necessarily a central vortex state. Yang and MacDonald (2002) showed that a (vortex) hole is created at the center of the dot for low electron numbers. When $N>13$ the hole locates at a finite distance from the center. In circularly symmetric systems, such a delocalized node would not be associated with the usual rotating charge current around a localized vortex core. A qualitatively similar regime of $N<13$ for the central vortex was obtained within a spin-density-functional analysis (Saarikoski and Harju, 2005). Calculations using the "rotating electron molecule" model reported a lower limit, $N<7$ (Li *et al.*, 2006). In the exact diagonalization studies in the LLL (Harju, 2005) the ground-state angular momenta for the first cusp state beyond the MDD state shows a marked change in the N dependence above $N=12$ [Fig. 12(b)]. For $N<12$ the node of the first cusp state is at the center of the electron droplet as indicated by its angular momentum $L=L_{\mathrm{MDD}}+N$. These solutions can be readily identified as vortex states. However, for $N\geqslant 12$ the angular momentum increase is almost independent of N, which is an indication that the node cannot reach the center but stays delocalized close to the edge, as shown in Fig. 13. This solution can also be interpreted as an edge excitation which helps to understand why different models and methods yield seemingly contradictory results for the MDD reconstruction, as discussed above.

The intermediate angular momentum states between the MDD and the $\Delta L=N$ central vortex states show a node in the wave function at a finite distance from the center (Oaknin *et al.*, 1995; Saarikoski, Harju, *et al.*, 2005) that can be interpreted as a delocalized vortex, i.e., a vortex approaching the center from the droplet surface as in the case of Figs. 9 and 10 for bosons. Note that these delocalized vortex states can be interpreted as center-of-mass excitations, as explained in connection with Eq. (17).

For larger electron numbers it is energetically more favorable to generate two (or even more) vortices already at $L/N=1$. In other words, the wave function shows two or more delocalized nodes at a finite distance from the center at $L/N=1$. This is contrary to Bose systems, where the central vortex state is the lowest-energy state at $L/N=1$ for any particle number [see Figs. 12(a) and 12(b)]. Apart from this fact, vortices in both fermionic and bosonic systems are manifest in the nodal structure of the wave function in a rather similar manner (Toreblad *et al.*, 2004; Borgh *et al.*, 2008).

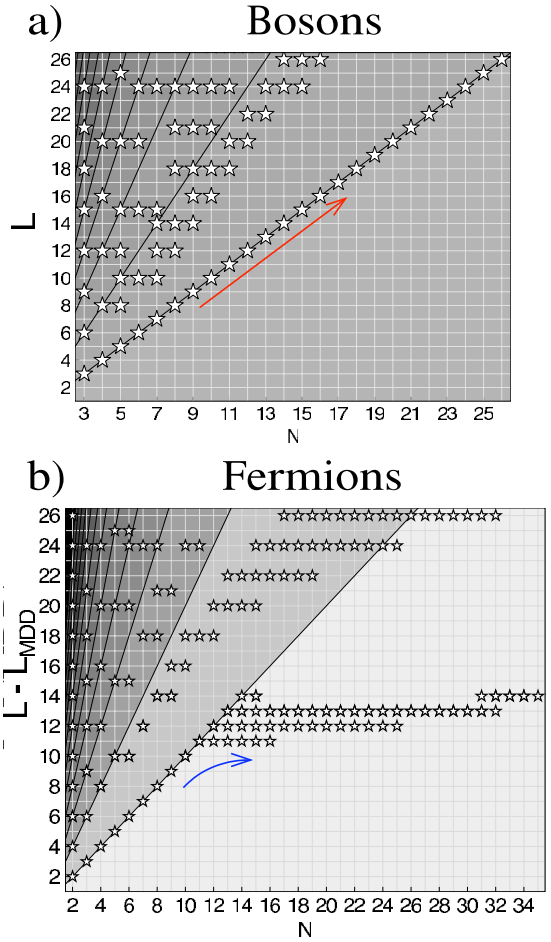

FIG. 12. (Color online) Systematics of boson and fermion ground states. When the external rotation Ω is gradually increased from zero, a droplet of N particles goes through a series of ground states with increasing angular momentum L. Stars mark these L values as a function of N for (a) boson droplets and (b) fermion droplets. Calculations are done with the exact diagonalization method in the lowest Landau-level approximation, and a harmonic confining potential Eq. (4). In the fermion results in (b), the angular momentum of the maximum density droplet L_{MDD} is subtracted from L. The linear N dependence of the first (N,L) combination in bosonic systems (arrow) indicates that the first L above the nonrotating state has a central vortex. Fermionic systems with repulsive interactions show a similar behavior only until $N=12$, where the breakdown mechanism of the MDD clearly changes (arrow), and a nonlocalized node emerges at a finite distance from the center. From Harju, 2005 and Suorsa, 2006.

B. Vortex clusters and lattices

When the angular momentum of the quantum droplet increases with rotation, additional vortices successively enter the cloud of particles. Normally, in a harmonic trap these vortices are all singly quantized and arrange in simple geometries, as observed for a rotating Bose-Einstein condensate in the early experiment by Madison *et al.* (2000); see Fig. 7. With increasing system size and rotation, the vortices order in arrays that resemble a triangular Abrikosov lattice (Abo-Shaeer *et al.*, 2001; Ho, 2001).

1. Vortex lattices in bosonic condensates

We begin by investigating the vortex structures along the yrast line, i.e., we study the states with highest angular momentum L at a given energy. Figure 14 shows the yrast line for $N=20$ bosons up to $L=3N$ calculated by exact diagonalization. The vortex is located at the center when $L/N=1$. The inset in Fig. 14 at $L=20$ shows the

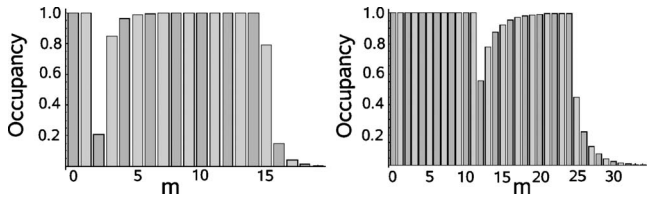

FIG. 13. Occupations of the single-particle (Fock-Darwin) eigenstates with angular momentum m of fermions in a harmonic trap at ground states with $L=L_{\mathrm{MDD}}+13$ for $N=15$ (left) and 25 (right). Since the mean particle distance from the center increases with m the high-N states resemble more edge excitations than central vortex states (cf. Fig. 12). From Suorsa, 2006.

pair-correlated density for that state, with a pronounced minimum at the origin. At angular momenta $L>N$, the slope of the yrast line changes abruptly, and the spectrum is no longer linear beyond the first cusp at $L/N=1$. The inset in Fig. 14 shows the angular momenta of the lowest-energy states for a given rotational frequency Ω of the trap that are obtained by minimizing the energy in the rotating frame, $E_{\mathrm{rot}}=E_{\mathrm{lab}}-\Omega L$. The pronounced plateaus correspond to stable states with vortices that successively enter the bosonic cloud with increasing trap rotation. Below a certain critical angular frequency, the cloud remains in the $L=0$ ground state. Beyond that frequency, the axially symmetric single vortex at the center becomes the ground state until more vortices penetrate the trap as the rotation increases.

In the exact results for small atom numbers, the vortices appear as clear minima in the pair-correlated densities, as here shown for the example of a two-vortex solution at $L/N=1.8$, and a three-vortex state, for L

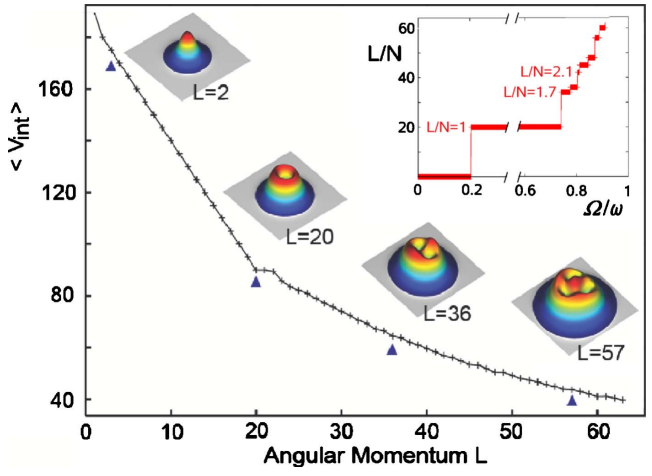

FIG. 14. (Color online) Yrast line of $N=20$ bosons in a harmonic confinement, obtained by the CI method in the lowest Landau level and for contact interactions between bosonic particles. The inset shows the total angular momentum of the ground state, plotted as a function of Ω/ω. Pair-correlated densities (renormalized in height) are shown for increasing angular momentum per particle, $l=L/N=0.1$, 1.0, 1.8, and 2.85 (as marked by the triangles). The reference point was chosen at high density for radii of order unity. From Christensson, Borgh, *et al.*, 2008

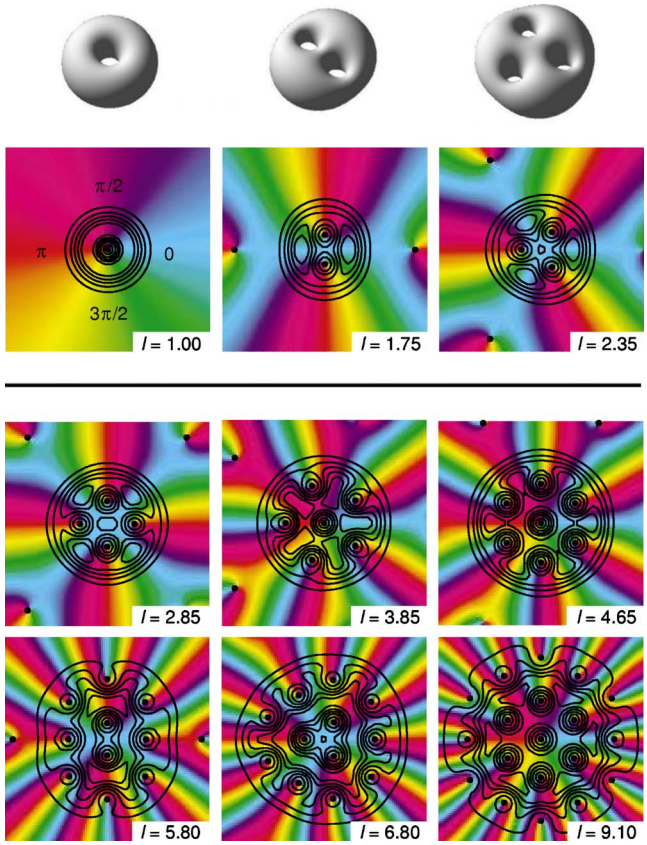

FIG. 15. (Color online) Vortices in a rotating cloud of bosons. Schematically shown are the vortex holes that penetrate the boson cloud with increasing angular momentum. The lower panel shows the phase of the order parameter, and its density contours. (The black dots indicate the vortex positions.) From Butts and Rokhsar, 1999.

=2.85, see Fig. 14. Related results of vortex formation in small systems were, for example, studied by Barberán *et al.* (2006), Dagnino *et al.* (2007), and Romanovsky *et al.* (2008).

For weakly interacting bosons, many states between angular momenta $L=N$ and $N(N+1)$ can be well described with the composite particle picture (Cooper and Wilkin, 1999; Viefers *et al.*, 2000). Cooper and Wilkin (1999) showed that for most states with a clear cusp in the yrast line the overlaps between the exact wave function and that of the Jain construction is in general close to 1 for particle numbers $N\leqslant 10$. Wilkin and Gunn (2000) furthermore showed that at some angular momenta in this region the so-called Pfaffian state is a good analytic approximation for the exact wave function.

These findings are similar to the results of the mean-field Gross-Pitaevskii method, where one finds successive transitions between vortex states of different symmetry. With increasing angular momentum, the arrays of singly quantized vortices are characterized by a phase jump of the order parameter around the density minima at the vortex cores (Butts and Rokhsar, 1999; Kavoulakis *et al.*, 2000).

Figure 15 shows schematically the equidensity surfaces for the unit vortex, a two-vortex and three-vortex

state in the upmost panel, as well as the contours and the corresponding phase of the order parameter at higher ratios $l=L/N$, as shown by Butts and Rokhsar (1999). At angular momenta beyond the unit vortex, the rotational symmetry of the mean-field solutions is broken. At $L \geqslant 1.75N$ the optimized Gross-Pitaevskii wave function shows a twofold symmetry when the second vortex has entered the cloud, very similar to the aforementioned experimental results for ^{87}Rb (Madison *et al.*, 2000), and in agreement with the pair-correlated densities in Fig. 14. Higher rotational frequencies introduce new configurations of vortices. At $l \approx 2.1$ there is a state with three vortices symmetrically arranged around the center of the trap. As $l=L/N$ increases, more and more vortices enter the cloud (Butts and Rokhsar, 1999; Kavoulakis *et al.*, 2000), and eventually the vortices arrange in a pattern that resembles a triangular lattice (Ho, 2001; Baym, 2003, 2005). This is in agreement with the experiments which were able to reach and image the angular momentum regime where large vortex arrays emerge (Abo-Shaeer *et al.*, 2001), reminiscent of the Abrikosov lattices in type-II superconductors. Stable multiply quantized vortices with phase shifts larger than 2π were not obtained (Madison *et al.*, 2000) for a one-component Bose gas in the purely harmonic trap, in agreement with the theoretical results discussed above.

As discussed in Sec. III.A, the effective mean-field potential in the Gross-Pitaevskii approach may break the rotational symmetry of the Hamiltonian to lower the energy. As a consequence, such a mean-field solution for the order parameter is not an eigenstate of the angular momentum operator and the solution may reflect the internal symmetry of the exact quantum state. Similar behavior has also been observed in density-functional studies of quantum dots (Reimann and Manninen, 2002) and is further discussed in the review by Cooper (2008).

Figure 16 shows the expectation value of the angular momentum of a bosonic cloud as a function of the angular velocity of the trap, as obtained from the Gross-Pitaevskii approach (Butts and Rokhsar, 1999). The discontinuities in $l=L/N$ correspond to the topological transformations of the rotating cloud that are associated with the occurrence of additional vortices, as discussed above.

In the purely harmonic trap, the oscillator frequency ω limits the angular rotation frequency Ω, see Eq. (1). When both quantities finally become equal, the condensate is no longer confined and the atoms fly apart.

2. Vortex molecules and lattices in quantum dots

The close analogy between the bosonic ground state, $|N00000\cdots\rangle$ at $L=0$, and the fermionic maximum density droplet state, $|111\cdots111000\cdots\rangle$ at $L_{\mathrm{MDD}}=N(N-1)/2$ (see Sec. II.F) suggests that vortex lattices may also emerge in fermionic systems to carry the angular momentum. Indeed, density-functional studies predicted the emergence of clusters or "vortex-molecule-like" geometric arrangements of vortices inside small droplets of electrons in quantum dots (Saarikoski *et al.*, 2004) when the

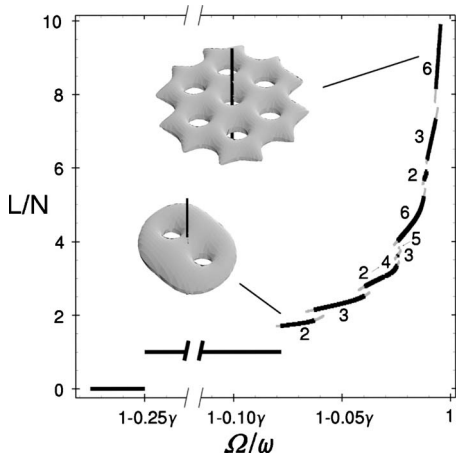

FIG. 16. Angular momentum per particle L/N as a function of the rotational frequency Ω/ω of the trap. The discontinuities correspond to the transitions between different symmetries. The insets show the surfaces of constant density in a spherical trap for states with two and six vortices. $\gamma=(2/\pi)^{1/2}aN/\sigma_z$, a the scattering length and σ_z the axial width of the ground state of a single particle in the trap. From Butts and Rokhsar, 1999.

angular momentum increases beyond the MDD. This happens in a similar way as in bosonic droplets at small rotation frequencies (Toreblad *et al.*, 2004). An example of these vortex molecules in few-electron quantum dots is shown in Fig. 17. Figure 18 shows a cluster of 14 vortices in a 24-electron quantum dot calculated with the density-functional method in a local spin-density approximation (see Sec. III.B).

These vortices correspond to off-electron nodes. The filling factor of the state in Fig. 18 can be approximated as $\nu \approx 0.63$. As in the bosonic systems vortex clusters are composed of single-quantized vortices (Saarikoski, Reimann, *et al.*, 2005). Remarkably, the structure of the vortices that appear localized on two concentric rings with four vortices on the inner, and ten vortices on the outer "shell," matches that of a classical Wigner molecule with 14 electrons at the verge of crystallization (Bedanov and Peeters, 1994). This also holds for the three- and four-vortex solutions shown in Fig. 17, where the triangle and square match the three- and four-particle classical Wigner-molecule configurations.

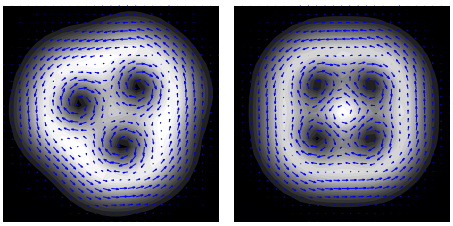

FIG. 17. (Color online) Vortex molecules in a six-electron droplet. Charge density (grayscale) and current density (arrows) show rotating currents around (a) three and (b) four localized vortex cores in density-functional calculations. From Saarikoski *et al.*, 2004.

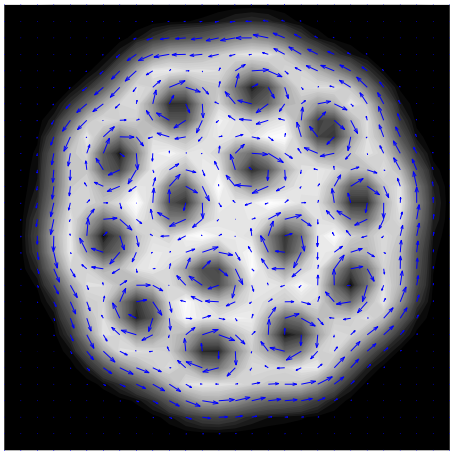

FIG. 18. (Color online) Electron density (grayscale) and current density (arrows) in a 24-electron quantum dot calculated with the density-functional method. The solution shows a cluster of 14 localized vortices arranged in two concentric rings. From Saarikoski *et al.*, 2004.

The clustering of vortices has also been analyzed with the CI method using reduced wave functions (see Sec. II.C.3) in the case of few-electron circular (Saarikoski *et al.*, 2004; Tavernier *et al.*, 2004, 2006; Stopa *et al.*, 2006) and elliptical (Saarikoski, Reimann, *et al.*, 2005) quantum dots. In these studies the formation of few-vortex molecules has been found to follow a similar pattern in both the CI method and the density-functional method.

Using the idea of the Bertsch-Papenbrock ansatz (Bertsch and Papenbrock, 1999) and assuming n fixed vortex sites, we can anticipate that the single determinant describing a vortex ring would be (Toreblad *et al.*, 2004)

$$\Psi_{nv} = \prod_{j=1}^{N}\prod_{k=1}^{n}(z_j - ae^{i2\pi k/n})|\mathrm{MDD}\rangle = \prod_{j=1}^{N}(z_j^n - a^n)|\mathrm{MDD}\rangle, \quad (47)$$

where a is the radius of the ring of vortices. This wave function is not an eigenstate of the angular momentum, but it can be projected out by collecting the states with a given power of a and symmetrizing the polynomial multiplying the $|\mathrm{MDD}\rangle$:

$$\Psi_{nv} = a^{n(N-K)}\mathcal{S}\left(\prod_{j=1}^{K} z_j^n\right)|\mathrm{MDD}\rangle, \quad (48)$$

where $\mathcal{S}$ is the symmetry operator and K determines the average radius of the vortex ring. For example, with $N=7$, $K=5$, and $n=3$, the most important configuration is $|1100011111000\cdots\rangle$, in agreement with the CI calculations (in the LLL approximation) for vortex rings by Toreblad *et al.* (2004). We discuss localization and fluctuations of vortices further in Sec. IV.C.

Equation (48) also elucidates the origin of different vortex types and the similarity of fermion and boson systems. The zeros of the symmetric polynomial $\mathcal{S}(\Pi z_j^n)$ give the free vortices, while the zeros of $|\mathrm{MDD}\rangle$ give the Pauli vortices. In a boson system, $|\mathrm{MDD}\rangle$ is replaced with the boson condensate $|0\rangle$ which has no zeros, and only the free vortices appear, as shown in Fig. 19.

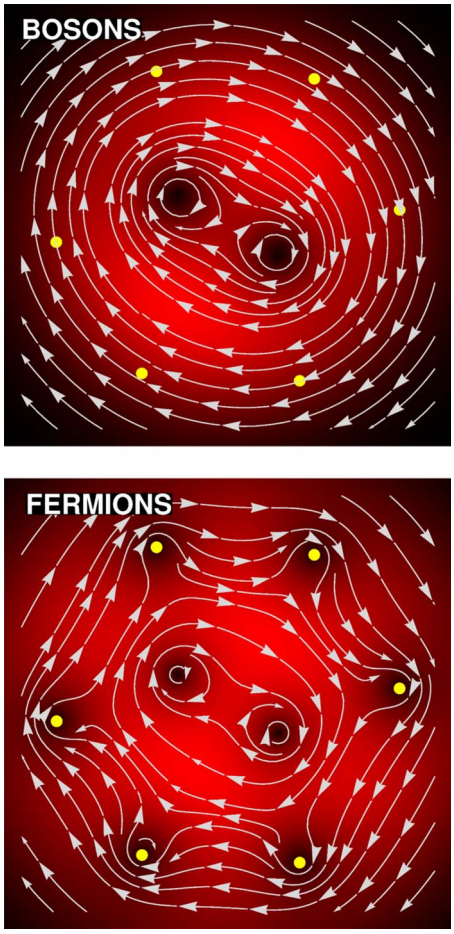

FIG. 19. (Color online) Reduced wave-function representation of the vortex structure of the model wave function Eq. (48) for bosons and fermions ($N=7$, $n=2$, $K=2$). The fixed particles are shown as light dots, the current field with arrows (logarithmic scale), and the particle density as shades of color (light color corresponding to high density).

Studies of electron-vortex correlations in quantum dots indicate that, at least in few-electron systems, the electron-vortex separation d_{e-v} can be approximated by a universal quadratic function of the filling factor, $d_{e-v} \sim d_{e-e}\nu^2$, where d_{e-e} is the average electron-electron separation (Anisimovas *et al.*, 2008). This shows that in the limit of high angular momentum (low ν) electrons tend to attract vortices closer to electron positions, which eventually leads to the formation of electron-vortex composites and the emergence of finite-size counterparts of the quantum Hall states.

The rotating electron molecule approach (Yannouleas and Landman, 2002, 2003) has also been used to analyze correlations between particles and vortices in electron droplets. However, this approach has been found to underestimate electron-vortex correlations (Anisimovas *et al.*, 2008) and vortex attachment to particles in the limit

of high angular momentum (Tavernier *et al.*, 2004).

The vortex-molecule-like characteristics of the states are expected to vanish gradually with increasing vorticity. However, exact diagonalization studies of few-electron systems with Coulomb interactions have suggested that the above-described vortex ordering into Wigner-molecule-like shapes continues down to a filling factor $\nu=\frac{1}{2}$, where the electron number equals the (off-electron) vortex number (Emperador, 2006). At $\nu=\frac{1}{2}$ the structure of the state is complex (Emperador *et al.*, 2005) and possible electron pairing in this regime has been studied (Harju *et al.*, 2006; Saarikoski *et al.*, 2008). This filling factor marks also the beginning of a regime $\nu<\frac{1}{2}$ where the vortex attachment to particles becomes pronounced (Emperador, 2006). We further discuss the breakdown of vortex molecules and the emergence of fractional quantum-Hall-liquid-like states in Secs. IV.C and IV.F, respectively.

3. Signatures of vortices in electron transport

For quantum dots in the fractional quantum Hall regime, where vortices have been predicted to form, electron transport measurements have revealed a rich variety of transitions associated with charge redistribution within the electron droplet (Ashoori, 1996; Oosterkamp *et al.*, 1999).

Quantum dots contain a tunable and well-defined number of electrons. The electron transport experiments in the Coulomb blockade regime at low temperatures (around 100 mK) measure the chemical potential

$$\mu(N) = E(N) - E(N-1), \tag{49}$$

which gives the minimum energy needed to add one more electron to the electron droplet. Transitions in the electron transport data can be seen as cusps or jumps in the chemical potential. Different quantum Hall regimes can be identified from these characteristic features of the chemical potential as a function of both the electron number and the magnetic field, see Fig. 20.

In experimental studies of vertical quantum dots, a harmonic external potential has been found to give a good approximation of the confining potential (Matagne *et al.*, 2002). The harmonic confinement strength $\hbar\omega_0$ is determined by the size of the quantum dot device and usually depends on the number of electrons N inside the quantum dot. The area of the electron droplet has been found to increase with the gate voltage suggesting that the electron density in the droplet remains constant (Austing, Tokura, *et al.*, 1999). Confining potentials scaling as $\hbar\omega_0 \sim N^{-1/4}$ in Koskinen *et al.* (1997) or $\hbar\omega_0 \sim N^{-1/7}$ in Saarikoski and Harju (2005) have been used in order to compare with experimental data.

The MDD state in quantum dots is the finite-size counterpart of the $\nu=1$ quantum Hall state. Its existence has been firmly established in experiments since it gives rise to a characteristic shape in the chemical potential at $\nu=1$ (Oosterkamp *et al.*, 1999). The MDD state assigns one Pauli vortex at each electron position giving a total magnetic flux of $N\Phi_0$. As the rotation is further increased, the MDD reconstructs (MacDonald *et al.*, 1993; Chamon and Wen, 1994; Goldmann and Renn, 1999; Reimann *et al.*, 1999; Toreblad *et al.*, 2006), and a vortex enters the electron droplet. This transition occurs approximately when the magnetic flux $\Phi=BA$ through the MDD of area A exceeds $(N+1)\Phi_0$. Subsequent transitions involve an increasing number of such off-electron vortices (Saarikoski *et al.*, 2004; Toreblad *et al.*, 2004). Assuming a constant electron density in the droplet, the change in B required for the addition of subsequent off-electron vortices in the droplet is $\Delta B=\Phi_0 n/N$. This result can be compared to density-functional calculations, which indicates a $1/N$ dependence of the spacing between the first major transitions after the MDD state. However, the limited accuracy of the available electron transport data at present does not allow to draw any more firm conclusions.

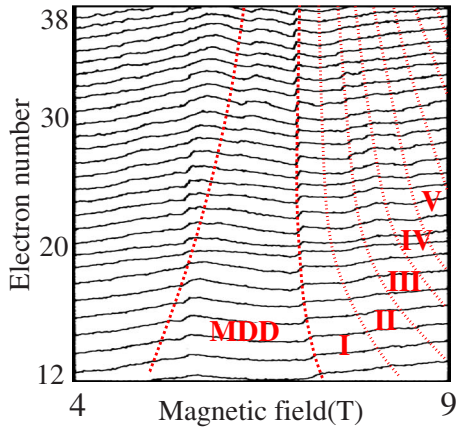

FIG. 20. (Color online) Current peaks in the electron transport experiments and transitions in the spin-density-functional theory (lines). The dashed lines denote the MDD boundaries and the roman numerals indicate number of vortices in the theory. Adapted from Saarikoski and Harju, 2005; the experimental data are from Fig. 2(b) in Oosterkamp *et al.*, 1999.

The different ground states obtained within density-functional theory are compared to electron transport data in Fig. 20. The transition patterns in theory and experiment show a narrowing of the stability domain of the MDD.

Closer examination of the chemical potential for different N values and comparison with the mean-field results reveal different quantum Hall regimes as the magnetic field is increased. Figure 21 shows the chemical potential for $N=13$ and 30.

The agreement with the electron transport data is best in the vicinity of the MDD domain. Experimental data show additional features not accounted for by the density-functional theory (open triangles in Fig. 21), which could be attributed to correlation effects, especially a transition to partially polarized states (Oaknin *et al.*, 1996; Siljamäki *et al.*, 2002). In a quantum Monte Carlo study by Güçlü *et al.* (2005) the frequency of transitions per unit of magnetic field was calculated in the $\nu<1$ regime and it was found to roughly correspond to the frequency in experiments. However, many of the cal-

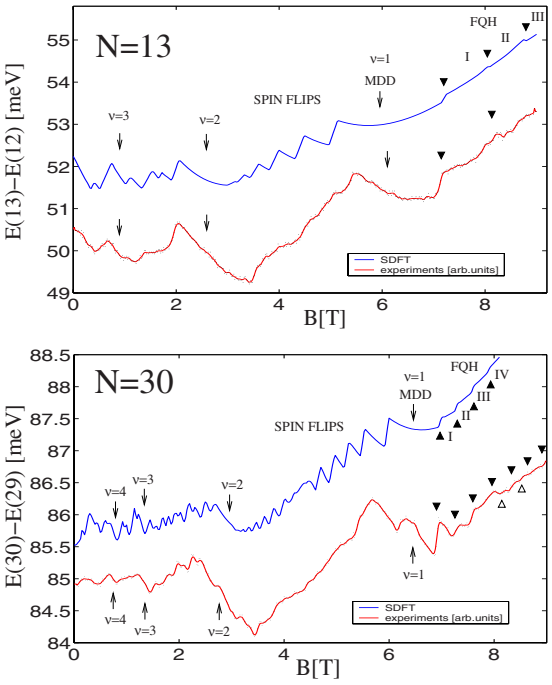

FIG. 21. (Color online) Chemical potential of a quantum dot device with $N=30$ (upper panel) and $N=13$ (lower panel) compared to the results from the spin-density-functional theory. The experimental data are from Oosterkamp *et al.* (1999). Noise in the experimental data has been reduced by using a Gaussian filter. In the calculations the confining potential is assumed to be parabolic with $\hbar\omega_0$ being 4.00 meV for $N=13$ and 3.51 meV for $N=30$. Finite-size precursors of different quantum Hall states are identified. The roman numbers between the filled triangles indicate the number of vortices inside the electron droplet predicted by the density-functional calculations. The open triangles mark other possible transitions which are beyond the reach of density-functional theory.

culated transitions give rise to small changes in angular momentum and energy. Direct comparison with experiments is therefore difficult due to noise in experimental setups and inevitable imperfections in the samples. Nishi *et al.* (2006) did experimental measurements and detailed modeling for few-electron quantum dots. High-accuracy electron transport data that would go deep into the fractional quantum Hall regime are still lacking for higher electron numbers.

Magnetization measurements of quantum dots could provide another way to probe for transitions caused by vortex formation inside electron droplets. Observed oscillations in the magnetic susceptibility $\chi=\partial M/\partial H$ have been analyzed, showing the de Haas–van Alphen effect in large arrays of quantum dots (Schwarz *et al.*, 2002). However, to resolve transitions in individual states in the regime of high angular momentum is challenging because the shapes of the quantum dots in the ensemble must be sufficiently uniform, and the number of electrons in the samples has to be small.

C. Localization of particles and vortices

We have seen above that localized vortices and vortex molecules have been observed in rotating bosonic systems, and similar structures were predicted to occur in rotating fermion droplets. Vortex localization can be seen as analogous to particle localization within the framework of the particle-hole duality picture, discussed in Sec. II.D. We start this section with a discussion of *particle* localization in 2D systems. Insight and concepts derived from these studies are necessary as we proceed to discuss the analogy between particle and vortex localization.

1. Particle localization and Wigner molecules

Wigner crystallization (Wigner, 1934) has been observed for electrons trapped at the surface of superfluid liquid helium (Andrei *et al.*, 1991) or in a two-dimensional electron gas in a semiconductor heterostructure (Pudalov *et al.*, 1993). Recent addition energy measurements of islands of trapped electrons floating on a superfluid helium film have revealed signatures of a Wigner-crystalline state (Rousseau *et al.*, 2009). In the low-density limit, the kinetic energy of the 2D electron gas becomes small and the interparticle interactions dominate. The crystalline phase is expected to emerge at the density parameter $r_s \approx 37a_B^*$, where a_B^* is the effective Bohr radius (Tanatar and Ceperley, 1989) (r_s is a radius of a circle containing on average one electron). This estimate is in agreement with recent computations by Attaccalite *et al.* (2002, 2003).

A finite system of a few (nearly) localized electrons is commonly referred to as a "Wigner molecule." In small quantum dots, these Wigner molecules take the shapes of simple polygons, depending on the number of electrons that can be resolved by classical electrostatics (Bolton and Rössler, 1993; Bedanov and Peeters, 1994). In the nonrotating case, the onset of electron localization occurs already at relatively high densities $r_s \approx 4a_B^*$ (Jauregui *et al.*, 1993; Egger *et al.*, 1999; Reimann *et al.*, 2000; Yannouleas and Landman, 2007). In this context it is interesting to note that in small systems most of the particles localize at the perimeter of the dot. For seven electrons, for example, six particles localize at the vertices of a hexagon, with the seventh particle at the dot center (Bolton and Rössler, 1993): the electrons along the perimeter essentially form a 1D system where the localization is even easier than in 2D (Kolomeisky and Straley, 1996; Viefers *et al.*, 2004). Localization in the radial direction takes place first followed by localization in the angular direction (Filinov *et al.*, 2001; Ghosal *et al.*, 2006).

In small electron systems there are no true phase transitions and the localization of electrons increases gradually with decreasing electron density (Reimann *et al.*, 2000). Inelastic light scattering experiments have only been used to probe excitations of moleculelike states in few-electron quantum dots in the high-density regime where, however, localization has not yet occurred (Kalliakos *et al.*, 2008). Addition-energy spectra obtained from Coulomb blockade experiments (Tarucha *et al.*, 1996) have been proposed as a direct probe for signatures of localization (Güçlü *et al.*, 2008). In large quan-

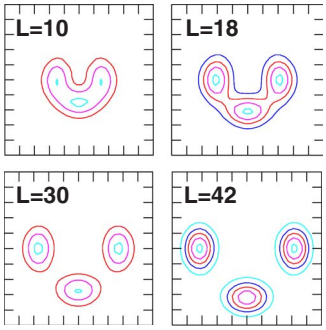

FIG. 22. (Color online) Pair-correlation functions of four fermions with repulsive Gaussian interactions at four different angular momenta $L=10$, 18, 30, and 42, respectively, showing that localization increases with rotation. The contour plots are in the same scale to demonstrate the expansion due to the rotation. From Nikkarila and Manninen, 2007a.

tum dots, the crystallization occurs in ringlike patterns, such as the shells of an onion (Filinov *et al.*, 2001; Ghosal *et al.*, 2006). A gradual rearrangement of addition energy spectra, which indicates a change in shell fillings, is then predicted to occur as the shell sizes of Wigner molecules differ from those of nonlocalized electrons. However, no experimental data yet exist in this regime.

Quantum dots are often modeled as circularly symmetric and the associated quantum states and ground-state electron densities therefore also have the same symmetry. The localization of particles takes place in the internal frame of reference. In the laboratory frame the localization is seen in the total density distribution only when using approximate many-particle methods which allow symmetry breaking, such as, for example, the unrestricted Hartree-Fock approach (Yannouleas and Landman, 1999). Other possibilities are to break the symmetry of the confining potential as, for example, by an ellipsoidal deformation (Manninen, Koskinen, *et al.*, 2001; Saarikoski, Reimann, *et al.*, 2005; Dagnino *et al.*, 2007, 2009; Dagnino, Barberán, and Lewenstein, 2009) or to analyze localization of the probing particle in the reduced wave function (Harju *et al.*, 2002; Saarikoski *et al.*, 2004). However, there are other straightforward methods to see the localization in exact calculation for circular confinement: Fig. 22 shows the pair-correlation function (conditional probability) for four particles at different values of the total angular momentum. Clearly, when the angular momentum increases, the particles are further apart and the localization becomes more pronounced. Another possibility is to study the rotational many-particle energy spectrum, which is more intricate, but also more revealing.

2. Rotational spectrum of localized particles

When the particles are localized, we may consider the system as a rotating "molecule" with a given point group symmetry. In the case of two identical atoms in a molecule the rotational spectrum shows a twofold periodicity in the angular momentum, which may be odd or even depending upon whether the atoms are bosons or fermions (Tinkham, 1964). Similarly, for N identical particles forming a ring, only every Nth angular momentum is allowed (Koskinen *et al.*, 2001) in a rigid rotation around the symmetry axis. For other angular momenta, the rotational state should be accompanied by an internal excitation. In the case of particles having no internal degrees of freedom (no spin), the only such excitations are vibrational modes of the molecule. Group theory can then be used to resolve the vibrational modes which are allowed to accompany a certain angular momentum eigenvalue (Maksym, 1996; Koskinen *et al.*, 2001; Viefers *et al.*, 2004).

Plotting the energies of the many-body system as a function of the angular momentum, the lowest energy (yrast line) has oscillations with a period of the symmetry group. The minima correspond to pure rotational states. Between the minima the states have vibrational excitations which increase the energy. Maksym showed that the energy spectrum of few electrons at high angular momenta can be quantitatively explained by a rotating and vibrating Wigner molecule (Maksym, 1996) which is the basis for the molecular approaches to correlations in quantum dots (Maksym *et al.*, 2000) and quantum rings (Koskinen *et al.*, 2001). Several other studies have later confirmed this observation; for a review, see Viefers *et al.* (2004). This molecular approach for rotating particles was also used by Yannouleas and Landman (2002, 2003), who introduced rotating electron molecule wave functions to describe rotating molecular states at high angular momenta. These wave functions are available in analytic form, with their internal structure constructed by placing Gaussian functions at classical positions of electrons in high magnetic fields.

Formulating a molecular model of a rotating system, we may approximate the many-particle spectrum (at zero magnetic field) by

$$E = \frac{L^2}{2I_L} + \sum_{\nu} \hbar\omega_{L\nu}\left(n_\nu + \frac{1}{2}\right), \tag{50}$$

where I_L is the moment of inertia of the Wigner molecule and $\omega_{L\nu}$ is the vibrational frequencies. I_L and $\omega_{L\nu}$ can be determined using classical mechanics in the rotating frame, and thus depend on the angular momentum as indicated with the subscript L. The eigenenergies Eq. (50) can be compared to those calculated from the exact diagonalization method.

To give an example for the signatures of localization in the many-body energy spectra, Fig. 23 shows the rotational three-particle spectrum. A broad range of low-lying states may be described quantitatively with the rotation-vibration model of Eq. (50).

Figure 23 also shows examples of the pair-correlation functions for a purely rotating state and for a state including vibrational modes. Similar observations have been reported for other vibrational modes and particle numbers (Maksym *et al.*, 2000; Nikkarila and Manninen, 2007a). A more detailed quantum-mechanical analysis of the molecular states has recently been reported by Yannouleas and Landman (2009).

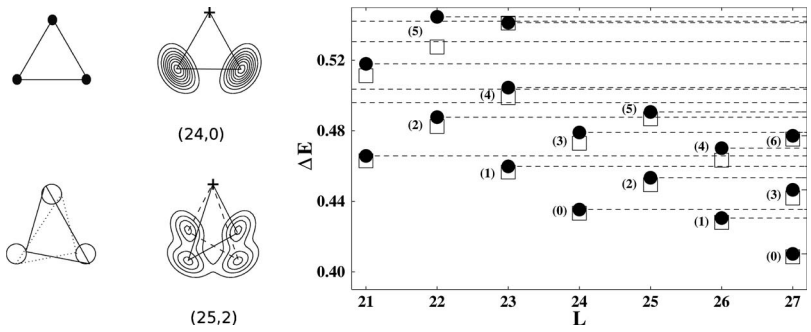

FIG. 23. Classical orbits and pair-correlation functions of localized electrons in rotating frame (upper panel). At angular momentum $L=24$ the lowest energy state is purely rotational while at $L=25$ a doubly excited rotational state is shown. In the rotating frame the classical motion shows a pseudorotation (middle left) while the pair correlation shows maxima at the classical turning points (middle right).The spectrum (lower panel) compares the exact energies (dots) with those of the classical model (squares). It shows a periodicity of $\Delta L=3$ in angular momentum, which agrees with the localization in a triangular geometry (see upper panel). The horizontal dashed lines indicate the center-of-mass excitations which occur at all angular momenta. From Nikkarila and Manninen, 2007b.

Finally, we should consider what happens to the rotational energy spectrum when the particles have internal degrees of freedom, say, spin. In the classical limit, the internal degrees of freedom separate from the spatial excitations (vibrations) since the Hamiltonian is spin independent. The different spin states of the system will eventually become degenerate. However, the existence of the different spin states will give more freedom to satisfy the required symmetry (bosonic or fermionic) of the total wave function. Again, group theory can be used to determine the spin states which are allowed for a given angular momentum and a given vibrational state (Maksym, 1996). The energies agree well with the classical model of Eq. (50) (Koskinen *et al.*, 2007).

The localization of the particles may in fact also be incomplete. This is indicated by the nonvanishing particle density in between the classically localized geometries, as well as small deviations in the symmetry of the Wigner crystal. The excited quantum Hall states (edge states) may especially show such structures, as discussed in connection with vortex formation, see Sec. IV.A. The lowest-lying excitations of a large electron droplet above the MDD state have been predicted to show particle localization into rings of electrons around a compact nonlocalized core of the MDD electrons (MacDonald *et al.*, 1993; Chamon and Wen, 1994). The wave functions of these states contain a single node at a finite distance from the center (i.e., a nonlocalized vortex, see Sec. IV.A.3), which leads to a separated ring of localized electrons at the edge, often referred to as the Chamon-Wen edge that has been much discussed (Goldmann and Renn, 1999; Reimann *et al.*, 1999; Manninen, Koskinen, *et al.*, 2001; Reimann and Manninen, 2002; Toreblad *et al.*, 2006). The localized edge state appears when the MDD begins to break up with the entrance of the first vortex, but before further vortex holes penetrate the cloud (see Sec. IV.C.4). It should be noted that the current-spin-density-functional theory (Vignale and Rasolt, 1987, 1988) with the local density approximation (Reimann *et al.*, 1999) largely overemphasizes the localization of electrons in the Chamon-Wen edge (Toreblad *et al.*, 2006).

3. Localization of bosons

In a nonrotating condensate, all bosons may occupy the same quantum state. In the regime of high angular momenta, however, rotation may induce localization in bosonic systems in the same way as in fermionic systems. In both cases, the rotation pushes the particles further apart, and the classical picture of a rotating and vibrating Wigner molecule (Maksym, 1996) sets in. The similarity of bosons and fermions in reaching the classical limit was suggested by Manninen, Viefers, *et al.* (2001) on the basis of Laughlin's theory (Laughlin, 1983) of the fractional quantum Hall effect, and has been subsequently studied more quantitatively: a detailed comparison of few bosonic and fermionic particles in a harmonic trap (Reimann *et al.*, 2006a) indicated similar localization effects in both systems. Note that for small particle numbers in the LLL the mapping between boson and fermion states discussed in Sec. II.D becomes increasingly accurate when the angular momentum increases (Borgh *et al.*, 2008), in accordance with the classical interpretation of the spectrum.

4. Vortex localization in fermion droplets

There is an apparent analogy between vortex localization and particle localization: we have seen that localized vortices cause minima in the electron density, with rotational currents around their cores. These "holes" arrange in vortex molecules, with shapes that indeed resemble those of Wigner molecules in the case of particle localization, discussed in Sec. IV.C.1. (Note that the Pauli vortices do not give rise to vortex structures in the electron density since each electron carries one such vortex.)

The vortex localization can be illustrated by the configuration mixing of the exact quantum states. If the configuration has, say, four vortices and $|11110000111111\cdots\rangle$

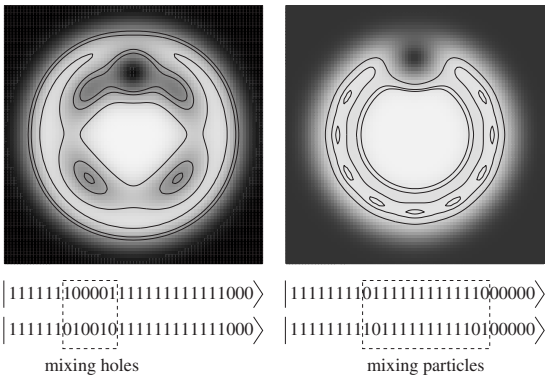

FIG. 24. Electron-electron pair-correlation functions showing localization of four vortices (left) and localization of electrons at the edge of the cloud in the case of one vortex (right). White color means high density, and some constant-density contours are shown. The two most important configurations are given in each case, demonstrating that mixing of single-particle states close to holes leads to hole localization, while correspondingly the mixing of particles localizes particles. The results are calculated with the CI method for 20 particles with angular momenta $L=242$ (left) and $L=202$ (right).

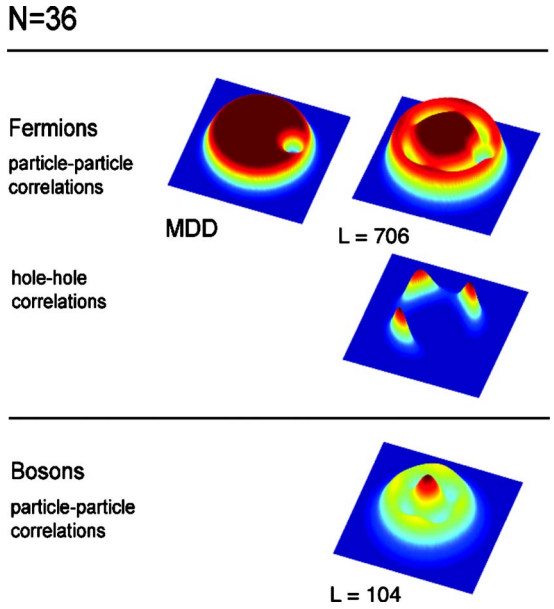

FIG. 25. (Color online) Pair-correlation functions for large fermion and boson systems with four vortices. The pair-correlation function of the MDD is displayed for comparison; it only shows the exchange-correlation hole at the reference point.

has the largest weight, other configurations with the same angular momentum, such as $|11101001011111\cdots\rangle$, have a finite weight. The CI method shows that the mixing of these states happens mostly around the holes in the filled Fermi sea, as shown in Fig. 24. This means that the holes are strongly correlated and may localize.

This can be directly compared to the localization of particles. As discussed in Sec. IV.C.1, the lowest-lying excitations of a large electron droplet above the MDD state were predicted to show particle localization into ringlike geometries, with a single vortex hole at a finite distance from the center (see Sec. IV.A.3). In this case, the configuration mixing is shifted to the outer edge of the droplet where it leads to a ring of strongly correlated particles as, for example, shown in Fig. 24.

The localization of particles and vortices in a circular system breaks the internal symmetry (unless a single vortex is localized at the center). The density-functional method, using a local approximation for the exchange-correlation effects, may show the localization of particles and vortices directly in the particle and current densities (see Fig. 18 and discussion of symmetry breaking in Sec. II.A.3) as discussed above. However, the true many-body wave function of the system must have the symmetry of the Hamiltonian. Figure 24 demonstrated that the localization of vortices can be seen in the pair-correlation functions by taking the reference point to be at the same radius as the vortices. Moreover, in a one-component fermion system, particle-hole duality (see Sec. II.D) can be used to gain insight into correlations between vortices. Transformation of a bosonic wave function to a fermionic one can be used to illustrate the vortex localization. Any fermion state can be written as a determinant of the MDD times a symmetric polynomial, where vortex structures are included in the latter (Manninen *et al.*, 2005). On the other hand, this polynomial is a good approximation to the exact boson wave function, as discussed in Sec. II.F.

Figure 25 shows examples of the particle-particle and hole-hole correlation functions which indeed reveal that vortices in both boson and fermion systems are well localized. This can be understood by considering the angular momentum of the system of holes, and the corresponding filling factor of the LLL. For example, in the case of four vortices, the hole filling factor is as low as about $1/9$, which corresponds to the value where the particles form a Wigner solid in an infinite system. In other words, when the electron filling factor approaches unity (from below), the hole filling factor approaches zero, forcing the holes to be localized.

Hole-hole correlations in Fig. 25 show clearly the effect of the zero-point fluctuation in the vortex position. To examine this further in the case of fermions, as an example we investigate the singly quantized vortex for six electrons in a harmonic confinement. As discussed in Sec. IV.A.3 the MDD state in this case, with angular momentum $L=15$, is characterized by a relatively flat electron density. The electrons occupy the six lowest levels of angular momentum in the lowest Landau level with occupancies $|11111100\cdots\rangle$. When the angular momentum increases, at stronger magnetic fields the MDD state is reconstructed and a vortex hole is created in the center. This state has angular momentum $L=21$. The single-particle determinant $|011111100\cdots\rangle$ with a weight 0.91 yields the largest contribution to the wave function in the lowest Landau level. Due to fluctuations, the exact many-body wave function includes other single-particle determinants corresponding to $L=21$, such as $|1011110100\cdots\rangle$ and $|11011100100\cdots\rangle$. However, since

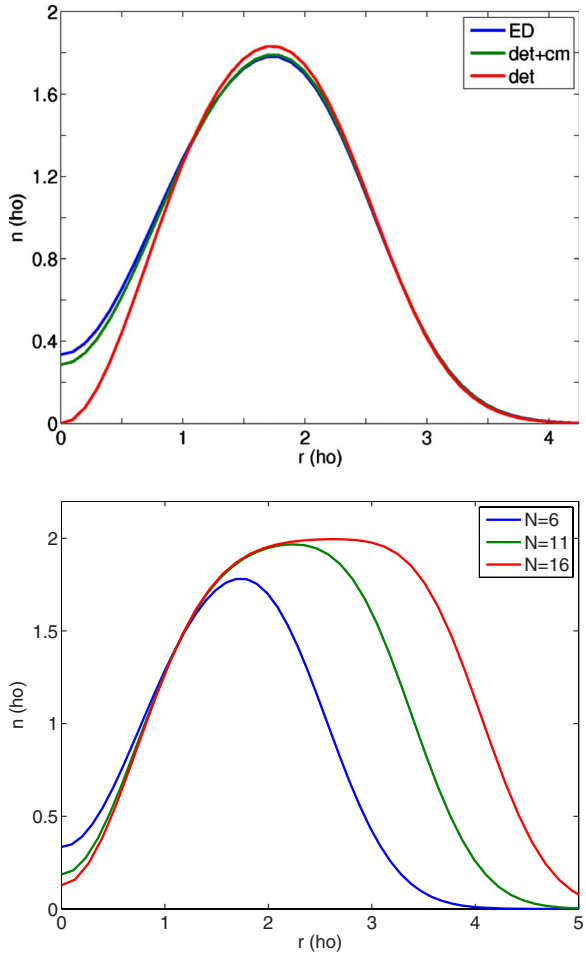

FIG. 26. (Color online) Radial electron densities. Upper panel: Radial electron densities in a harmonic trap ($\omega=1$) in a six-electron droplet with a central vortex at $L=21$ (in harmonic oscillator units). The exact solution in the LLL is shown by the line, a single-determinant wave function which describes a central vortex is shown by another line, and a single-determinant wave function in the center of mass (CM) transformed coordinates $z_i \rightarrow z_i - z_{\mathrm{CM}}$ is shown by the third line. Lower panel: Radial electron densities for central vortex states $L=L_{\mathrm{MDD}}+N$, showing that vortex localization increases with electron number N due to decrease in the center-of-mass motion.

their weights are relatively small, the state can be characterized by a rather flat maximum density droplet configuration with a vortex hole in the center. The electron density of this state indeed shows a deep hole in the center and a rotating current around it (upper panel of Fig. 26). Fluctuations in the vortex position cause the particle density to remain finite in the center of the confining potential. A single-determinant wave function $|01111100\cdots\rangle$ transformed into the center-of-mass coordinates $z_i \rightarrow z_i - z_{\mathrm{CM}}$ shows a density profile that is close to the exact results (upper panel of Fig. 26). The quantum-mechanical zero-point motion of the vortex hole leads to a finite density at the vortex core. The center-of-mass fluctuations decrease with electron number, which is reflected by localization increasing with particle number (lower panel of Fig. 26).

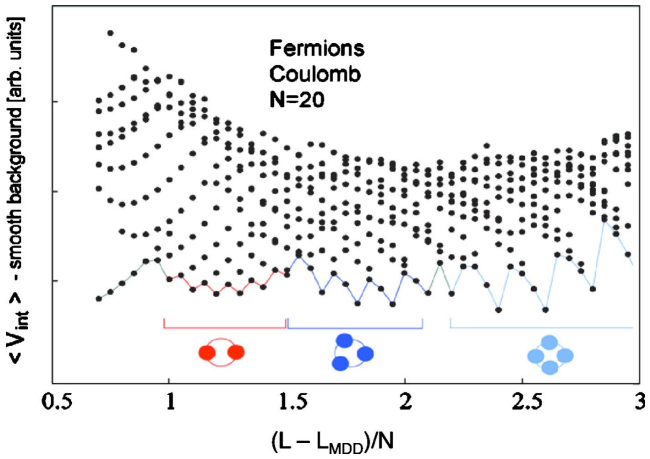

FIG. 27. (Color online) Fermion low-energy spectrum for 20 particles. The lowest energy many-particle states as a function of the total angular momentum (yrast states) are connected with lines to guide the eye. A smooth function of angular momentum was subtracted from the energies to emphasize the oscillatory behavior of the yrast line. The periodicity of the oscillation reveals the number of localized vortices as shown schematically. From Reimann *et al.*, 2006b.

5. Vortex molecules

A section of the many-particle energy spectrum for $N=20$ electrons for different angular momenta L is shown in Fig. 27 (Reimann *et al.*, 2006b). The yrast line shows periodic oscillations, with the oscillation length (in units of L) equal to number of localized vortices in the system. The reason behind these periodic oscillations in the energy spectrum is deeply connected with the above-mentioned particle-hole duality and vortex localization: they are signatures of two, three, and four vortices localized at the vertices of simple polygons with C_{2v} symmetry. For polarized fermions as in Fig. 27, the rigid rotation of the vortex "molecule" with n-fold symmetry is allowed only at every nth angular momentum, corresponding to a minimum (cusp) in the yrast line. At intermediate angular momenta, the rigid rotation is accompanied by other excitations, such as vibrational modes, that result in higher energies (Nikkarila and Manninen, 2007a). Figure 28 compares a small part of the spectrum to that for three electrons. The marked similarity of these spectra demonstrates not only that the vortices are localized in a triangle, such as the three electrons, but also that elementary excitations of the many-particle energy spectrum are vibrational modes of the vortex molecule.

Under certain circumstances the particle and current densities of the (exact) many-body state may show directly the formation of vortex molecules. This may, for example, be the case for a broken rotational symmetry of the system as predicted for elliptically confined quantum dots (Manninen, Koskinen, *et al.*, 2001; Saarikoski, Reimann, *et al.*, 2005). Figure 29 shows the electron density of an elliptical six-electron quantum dot calculated by exact diagonalization.

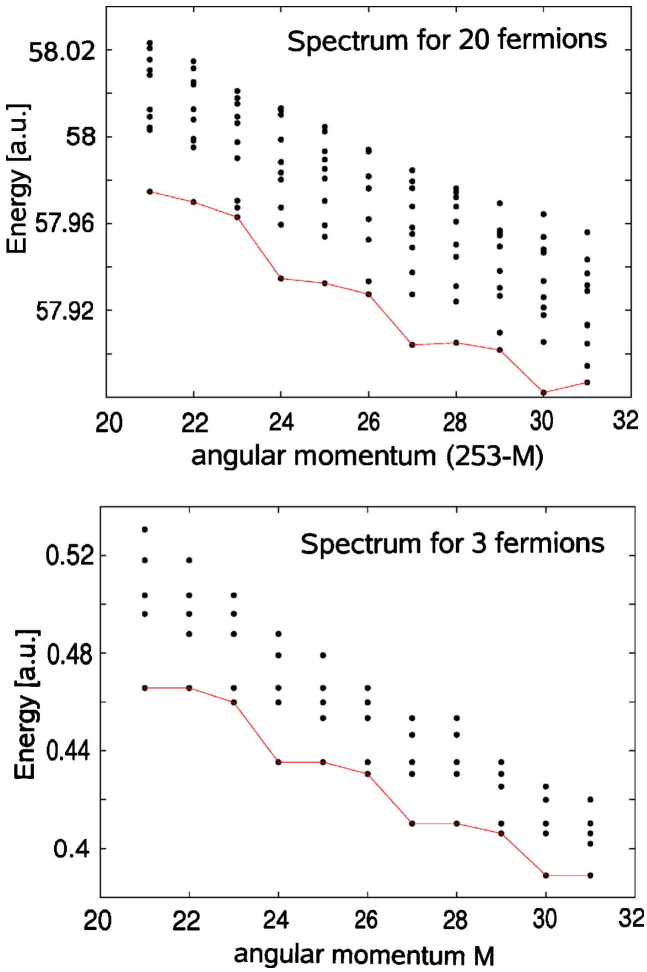

FIG. 28. (Color online) Fermion yrast spectrum for 20 particles and three vortices (upper panel) and three particles (lower panel) show both the periodicity of $\Delta L=3$ associated with the threefold rotational symmetry of the vortex molecule in the former case and electron molecule in the latter case. From Manninen *et al.*, 2006.

Two localized vortices can be identified as minima in the charge density, around which the current shows the typical loop structure. In highly eccentric confining potentials, vortex structures containing three and more localized vortices were also predicted to form (Saarikoski, Reimann, *et al.*, 2005). The effect of fluctuations in the vortex positions is also seen in this case. To some extent, electron localization is observed as well. In this case, the wave function can be characterized by two holelike quasiparticles at the center of a ring of six electrons. It should be noted that Fig. 29 shows the exact particle density and not the mean-field particle density. Since elliptically deformed quantum dots have been realized experimentally (Austing, Sasaki, *et al.*, 1999) this may be the most direct way to image vortex structures in quantum dots. Localized vortex structures have also been predicted to emerge in other quantum dot geometries (Helle *et al.*, 2005; Saarikoski, Reimann, *et al.*, 2005).

A perturbative approach to visualize vortices in the particle density is to include a point perturbation in the external potential (Christensson, Borgh, *et al.*, 2008),

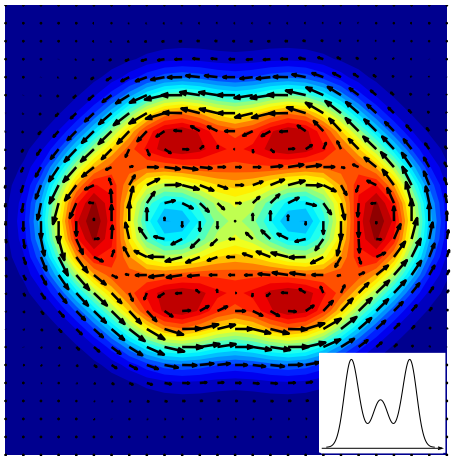

FIG. 29. (Color online) Electron density and current density (arrows) of an elliptically confined six-electron droplet with two localized vortices, calculated by the exact diagonalization method. The confinement strength is $\hbar\omega_0=5.93$ meV, the eccentricity of the elliptic confining potential $\delta=1.2$, and the magnetic field is $B=17$ T. Inset: Profile of the electron density at the longest major axis shows fluctuations in the vortex positions, which causes electron density to remain finite at the density minima. Adapted from Saarikoski, Reimann, *et al.*, 2005.

which can pin the vortices. The resulting particle density shows the vortex localization. An example is shown in Fig. 30 for a system of eight electrons. With this small perturbation, the expectation value of the angular momentum has a nearly similar dependence on the rotational frequency than the unperturbed system. It is thus expected that each angular momentum jump in the nonperturbed system corresponds to addition of one vortex as seen in the perturbed system.

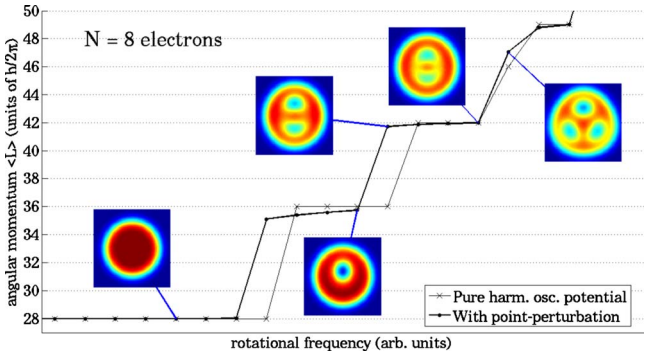

FIG. 30. (Color online) Angular momentum as a function of the rotational frequency of the parabolic trap with $N=8$ electrons in the lowest Landau level. The unperturbed result (thin line) is comparable to the expectation value of angular momentum in the presence of an added point perturbation which breaks the rotational symmetry (thick solid line). The insets show the densities as shades of color in the perturbed system. The vortices appear as pronounced minima in the density distribution, their number increasing with the trap rotation. Results are calculated with the exact diagonalization method (Christensson, Borgh, *et al.*, 2008).

D. Melting of the vortex lattice

After single vortex lines in rotating condensates were experimentally realized by phase imprinting techniques (Matthews *et al.*, 1999), many experimental studies concerned the formation of lattices of vortices in bosonic cold-atom gases in the regime of high particle-to-vortex ratio (filling factor) $\nu_{pv}=N/N_v$ (Chevy *et al.*, 2000; Madison *et al.*, 2000, 2001). The modes of the vortex lattice (Baym, 2003, 2004) as well as the structure of the vortex cores were analyzed (Coddington *et al.*, 2003, 2004; Schweikhard *et al.*, 2004). When the vortex density increases with the angular momentum, it is expected that for rapid rotation the vortex density may finally become comparable to the particle density (Cooper *et al.*, 2001; Fetter, 2001; Ho, 2001). An interesting issue is how the system then changes with the increasing particle-to-vortex ratio (Baym, 2005). At rapid rotation, strongly correlated states analogous to fractional quantum Hall states may emerge (Wilkin *et al.*, 1998; Cooper, 2008; Viefers, 2008). These states are quantum liquidlike states of particles and vortices where correlations may give rise to the formation of particle-vortex composites. It is believed that a phase transition occurs with a vortex density somewhere between the rigid vortex lattice and the quantum liquid of vortices. This transition is often referred to as "melting." However, the process is not fully understood and calculations yield different estimates for the critical vortex density. Moreover, in present day experiments the particle-to-vortex density is usually very high, $\nu_{pv}\gtrsim 500$ (Schweikhard *et al.*, 2004).

1. Lindemann melting criterion

The vortex density at the transition from localized vortex lattice states to liquidlike states can be approximated by assuming that the melting process is analogous to the melting of solids when atomic vibrations increase above a threshold amplitude. In the Lindemann model the melting point of solids is determined from the condition that when thermal vibrations reach a critical amplitude, melting of the material occurs (Lindemann, 1910). This amplitude in solids is often approximated to be around 10–20 % of the lattice spacing. Using an analogous idea, the melting point of the vortex lattice can be approximated from the condition that thermal and quantum zero-point vibrations reach a critical threshold amplitude (Blatter and Ivlev, 1993).

Rozhkov and Stroud (1996) studied superconductors at zero temperature to obtain an estimate for the vortex density where zero-point fluctuations become large enough to melt the vortex lattice. Their study was motivated by the presence of large quantum fluctuations in high-T_c materials but their results gave also an estimate of the vortex lattice melting in ultracold rotating Bose-Einstein condensates. Using the Lindemann criterion they approximated that melting takes place at particle-to-vortex filling factor $\nu_{pv}\sim 14$ at a presumed threshold zero-point vibration amplitude of 14% of the nearest-neighbor intervortex distance.

Other calculations using the Lindemann criterion have given comparable estimates of the filling factor at the vortex lattice melting [see also the discussion in the reviews by Cooper (2008) and Fetter (2009)]. Sinova *et al.* (2002) reported that the critical density in their model system of rapidly rotating bosons corresponds to $\nu_{pv}\sim 8$. Baym (2003, 2004, 2005) analyzed normal modes of vortex lattice vibrations in the mean-field limit and found that the vortex lattice melts at $\nu_{pv}\sim 10$.

2. Transition to vortex liquid state

The predictive power of the Lindemann model is poor because melting in solids is known to be a cooperative phenomenon, and the process therefore cannot be accurately described in terms of the mean vibration amplitude of a single particle. However, Rozhkov and Stroud (1996) obtained another estimate $\nu_{pv}\sim 11$ for the melting point of the vortex lattice by comparing the energy of a Wigner crystal model wave function to the energy of a Laughlin-type wave function. These wave functions were assumed to correspond to the ordered vortex-lattice state and the vortex-liquid state, respectively. Exact diagonalization calculations with contact interactions in a periodic toroidal geometry showed that the excitation gap collapsed at $\nu_{pv}\sim 6$, which was interpreted as a lower bound for a vortex lattice melting (Cooper *et al.*, 2001). The associated vortex-liquid states at integer and half-integer ν_{pv} were shown to be, in general, well described with so-called parafermion states studied by Read and Rezayi (1999).

In contrast to bosonic systems, the vortex lattice melting has not been studied theoretically in fermion systems. However, we can obtain an estimate for a corresponding transition using the particle-hole duality (Sec. II.D). There is a transition from the fractional quantum Hall liquid to localized electrons (i.e., the formation of a Wigner crystal) when the filling fraction of the LLL decreases below $\nu\approx 1/7$ (Lam and Girvin, 1984; Pan *et al.*, 2002). There are about 6 to 8 vortices per particle, not counting the Pauli vortices, at the transition point. Using the particle-hole duality we can now reverse the role of particles and vortices. In the dual picture a lattice of localized vortices then melts to a quantum Hall liquid when the particle-to-vortex ratio decreases to a value between 6 and (about) 8. This corresponds to a filling factor between $\nu\approx 0.8$ and 0.9, where a vortex lattice is expected to melt in a 2DEG. The close relation between boson and fermion states in the LLL [Eq. (21)] would also suggest that in boson systems the vortex lattice should melt when the particle-to-vortex ratio decreases to about 8, which is not too different from the values mentioned above.

In conclusion, even though the results of different calculations show a considerable variation for the melting point, they all indicate vortex lattice melting well before the number of vortices in the system becomes comparable to the particle number. However, much of the details are not understood, and experiments do not yet reach the transition regime. The transition may happen

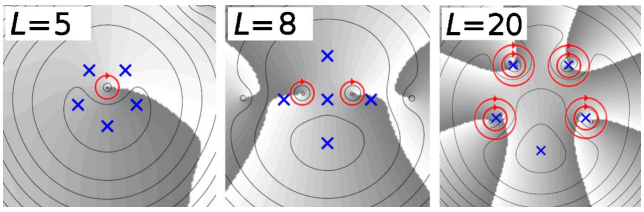

FIG. 31. (Color online) Reduced wave functions of a bosonic five-particle system in a harmonic trap, showing the formation of one and two free vortices in the region of high particle density (marked as circles) at low angular momenta $L=5$ and $L=8$, respectively (left and middle). When the angular momentum increases, two vortices are finally captured by each particle to form a state which is approximated by the bosonic Laughlin state $m=2$ (two concentric circles) at $L=20$ (right). Particle interactions are Coulombic here and the probe particle is at the bottom. After Suorsa, 2006.

gradually and go through several intermediate states with increasing vortex delocalization or, as the name explicitly suggests, it may occur through an abrupt loss of vortex ordering.

3. Breakdown of small vortex molecules

As discussed, rotation in the intermediate angular momentum regime in small quantum droplets may give rise to formation of vortex molecules which are analogs of vortex lattice states of infinite systems. However, in finite-size systems, edge effects may play an important role. This was also noted in the context of Wigner crystallization in quantum dots, where the onset of localization occurs at electron densities which are much higher than the corresponding values for the infinite 2D electron gas. The importance of edge effects has also been pointed out for bosonic systems (Cazalilla *et al.*, 2005).

Partly, localization effects account for the fact that also in small systems the $\nu=1/3$ state appears localized as, for example, visible in the pair-correlation functions. The same applies to vortices, and in very small systems it is difficult to make a difference between a vortex molecule and a vortex liquid since both show similar short-distance correlations.

The analysis of few-electron quantum dots using the exact diagonalization method has shown that the final breakup of vortex molecules and the transition into the fractional quantum Hall regime of electrons is associated with the formation of composites of particles and vortices (Saarikoski *et al.*, 2004). Electrons "capture" free vortices, breaking up the vortex molecules. Similar processes have also been reported for bosons in the LLL by analyzing the vortex attachment with reduced wave functions (see Fig. 31).

These calculations suggest, however, that vortices continue to show ordering at surprisingly low particle-to-vortex filling factors, well below the obtained stability limits of vortex lattices in bosonic condensates. This is also evident for fermions, as shown in Fig. 24, where hole correlations show vortex molecules at very high angular momentum and large zero-point fluctuations. In the case of fermions, vortex localization may continue to filling factors down to $\nu=\frac{1}{2}$ where a transition from prominent vortex localization into particle localization occurs (Emperador, 2006). These calculations showed signs of vortex-hole bunching and the formation of concentric rings of localized vortices, until the number of (free) vortices was equal to the number of particles. Below $\nu=\frac{1}{2}$, no such signatures are seen. Instead, this regime is characterized by particle localization. The conditional probability densities begin to show prominent localized structures (Koskinen *et al.*, 2001; Yannouleas and Landman, 2007). The corresponding bosonic case has not been studied, but due to close analogies of bosonic and fermionic states similar results are expected to hold also for small bosonic droplets where vortex localization should disappear at $\nu_{pv}=1$.

These results suggest that signatures of vortex localization in small systems disappear at a particle-to-vortex ratio which is an order of magnitude lower than the value where vortex lattice melting occurs in large bosonic condensates. However, as mentioned, in small systems the separation of liquid and solid is difficult, and the observed transition is also related to the formation of composite particles (see Sec. IV.F).

E. Giant vortices

In multiply quantized vortices, the phase changes several integer multiples of 2π when encircling the singularity. However, they are not stable in a purely harmonic confinement potential. The existence of many singly quantized vortices is energetically preferred, and the effective repulsive interaction between the vortex cores leads to a lattice of singly quantized vortices (Butts and Rokhsar, 1999; Castin and Dum, 1999; Lundh, 2002). The instability of multiply quantized vortices in harmonic potentials, and the breakup into singly quantized vortices was further discussed by Pu *et al.* (1999) and Möttönen *et al.* (2003). Disintegration of a multiple quantized vortex has also been observed experimentally (Shin *et al.*, 2004).

Rotating condensates in *anharmonic* potentials that rise more rapidly than r^2, however, show a behavior that is different from purely harmonic traps. Most commonly, a quartic perturbation is added to the oscillator confinement.[5] Due to the anharmonicity it is possible to rotate the system sufficiently fast such that the centrifugal force may create a large density hole at the trap center. So-called "giant" vortices with a large core at the center may exist that originate from multiple quantization. Singly quantized vortices may also form a close-packed ensemble inside a large density core. In addition, for certain parameter ranges, the usually quantized lat-

[5]See, e.g., Fetter (2001), Kasamatsu *et al.* (2002), Lundh (2002), Fischer and Baym (2003), Kavoulakis and Baym (2003), Jackson and Kavoulakis (2004), Jackson *et al.* (2004), Fetter *et al.* (2005), Fu and Zaremba (2006), and Blanc and Rougerie (2008).

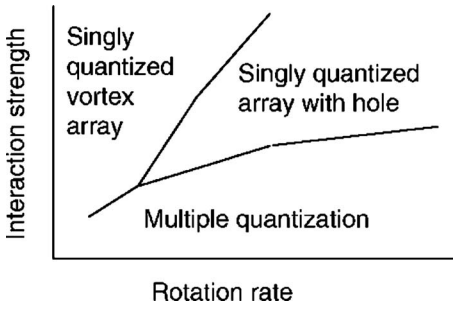

FIG. 32. Schematic phase diagram of the ground states of a bosonic cloud in an anharmonic confinement. From Kavoulakis and Baym, 2003.

tice exists. Kavoulakis and Baym (2003) found a rich phase diagram, for which a schematic is given in Fig. 32, showing the different possible phases as a function of the interaction strength and the trap rotation.

In the following, we discuss the formation and structure of such giant vortex states both in bosonic and in fermionic quantum droplets.

1. Bose-Einstein condensates in anharmonic potentials

Lundh (2002) proposed that in the presence of anharmonicity of the confining trap potential multiply quantized vortices with a giant vortex core could exist in a rotating condensate, and calculated the ground-state vortex structures within the Gross-Pitaevskii formalism. In fact, vortices in these states are not truly multiple-quantized vortices but rather dense-packed ensembles of single-quantized vortices (Kasamatsu *et al.*, 2002; Fischer and Baym, 2003). Phase singularities do not completely merge into the same point because the residual interaction between phase singularities is logarithmic as a function of intervortex separation in the region of low particle density surrounding the cores. Despite this fact, the composite core has a large and uniform spatial extent. Therefore, the name "giant vortex" was coined for these structures. Depending on the strength of the anharmonicity, the condensate can exist in a phase where only single-quantized vortices occur, in a state where all vortices form a giant vortex, and in a mixed phase where both giant and single-quantized vortices exist (Kasamatsu *et al.*, 2002; Kavoulakis and Baym, 2003; Jackson and Kavoulakis, 2004; Jackson *et al.*, 2004). An example of the latter is shown in Fig. 33.

We further note that anharmonicity, which is required for giant vortex formation, may be induced also via the presence of another, distinguishable particle component. The interaction between the particles would then create an *effectively* anharmonic potential for the particle components which may induce giant vortex formation (Bargi *et al.*, 2007; Christensson, Bargi, *et al.*, 2008; Yang *et al.*, 2008). This is discussed in Sec. V in the context of multicomponent quantum droplets.

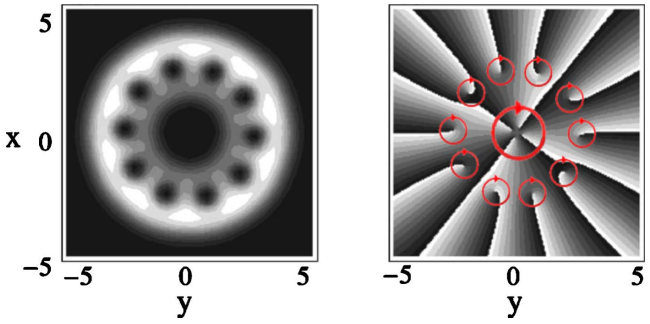

FIG. 33. (Color online) A rotating Bose-Einstein condensate in a mixed state with a giant vortex in the center surrounded by ten single-quantized vortices. The giant vortex is composed of four phase singularities. The left panel shows the particle density (white is high density and black is zero density) and the right panel shows the phase profile. Locations of phase singularities are marked with circles. The large circle marks the ensemble of four phase singularities in the core of the giant vortex. Adapted from Kasamatsu *et al.*, 2002.

2. Giant vortices in quantum dots

Giant vortex structures are predicted to also form in fermionic droplets with repulsive interactions, as shown by exact diagonalization calculations for few-electron quantum dots (Räsänen *et al.*, 2006). Similarly to the bosonic case, giant vortices emerge in anharmonic confining potentials and their structure shows a large core with multiple phase singularities. It was found that even a slight anharmonicity in the confining potential is sufficient for these giant vortex states to become energetically favorable. In addition to the particle interactions, fluctuations tend to keep phase singularities separated, broadening the charge deficiency in the core to a larger area (see Fig. 34). The electron density of a central giant vortex state shows a ringlike distribution.

Unlike bosonic systems, giant vortices with repulsive fermions were only found in the limit of small numbers

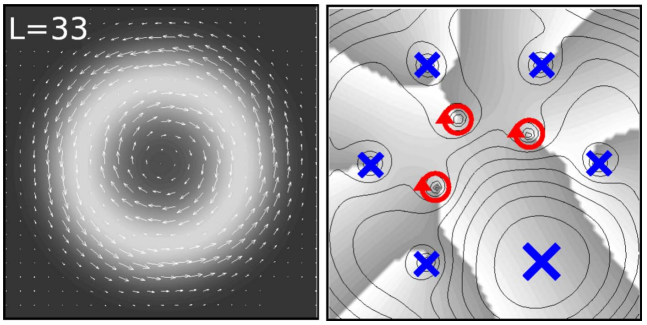

FIG. 34. (Color online) A giant vortex in a six-electron quantum dot calculated with the exact diagonalization method. The left panel shows the particle density (black is low density) and current density (arrows), and the right panel shows the reduced wave function, where phase singularities are marked with circles and electron positions with crosses. The giant core in this case comprises three phase singularities. Interactions and fluctuations keep the phase singularities separated. The probe electron is on the bottom right. From Räsänen *et al.*, 2006.

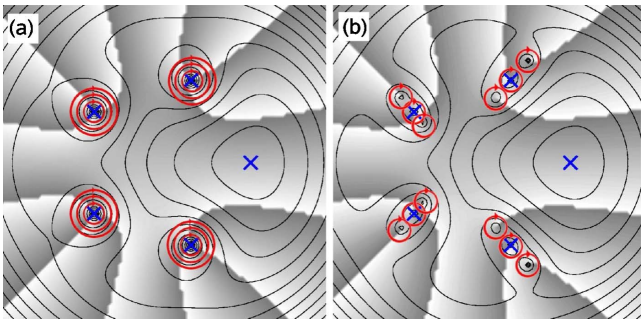

FIG. 35. (Color online) The reduced wave functions for (a) the approximate Laughlin state $\nu=\frac{1}{3}$ and (b) the exact $L=30$ ground state for five electrons in a parabolic external potential. The Laughlin state fixes a triple vortex (concentric rings) on each electron position (crosses). In the exact solution there are clusters of three vortices near each electron.

of particles. This could be seen as another manifestation of the tendency of vortices to drift toward the edge of the droplet in the limit of large particle numbers (see Sec. IV.A.3), breaking apart the giant vortex pattern at the center. In electron droplets interacting via Coulomb forces, density-functional calculations predicted that giant vortex formation is generally limited to systems with less than 20 fermions (Räsänen *et al.*, 2006).

F. Formation of composite particles at rapid rotation

In the regime of high vorticity, electron-vortex correlations are particularly strong and cause vortices to be bound to electrons. This regime is ultimately linked with the fractional quantum Hall effect in the 2D electron gas. Actually, early works aiming to explain this effect used a disk geometry (Girvin and Jach, 1983; Laughlin, 1983) and are in fact more relevant for quantum dots than for the bulk properties of quantum Hall systems.

Figure 35 shows the nodal structure of the reduced wave function for the Laughlin state for $N=5$ electrons as well as the corresponding $L=30$ state obtained with the CI method. In the Laughlin $\nu=\frac{1}{3}$ state, there are three vortices on each electron position, one Pauli vortex and two extra vortices, as shown in Fig. 35(a). In the exact wave function, there are clusters of three vortices near each electron (except near the probe electron). There is one vortex on top of each electron position, as required by the Pauli principle, but, in addition, there are two vortices very close by, separated by their mutual repulsion to opposite sides. Calculations show that small changes in the position of one of the fixed electrons in the reduced wave function causes the vortex to be dragged along with the electron, which indicates vortex attachment to the electron. The overlap between the exact state and the Laughlin approximation is 0.98. The state can be interpreted as a finite-size precursor of the $\nu=\frac{1}{3}$ fractional quantum Hall state, for which the Laughlin wave function yields an accurate description. However, in contrast to the Laughlin state, the attachment of nodes to particles in the exact wave function shows a small spatial separation.

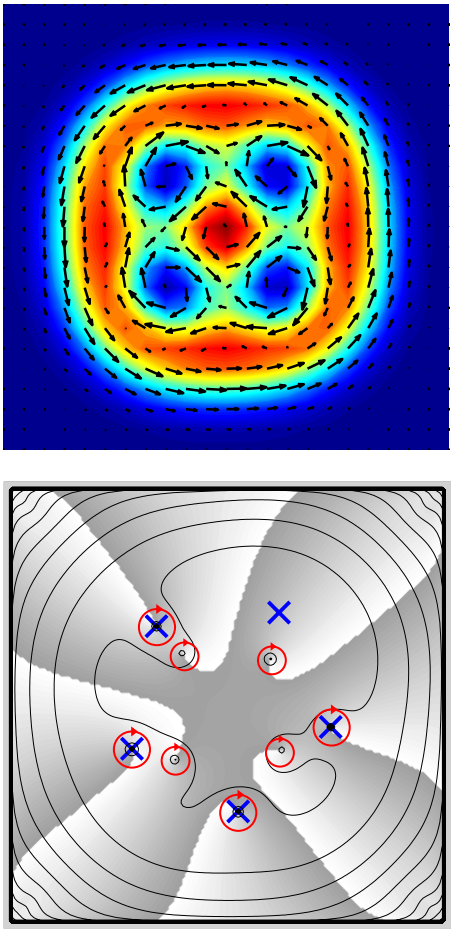

FIG. 36. (Color online) A $\nu=\frac{1}{3}$ state of five electrons in a harmonic trap. Top: Electron density from the density-functional method and current density (arrows). The confinement strength is $\hbar\omega_0=5$ meV and the magnetic field is $B=18$ T. Bottom: Reduced wave function for the same state constructed from the Kohn-Sham single-particle states. The probe electron is at the top right.

The attachment of vortices to particles also explains the absence of vortices for the probe electron in the exact many-body state (see Fig. 35). In the fractional quantum Hall regime, the density-functional method failed to reveal the correct nature of the ground state. The solutions of the spin as well as current-spin-density-functional theory show only a cluster of vortices inside the electron droplet, but these methods are unable to associate two extra vortices to each electron (Saarikoski, Harju, *et al.*, 2005); see Fig. 36.

The density-functional approach fails to properly include these correlations. A single-determinantal wave function constructed from the self-consistent Kohn-Sham orbitals yields an approximate description for few-vortex states near $\nu=1$, but the overlaps with the exact wave functions diminish as the angular momentum of the system increases. Figure 37 shows that for a five-electron system at $\nu=1/3$ the overlap is only of the order of 0.5. Compared to this, the overlap with the Laughlin

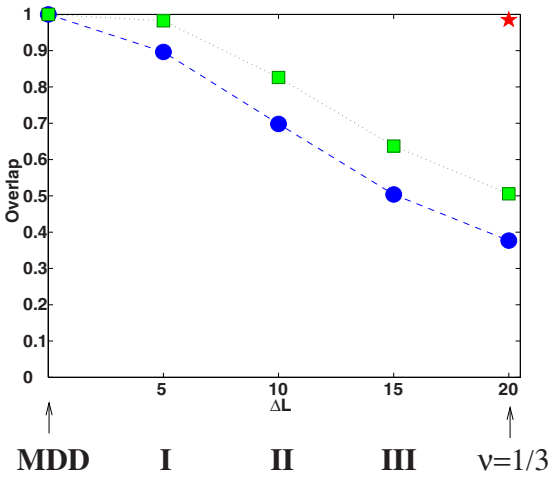

FIG. 37. (Color online) Overlap of a single-determinant wave function with the exact one as a function of the angular momentum increase with respect to the MDD state $\Delta L = L - L_{\mathrm{MDD}}$ for five electrons in parabolic confinement. The higher points (squares) are obtained with a coordinate transformation to the center of mass $z_i \rightarrow z_i - z_{\mathrm{CM}}$ and the lower ones (circles) without it. The star at $\Delta L = 20$ shows the overlap with the Laughlin $\nu = 1/3$ state. The roman numbers count the vortices inside the electron droplet. From Harju, 2005.

$\nu = 1/3$ wave function that amounts to 0.98 is high.

When the angular momentum of the droplet increases further, additional vortices appear in the Laughlin-like state and the filling factor decreases below $\nu = 1/3$. These vortices are not bound to composite particles, rather they correspond to the Laughlin excitations with fractional charge. The pattern of vortex formation is expected to be similar to that after the MDD: first a single vortex enters from the surface and moves toward the center until it is energetically favorable to have two vortices, etc. This is illustrated in Fig. 38, which shows the vortex sites for a five-electron system determined from the reduced wave function. Again, a similar behavior is expected in the case of bosonic particles. However, despite the recent progress in realizing BECs at extreme rotation (Lin *et al.*, 2009), an analysis of these states appears still to be beyond the current experimental capabilities.

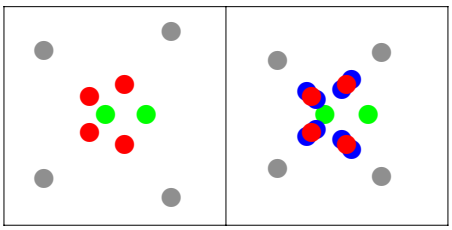

FIG. 38. (Color online) Schematic of the sites of vortices, determined from the reduced wave function of an exact diagonalization for five electrons with angular momentum $L = 16$ (six above the MDD, left) and $L = 36$ (six above the state with filling factor 1/3, right). Fixed electron positions with Pauli vortices, vortices attached to electrons making composite particles, and free vortices inside the electron droplet are denoted by bullets. Free vortices outside the droplet are shown by gray bullets.

There are two basic mechanisms to unbound the vortices from the particles, namely the softening of the interaction potential by the finite thickness of the system, and second by impurities. When the system has a finite thickness, the incompressible $\nu = 1/3$ Laughlin state breaks down as the vortices are gradually less bound to the electron coordinates. This effect is in contrast to the screening of the Coulomb interaction energy whereby, in the strong-screening limit, the zeros are exactly localized to the electron positions (Tölö and Harju, 2009). We should also mention that repulsive impurities attract vortices at the impurity position (Bårdsen *et al.*, 2009).

V. MULTICOMPONENT QUANTUM DROPLETS

Multicomponent quantum droplets are composed of different particle species that may, for example, be different atoms, different isotopes of the same atom, different spin states of an atom or electron, or even different hyperfine states of an atom. In such systems intercomponent interactions can modify the many-body wave function significantly.

The properties of multicomponent BECs have been discussed, both experimentally and theoretically, over the past few years. For recent reviews on multicomponent BECs, see Kasamatsu *et al.* (2005a) and Fetter (2009). We do not attempt to cover the vast literature on binary or spinor BECs but instead set our focus mainly on structural properties and vorticity of few-particle droplets and the analogies between bosonic and fermionic two-component systems. Only a brief outlook on spinor condensates with more components is given at the end of this section.

Theoretical studies of multicomponent quantum liquids were performed in the 1950s for superfluid helium mixtures, see, for example, the early works by Guttman and Arnold (1953), Khalatnikov (1957), and Leggett (1975). Examples for vortex patterns include the Mermin-Ho vortex (Mermin and Ho, 1976) and the Anderson-Toulouse vortex (Anderson and Toulouse, 1977). These vortices are nonsingular and the order parameter is continuously rotated by superposing a texture on it (see below). Recently doubly quantized vortices in the A phase of ^{3}He were found by Blaauwgeers *et al.* (2000). With ultracold atoms, condensate mixtures may be achieved using different atomic species, such as ^{87}Rb and ^{41}K (Modugno *et al.*, 2002) or, for example, the different isotopes of ^{87}Rb (Burke *et al.*, 1998; Bloch *et al.*, 2001) in the same trap.

Another possibility to create multicomponent condensates is given by the different hyperfine states of the same atom, as, for example, ^{87}Rb with the hyperfine states $|F=1, m_f=-1\rangle$ and $|F=2, m_f=1\rangle$ (Myatt *et al.*, 1997; Hall, Matthews, Ensher, *et al.*, 1998; Hall, Matthews, Wieman, *et al.*, 1998; Matthews *et al.*, 1998, 1999). The atoms in the two states have nearly equal intercomponent and intracomponent scattering lengths, and the

spin flip rate is small due to weak hyperfine coupling, which yields a stable two-component system with a long lifetime (Julienne *et al.*, 1997; Kasamatsu *et al.*, 2005a). In fact, the first experiment by Matthews *et al.* (1999) creating vortices in a BEC made use of these internal spin states, following a suggestion by Williams and Holland (1999): they proposed a phase-imprinting technique, where an external coupling field was used to control independently the two components of the quantum gas. In this way, angular momentum could be induced in one component that formed a quantized vortex around the nonrotating core of the other component when the coupling was turned off. Since the magnetic moments for the ^{87}Rb atoms in the two hyperfine states are nearly equal, they could be confined by the same magnetic trap.

Optical traps have the advantage that one is not restricted by certain hyperfine spin states. Already in 1998, experimentalists at MIT could create a BEC of ^{23}Na (Stamper-Kurn *et al.*, 1998; Stenger *et al.*, 1998) where different "spinor" degrees of freedom of the atomic quantum gas can be trapped simultaneously. Other examples are ^{39}K and ^{87}Rb (Barrett *et al.*, 2001). In these alkali systems one can trap the three projections of the hyperfine multiple with $F=1$, adding three (internal) degrees of freedom to the system. However, population exchange (without trap loss) among the hyperfine states may occur due to spin-relaxation collisions (Stenger *et al.*, 1998). The dynamical loss of polarization of a BEC due to spin flips was examined by Law *et al.* (1998). Larger atom spins can also be realized as, for example, with ^{85}Rb and ^{133}Cs. Such condensates show a wealth of quantum phenomena that do not occur in simple scalar condensates (Ho, 1998; Ohmi and Machida, 1998). The interactions between the different components of the trapped cold-atom gas may lead to topologically interesting, new quantum states.

Rotating two-component fermion droplets may be realized with electrons in quasi-two-dimensional quantum dots (Reimann and Manninen, 2002) with a spin degree of freedom. Usually, the magnetic field causes polarization of the droplet due to the Zeeman coupling. However, in 2D electron systems, the Zeeman splitting can be tuned by applying external pressure (Leadley *et al.*, 1997) or by changing the Al content in a GaAs/Al_xGa_{1-x}As sample (Weisbuch and Hermann, 1977; Salis *et al.*, 2001). In systems with low Zeeman coupling the regime of vortex formation beyond the maximum density droplet is associated with various spin polarization states (Siljamäki *et al.*, 2002). These states occur in much analogy to those in two-component bosonic systems (Saarikoski *et al.*, 2009). In the regime of rapid rotation, some of the many-electron states can also be identified as finite-size counterparts of nonpolarized quantum Hall states, such as the much studied $\nu=\frac{2}{3}$ and $\frac{2}{5}$ states (Chakraborty and Zhang, 1984; Xie, Guo, and Zhang, 1989).

A. Pseudospin description of multicomponent condensates

For a bosonic condensate with n components, the order parameter ψ becomes of vector type $(\psi_1,\psi_2,\ldots,\psi_n)$. One may interpret this as a "pseudospin" degree of freedom (Kasamatsu *et al.*, 2005a, 2005b). As an example, for $n=2$ distinguishable particles of type A or B the order parameter is then a spinor-type function, $\psi=(\psi_A,\psi_B)$, and the pseudospin $\mathbf{T}$ points "up" $(T=1/2)$ or "down" $(T=-1/2)$ for either of the two components in the absence of the other. This concept straightforwardly extends to higher half-integer as well as integer pseudospins.

When rotation is induced in the multicomponent or spinor system, vortex formation becomes much more complex due to the increased freedom of the system to carry angular momentum. Spatial variations in the directions of the atomic spins may lead to different patterns, such as the aforementioned spin textures. For atomic quantum gases, these structures were investigated theoretically.[6] Many theoretical studies applied the spin-dependent Gross-Pitaevskii formalism. The Thomas-Fermi approach has been used to determine the density profiles of ground state and vortex structures for two-component mixtures of bosonic condensates (Ho and Shenoy, 1996). This approach was later simplified to describe segregation of components in the presence of vorticity (Jezek *et al.*, 2001; Jezek and Capuzzi, 2005).

In their most general form, the two-body interactions are often parameterized by $V_{ij}=[c_0+c_2(\mathbf{T}_i\cdot\mathbf{T}_j)]\delta(\mathbf{r}_i-\mathbf{r}_j)$ with the usual contact interactions of strengths c_0. For $c_2>0$, i.e., repulsive spin-dependent interactions as, for example, for ^{23}Na, the system minimizes the total spin. Consequently, this parameter regime is called the "antiferromagnetic" one, while for $c_2<0$ as, for example, for ^{87}Rb, the spin interactions are called "ferromagnetic" (Ho, 1998; Stamper-Kurn *et al.*, 1998; Stenger *et al.*, 1998; Miesner *et al.*, 1999). Typically, the ratio of the spin-dependent and spin-independent parts of the contact interaction is of the order of a few percent. In the following we set $c_2=0$ and restrict the discussion to the special case of SU(2) symmetry, unless otherwise stated.

B. Two-component bosonic condensates

We now consider a bosonic gas of atoms that is a mixture of two distinguishable species A and B with fixed numbers of atoms N_A and N_B. The majority of experimentally studied two-component gases has similar interactions between the like and unlike species. Similar s-wave scattering lengths yield a small inelastic spin exchange rate (Julienne *et al.*, 1997), providing a stable

[6]See, e.g., Ho (1998), Ohmi and Machida (1998), Yip (1999), Al Khawaja and Stoof (2001a, 2001b, 2001c), Chui *et al.* (2001), Isoshima *et al.* (2001), Stoof *et al.* (2001), Isoshima and Machida (2002), Kita *et al.* (2002), Martikainen *et al.* (2002), Mizushima, Machida, and Kita (2002a, 2002b), Mueller (2004), and Reijnders *et al.* (2004).

two-component system with a long lifetime (Kasamatsu *et al.*, 2005a). Therefore, the case $g_{AA} \approx g_{BB} \approx g_{AB}$ (with interaction strengths as defined in Sec. IV.A) appears as the most relevant one. Thus, we first assume equal and (pseudo)spin-independent coupling strengths g between all particles and also choose the harmonic trapping potentials for the two components to be identical. As mentioned, the two-component Bose gas is then described by a pseudospin 1/2 and the order parameter is a vector, (ψ_A, ψ_B).

As shown in Sec. IV, for repulsive interactions a condensate with only one kind of atoms that is brought to rotation develops a single vortex at the trap center at $L/N=1$. With increasing angular momentum, the single component, so-called "scalar," condensate nucleates an increasing number of vortices inside the condensate, until the triangular Abrikosov vortex lattice is formed (Madison *et al.*, 2000; Abo-Shaeer *et al.*, 2001). For weakly interacting and dilute gases, this was also found within Gross-Pitaevskii mean-field theory (Butts and Rokhsar, 1999; Kavoulakis *et al.*, 2000). The case of a two-component gas is more complex since the system may divide its angular momentum between its components. One possibility is that one component is at rest, while another carries all the angular momentum. The component at rest may then fill the core of the first vortex in the other component, creating a so-called *coreless* vortex state. When the rotation increases, the Abrikosov lattice of the scalar condensate now may become a lattice of such coreless vortices. The vortex lattice geometry depends crucially on the interactions between the components and the sizes and numbers of components.

1. Asymmetric component sizes

Figure 39 shows the mean-field (Gross-Pitaevskii) densities and phases of the order parameters ψ_A and ψ_B for a two-component condensate with unequal particle populations $N_B > N_A$ (Bargi *et al.*, 2007, 2008).

At $L/N_A=1$, the system forms a single vortex in the smaller component A, which is seen in the phase plot of the order parameter in Fig. 39. The phase jump is 2π along any closed path encircling the origin. The larger component rests at the origin $L_B=0$ with no vorticity (and, correspondingly, a flat phase profile in the order parameter). When the angular momentum reaches $L=N_B$, a singly quantized coreless vortex is formed in the larger component B, while the component A now is stationary at the origin.

Referring back to the work of Skyrme in the context of nuclear and high-energy physics (Skyrme, 1961, 1962) such coreless vortices were also called "Skyrmions," see the review by Kasamatsu *et al.* (2005a).[7]

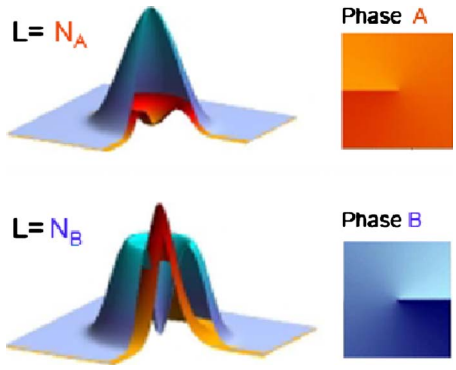

FIG. 39. (Color online) Densities (left) and phases (right) in a two-component rotating Bose-Einstein condensate, as obtained from the Gross-Pitaevskii equations, for a ratio of atom numbers in the two components of $N_A/N_B=0.36$ and equal coupling strengths $g_{AA}=g_{AB}=g_{BB}=50$ a.u. (The densities are cut in one quadrant in order to visualize them for both components in one diagram.) The rotational frequency is $\Omega=0.45$. The upper panel shows a coreless vortex at angular momentum $L=N_A$, where the smaller component A shows a unit vortex at the center, as seen from the phase of Ψ_A plotted to the right (from dark to light shading), changing by 2π when the center is encircled once. The phase singularity is absent in B component. The lower panel shows the case $L=N_B$, where now the larger component encircles the smaller one, filling the unit vortex at the center. The phase singularity consequently now occurs in the order parameter of B component, as shown to the right (from dark to light). From Bargi *et al.*, 2008.

A graphic illustration of the pseudospin behavior in a single coreless vortex state is given in Fig. 40 by Mueller (2004), showing the top and perspective view of such a Skyrmion in a two-component system. As L increases, beyond $L=N_B$, a second vortex enters the larger component B, merging with the other vortex at $L=2N_B$. The smaller component A remains localized at the center, and the system as a whole has a twofold phase singularity at the center. An example is shown in Fig. 41. The central minimum in the density of the larger component B expands with increasing angular momentum. It encircles the smaller one, that is nonrotating and localized at the trap center. A phase change of 4π in a closed path around the center indicates a vortex that is twofold quantized. At $L=3N_B$ a triple phase singularity emerges at the center, but eventually the scenario breaks down with increasing rotation frequency.

In single-component quantum liquids, multiply quantized vortices are not favored in parabolic potentials. However, any external potential that grows more rapidly than quadratically may give rise to these giant vortex structures (Lundh, 2002; Kavoulakis and Baym, 2003) discussed in Sec. IV.E. In two-component systems, it was found that the smaller nonrotating component at the trap center may effectively act as an additional potential to the (harmonic) trap confinement, rendering the potential effectively anharmonic close to the trap center for the rotating component (Bargi *et al.*, 2007). With increasing rotation, both components carry a finite frac-

[7]This terminology has also been used for analogous textures in liquid ^{3}He-A (Mermin and Ho, 1976; Anderson and Toulouse, 1977; Salomaa and Volovik, 1987) and in quantum Hall states (Lee and Kane, 1990; Sondhi *et al.*, 1993; Barrett *et al.*, 1995; Aifer *et al.*, 1996; Oaknin *et al.*, 1996).

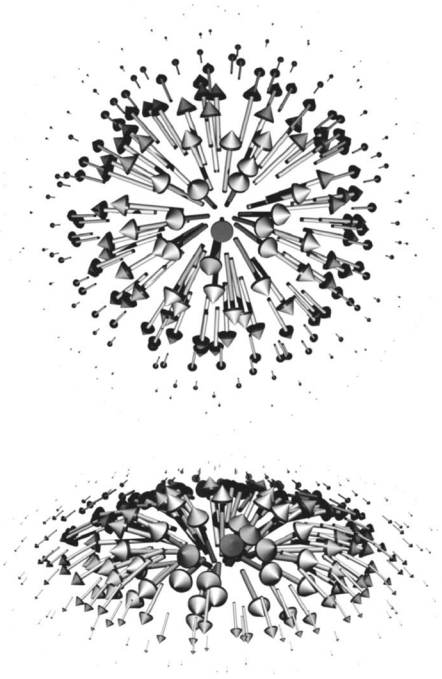

FIG. 40. Schematic of a Skyrmion (top and perspective). The spin tilts from "up" for one component at the center, where one component shows a maximum density filling the vortex in the other component, to "down" toward the edge. From Mueller, 2004.

tion of the total angular momentum, and multiply quantized or giant vortex states are no longer energetically favorable.

In exact diagonalization studies of multicomponent systems, the additional degree of freedom through the pseudospin increases the dimension of the Hamiltonian matrix significantly, which leads to severe restrictions in the particle numbers or angular momenta that can be studied. Nevertheless, the results obtained for few-particle systems confirm the existence of Anderson-Toulouse and Mermin-Ho types of coreless vortices, as obtained within the Gross-Pitaevskii approach. For a two-component system with $N_A+N_B=8$ bosons with contact interactions in a harmonic trap, Fig. 42 shows the total angular momentum L as a function of the rotational frequency Ω/ω. As in the case of scalar Bose gases (see Fig. 14), plateaus with increasing Ω can be associated with vortices that successively enter the bosonic cloud with increasing trap rotation (Butts and

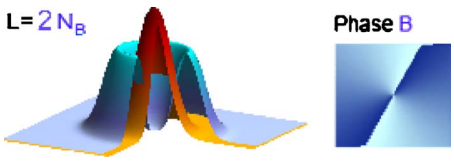

FIG. 41. (Color online) Densities (left) and phases (right) of the Gross-Pitaevskii order parameters in a two-component rotating Bose-Einstein condensate with a coreless vortex with a double phase singularity. For notation see Fig. 39. Adapted data from Bargi *et al.*, 2008.

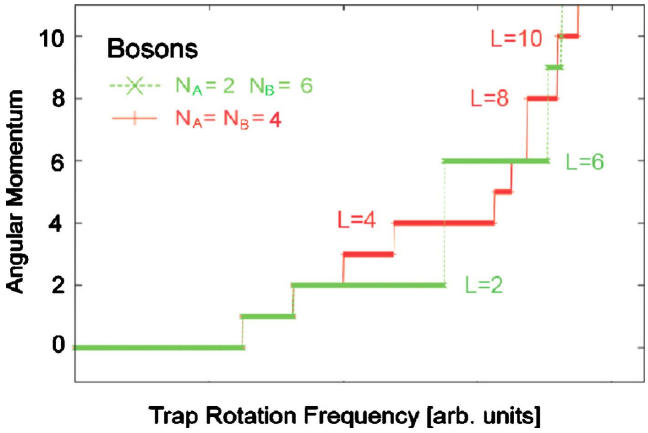

FIG. 42. (Color online) Angular momentum as a function of the trap rotation frequency (in arbitrary units) for $N=8$ bosons with equal masses and interactions, in a harmonic trap, for equal population ($N_A=N_B=4$) and unequal population ($N_A=2$ and $N_B=6$). From Bargi *et al.*, 2010.

Rokhsar, 1999; Kavoulakis *et al.*, 2000). These plateaus correspond to cusp states along the yrast line in the two-component system (Bargi *et al.*, 2010).

The exact quantum states retain the symmetry of the Hamiltonian, and thus one must turn to conditional probability densities (pair-correlation functions) and reduced wave functions to map out the internal structure of the wave function, as discussed in Sec. II. For unequal populations of the two species, here $N_A=2$ and $N_B=6$, at those angular momenta where the pronounced plateaus occur in the L versus Ω plot in Fig. 42, the pair correlations are shown in Fig. 43.

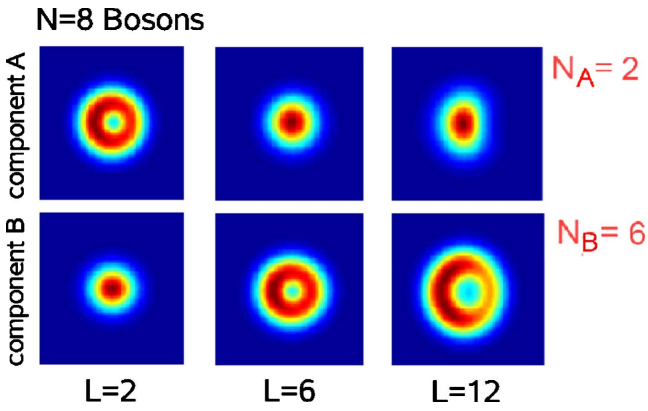

FIG. 43. (Color online) Density plots of conditional probabilities for a two-component few-boson system in a harmonic trap, with two bosons in component A and six bosons in component B. The reference point was chosen in component B at an off-center position close to the maximum of the probability density. Axes are from (−4,4) in atomic units. The scale in the density plots is from zero to maximum. (To increase the visibility, the plot range of the conditional probabilities in the two components was re-scaled to the same constant in all panels.) The charge deficiency of the vortex cores causes deep minima to appear in the pair-correlation functions. Adapted from Bargi *et al.*, 2010.

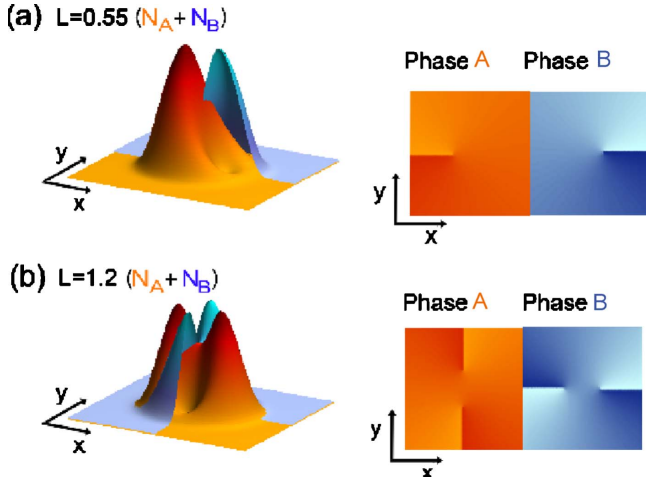

FIG. 44. (Color online) Mean-field order parameters (left) and phases (right) of a symmetric condensate with $N_A=N_B$, at $L=1.2(N_A+N_B)$, for equal coupling strengths $g_{AA}=g_{AB}=g_{BB}=50$, showing (a) one and (b) two interlaced coreless vortices in the two components. Component B is only shown in a half-plane to make the vortex in the component A visible. Adapted from Bargi *et al.*, 2008.

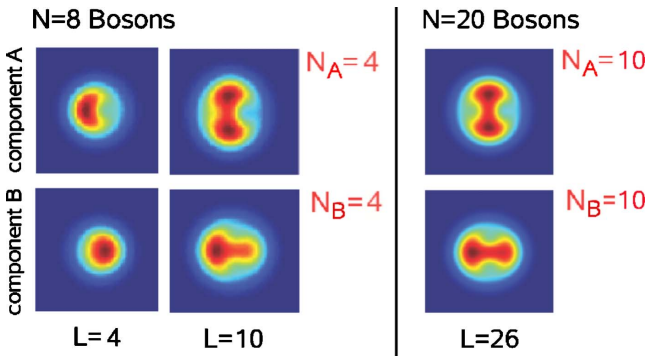

FIG. 45. (Color online) As in Fig. 43, but for equal components $N_A=N_B=4$ (left panel). The density minima in one component coincide with the density maxima in the other component. This suggests that these states are finite-size precursors of interlaced vortex lattices that occur in the limit of large N. The picture becomes much more clear for larger particle numbers, as shown in the right panel for $N=20$ and $L=26$. From Bargi *et al.*, 2010.

At $L=2$ a vortex is seen as a hole at the center in the smaller component, encircling the larger component that forms a Gaussian at the trap center. At angular momentum $L=6$ a single vortex is created in the larger component, as seen in the middle panel. Twice this angular momentum creates a twofold quantized vortex structure in the larger component. The existence of coreless vortices, as predicted by the Gross-Pitaevskii equation in the mean-field limit (Sec. V.B), is accurately reproduced by the exact solutions in the few-body regime.

2. Condensates with symmetric components

When the cloud has equal populations of the two components, i.e., $N_A=N_B$, a different scenario emerges: a vortex enters each of the components from "opposite" sides, reaching a minimum distance of one oscillator length from the center of the trap when $L=N_A=N_B$ (Christensson, Bargi, *et al.*, 2008). An example is given by the Gross-Pitaevskii solution shown in the upper panel of Fig. 44.

Similarly to the one-component case, increasing rotation adds more vortices to the cloud. For two equal components, the vortices become interlaced, with density maxima in one component located at the vortices in the other, minimizing the interaction energy between the different components (lower panel of Fig. 44). In the limit of large N and L a lattice of coreless vortices is formed (Kasamatsu *et al.*, 2005a).

These Gross-Pitaevskii results are in good correspondence with exact diagonalization results of few-particle systems. The left panel of Fig. 45 shows conditional probability densities of a symmetric configuration $N_A=N_B=4$. When $L=N_A=N_B=4$, the clouds separate, with a vortex hole emerging at the maximum density location in the other component. These solutions correspond to a Mermin-Ho vortex (or a meron pair, where each meron accounts for half of the spin texture of the coreless vortex) as obtained in Gross-Pitaevskii theory (Kasamatsu *et al.*, 2005a).

For higher angular momenta, as here for $L=10$, the correlation functions indicate interlaced vortices as in Fig. 44 above, with density maxima in one component localizing at the minima (vortex cores) in the other component. The interlaced pattern of density minima and maxima becomes more apparent with higher particle number as shown in the right panel of Fig. 45 for $N=20$ bosons, where $N_A=N_B=10$, at angular momentum $L=26$.

The conditional probability densities average out the effect of phase singularities as signatures of vortices. However, the nodal structure of the many-body state may straightforwardly be probed by reduced wave functions (Saarikoski *et al.*, 2009) (see Sec. II.C.3), as shown in Fig. 46 for a system with $N_A=N_B=3$ bosons.

Coreless vortices form one by one as the angular momentum increases: in the example shown here for $L=6$ and $L=12$, the phase singularities in one component occur at the most probable positions of the particles of the other component, indicating formation of two and three coreless vortices, respectively, in each particle component (Fig. 46).

3. Vortex lattices and vortex sheets

Vortex lattices in two-component bosonic condensates may show a variety of different structures, depending on the strength and sign of the interspecies interaction (Mueller and Ho, 2002). In the antiferromagnetic case ($c_2>0$), for weak interactions square lattices form, whereas for strong interactions the vortices are arranged into triangular Abrikosov lattices. In the former case the square lattice is energetically favored because the antiferromagnetic interaction between adjacent vortex holes makes a triangular lattice frustrated (Kasamatsu *et al.*,

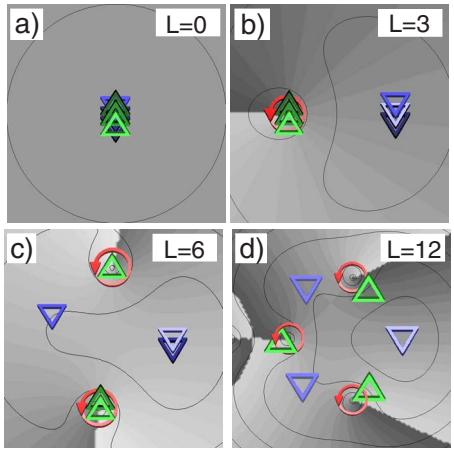

FIG. 46. (Color online) Reduced wave functions in a symmetric system of $N_A=N_B=3$ bosons, showing the correlations between phase singularities (circles) with the most probable positions of the particles of opposite species (triangles). This is an indication for the formation of coreless vortices one by one in the system as the angular momentum increases. (a) The nonrotating state, (b) a state with one coreless vortex per particle species, c) two coreless vortices, and (d) three coreless vortices are shown. Note that for identical components A and B, the reduced wave functions for the two species are necessarily symmetric, and only one component is shown here. From Saarikoski *et al.*, 2009.

2003). At $c_2=0$ the system has metastable states such as a stripe phase. In the regime of ferromagnetic interspecies coupling ($c_2<0$), spin domains spontaneously form. These vortex sheets form "serpentinelike" structures that are nested into each other (Kasamatsu *et al.*, 2003; Kasamatsu and Tsubota, 2009). A number of metastable lattice structures that were energetically almost degenerate have also been found in an antiferromagnetic spin-1 BEC (Kita *et al.*, 2002).

C. Two-component fermion droplets

Recent electronic structure studies of quantum dots with spin degrees of freedom predicted the formation of coreless vortices in fermion droplets analogously to the bosonic case (Dai *et al.*, 2007; Koskinen *et al.*, 2007; Petković and Milovanović, 2007; Saarikoski *et al.*, 2009). This comes as no surprise since analogies in the structure between fermion and boson states (Sec. II.F) are not limited to single-component systems, but an approximate mapping between two-component fermion and boson states can be constructed as well. In the following we discuss coreless vortices in fermion droplets and some of the consequences of the fermion-boson analogy with few-electron droplets as a particular example.

1. Coreless vortices with electrons

The angular momentum for a system with eight fermions with both balanced ($N_A=N_B=4$) and unbalanced ($N_A=2, N_B=6$) component sizes is shown as a function

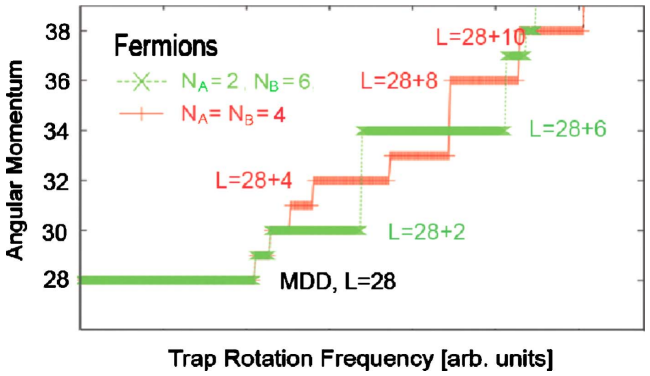

FIG. 47. (Color online) Angular momentum as a function of the trap rotation frequency (in arbitrary units) for $N=8$ fermions with symmetric and asymmetric component occupations, in Fig. 42. From Bargi *et al.*, 2010.

of the trap rotation frequency in Fig. 47. The staircase shape is strikingly similar to the bosonic counterpart (Fig. 42) with $L_{\text{boson}}=L_{\text{fermion}}-L_{\text{MDD}}=L_{\text{fermion}}-28$. In the fermion case with asymmetric components $N_A=2$ and $N_B=6$, the first pronounced plateaus appear at $L=L_{\text{MDD}}+N_A=28+2$ and $L=L_{\text{MDD}}+N_B=28+6$, which correspond to a coreless vortex in the A and B components, respectively. In the case of symmetric component occupations $N_A=N_B=4$ the first major plateau moves to $L=L_{\text{MDD}}+4$ and the coreless vortex configuration is analogous to a meron pair (Petković and Milovanović, 2007) in bosonic systems. The lengths of these plateaus indicate that coreless vortex states are also stable in fermion systems.

The fermionic "quantum-dot" analog to the unbalanced few-boson system (with $N_A=2$ and $N_B=6$) discussed above would be a system with $N=8$ electrons and fixed $S_z=2$, which demands two spins antiparallel to the external magnetic field (component A) and six spins parallel to the field (component B). Both components form compact maximum density droplets independently at $L_{\text{MDD}}=28$ that corresponds to the $L=0$ nonrotating condensate in the bosonic case. When the angular momentum exceeds that of the MDD by two units of $\hbar$, a hole forms at the center of the smaller component which is associated with a vortex state, while the larger one remains a MDD. This can be seen from the pair-correlated density shown in Fig. 48. Note that in the case of fermions, there is a clearly visible exchange-correlation hole around the reference point in the pair correlation. This is due to the Pauli principle which is naturally absent in the bosonic case. Due to the strong repulsion between fermions, this hole is mirrored in the other component. For larger angular momentum, multiply quantized vortices are found in the larger component, in direct analogy to the bosonic case discussed above. This happens in our example for $L_{\text{fermion}}=L_{\text{MDD}}+6$ and $L_{\text{fermion}}=L_{\text{MDD}}+12$ (shown in Fig. 48).

The case of equal components corresponds to fixed $S_z=0$. For $L=N_A=N_B$, just as in the bosonic case, a vortex appears at some distance from the trap center, with a

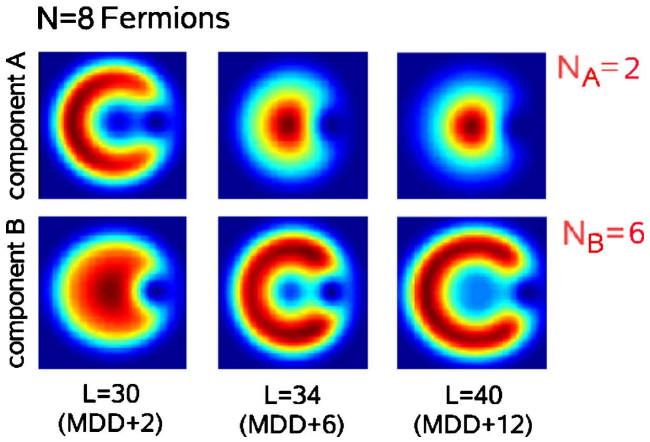

FIG. 48. (Color online) Pair-correlated densities for fermions, as in Fig. 43, but here for *fermions* with Coulomb interactions (N_A=2 and N_B=6). Angular momenta corresponding to the pronounced plateaus in Fig. 47 are shown. Compared to the bosonic case the densities show analogous structures except for an additional exchange hole at the reference point in component B which is reflected also in the component A due to Coulomb repulsion. From Bargi *et al.*, 2010.

density maximum on the other side, and vice versa. These textures are again similar to the meron pairs in the bosonic two-component system discussed above. For higher angular momenta, the interlaced vortex lattice is seen for fermions at $L=L_{\mathrm{MDD}}+8$ and $L=L_{\mathrm{MDD}}+10$ (see Fig. 49). (Note again the occurrence of the exchange hole, that should not be confused with the holes of off-electron vortices.)

Figure 50 shows the reduced wave functions [see Eq. (11)] for a two-component fermion droplet with Coulomb interactions and N=6 particles, with symmetric component occupations $N_A=N_B=3$. The sequence of states in this figure shows the formation of coreless vortices one by one inside the fermion droplet, in analogy to the bosonic case in Fig. 46, with the angular momenta for boson and fermion systems shifted by $L_{\mathrm{fermion}}=L_{\mathrm{boson}}+L_{\mathrm{MDD}}$. In comparison to the bosonic case, for fermions the Pauli vortices keep the particles further apart.

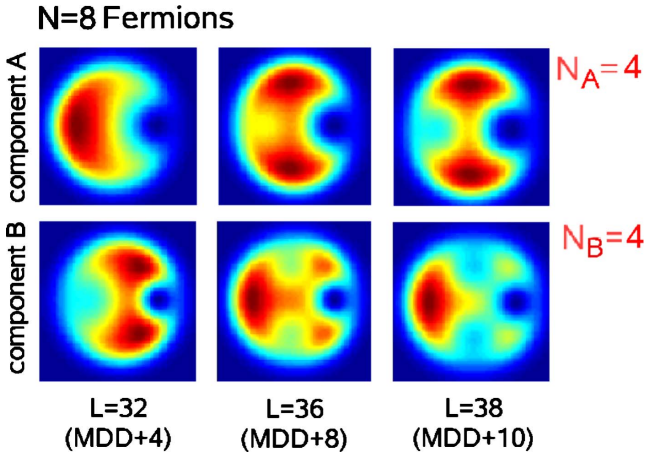

FIG. 49. (Color online) Pair-correlated densities for fermions, as above, but for S_z=0, i.e., equal components (N_A=4 and N_B=4). From Bargi *et al.*, 2010.

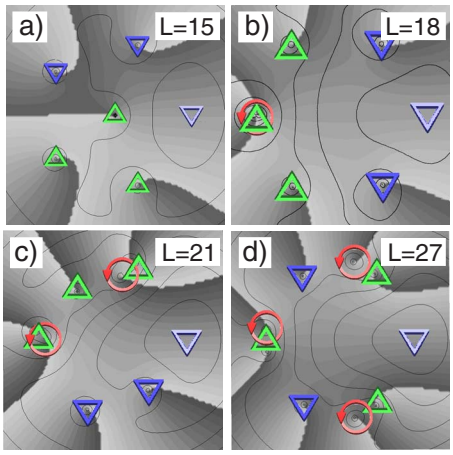

FIG. 50. (Color online) Reduced wave functions in a two-component system. In a two-component fermion droplet with symmetric occupations $N_A=N_B=3$ the reduced wave function in the lowest Landau level reveals coreless vortices as correlations between phase singularities (circles) with the most probable positions of the particles of opposite spin (triangles). (a) The MDD state with total spin S=3 and S_z=0, (b) a state with one coreless vortex per particle species, (c) two coreless vortices, and (d) three coreless vortices are shown. This sequence of states is analogous to that of a bosonic system in Fig. 46. Note that vortices of the MDD state are not shown in order to ease the comparison to the bosonic case. From Saarikoski *et al.*, 2009.

2. Quantum dots with weak Zeeman coupling

The formation of coreless vortices, as discussed, can also be observed in quantum dots where Zeeman coupling is weak. Then, the first reconstruction of the MDD may not be directly into the completely polarized states with one additional vortex, but into an excitation which is reminiscent of the vortex state, with one spin flipped antiparallel to the magnetic field. This transition would be followed by a second one, involving a spin flip into the completely polarized state (Oaknin *et al.*, 1996). Siljamäki *et al.* (2002) studied the effect of Landau-level mixing in the MDD reconstruction, using the variational quantum Monte Carlo method. They found significant changes in the ground states for systems consisting of up to seven electrons. Figure 51 shows the different states of a six-electron quantum dot in the vicinity of the MDD.

The partially polarized state after the MDD has a leading determinant of the form $|01111100\cdots\rangle$ for the majority-spin component and $|100\cdots\rangle$ for the minority-spin component: the vortex hole at the center of the dot in the majority-spin component is filled by a particle with opposite spin polarization. Consequently, the state shows formation of a coreless vortex and is completely analogous to the case of asymmetric particle populations in a two-component bosonic system, as discussed in Sec.

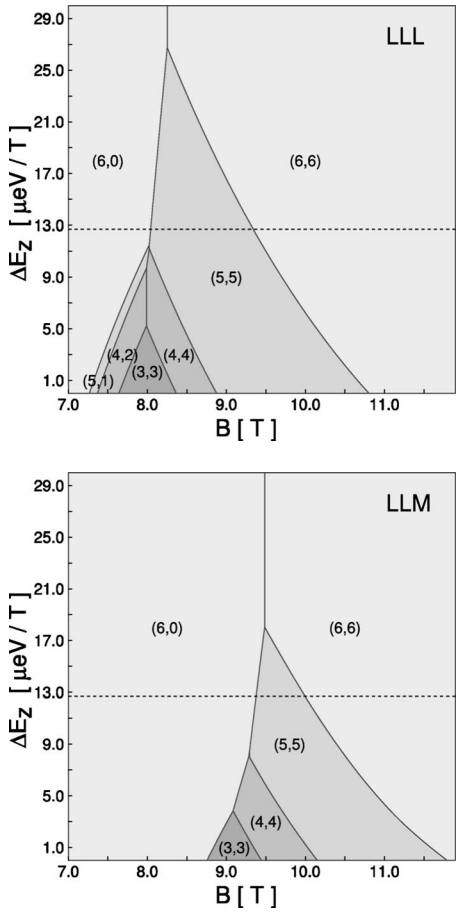

FIG. 51. Partially polarized states beyond the maximum density droplet reconstruction, obtained from a variational Monte Carlo study by Siljamäki *et al.* (2002). The diagrams show the different states of a six-electron quantum dot as a function of the magnetic field and the strength of the Zeeman coupling per spin in the lowest Landau-level (LLL) approximation (upper panel) and including Landau-level mixing (LLM) (lower panel). The states are labeled as $(N_\uparrow,\Delta L)$, where $N_\uparrow$ is the number of electrons with spins parallel to the magnetic field and $\Delta L = L - L_{\mathrm{MDD}}$ is the additional angular momentum with respect to the MDD. The Zeeman coupling strength for GaAs is marked by dashed lines. The confinement strength is $\hbar\omega = 5$ meV and the material parameters are for GaAs, $m^*/m_e = 0.067$ and $\epsilon_r = 12.4$.

V.B.1. The minority-spin component has a MDD-like structure, which corresponds to the nonrotating component in the bosonic case, and the majority-spin component shows a single vortex core localized at the center.

3. Nonpolarized quantum Hall states

In the regime of rapid rotation vortices are expected to also attach to particles in two-component quantum droplets. One of the studied model wave functions for two-component states was introduced to explain the quantum Hall plateau at $\nu = 2/3$ (Halperin, 1983):

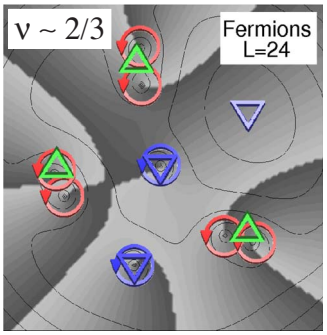

FIG. 52. (Color online) Reduced wave function of the $L=24$ fermion state with symmetric occupations $N_A = N_B = 3$. The nodal structure closely corresponds to that of the $q=2, p=1$ Halperin wave function with one phase singularity in the component of the probing particle and two phase singularities in the opposite component. The approximate Landau-level filling for the above finite-size system is $\nu \approx 2/3$, just as for the Halperin state proposed to describe the $\nu = 2/3$ quantum Hall plateau. The symbols in the figure were explained in Fig. 3. From Saarikoski *et al.*, 2009.

$$\psi = \prod_{i<j}^{N/2} (z_i - z_j)^q \prod_{k<l}^{N/2} (\tilde{z}_k - \tilde{z}_l)^q \prod_{m,n}^{N/2} (z_m - \tilde{z}_n)^p, \tag{51}$$

where q is an odd integer (due to fermion antisymmetry), p is a positive integer, and the Gaussians have been omitted. The last product in Eq. (51) attaches p vortices to each electron with opposite spin and these can be interpreted as coreless vortices. The corresponding nodal structure can also be found in spin-compensated few-electron systems near the $\nu = 2/3$ filling. Figure 52 shows the reduced wave function of the $N_A = N_B = 3$, $L = 24$ electron state where one (Pauli) vortex is attached to each particle of the same spin and two (coreless) vortices are attached to particles of the opposite spin, in good agreement with the Halperin model with $q=1$ and $p=2$ (Saarikoski *et al.*, 2009). However, despite the correspondence in the nodal structures, the overlap of this state with the Halperin wave function has been found to be small for large particle numbers due to a mixing of spin states in the Halperin model (Koskinen *et al.*, 2007).

D. Bose gases with higher spins

Experimentally the investigations with two-component quantum gases have been extended to higher pseudospins ($T=1$) (Leanhardt *et al.*, 2003). For a rotating trap in the LLL approximation, the phase diagram of pseudospin $T=1$ bosons was studied by Reijnders *et al.* (2004), both using mean-field approaches and numerical diagonalization. The stability of the Mermin-Ho and Anderson-Toulouse vortices has been demonstrated for rotating ferromagnetic condensates with pseudospin $T=1$ (Mizushima, Machida, and Kita, 2002b, 2002c). At small rotation the ground state is a coreless vortex. As an example, Fig. 53 shows the ground-state structure of a ferromagnetic $T=1$ spinor

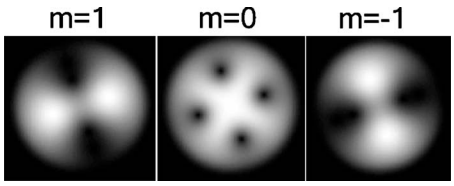

FIG. 53. Density plots of the Gross-Pitaevskii order parameters of the three components ($m=-1,0,1$) for a $T=1$ ferromagnetic condensate (see text). The calculation was performed for 1.7×10^4 bosonic atoms of ^{87}Rb. Length units in the figure are in oscillator lengths. The total angular momentum per particle for the state shown was $L/N=1.85$, and the rotation frequency in units of the trap frequency was $\Omega=0.17$. White color indicates maximum density. From Martikainen *et al.*, 2002.

condensate for the three different components of the order parameter (Martikainen *et al.*, 2002). The three-dimensional trap was chosen with strong confinement in the z direction of a harmonic trap, such that the system was effectively two dimensional. The density distributions (where light shade corresponds to the maximum density) in the x-y plane are shown for $m=1$, 0, and −1. The $m=\pm1$ components show two coreless vortices in much similarity to the two-component case discussed above. The third component, $m=0$, shows a regular array of four vortices that occur at the same positions of the coreless vortices.

VI. SUMMARY AND OUTLOOK

In finite systems with only a small number of particles, vortex formation can be studied by a numerical diagonalization of the many-body Hamiltonian. Often, a reasonable approximation is to assume the confinement to be a two-dimensional harmonic oscillator and to restrict the single-particle basis to the lowest Landau level. This is in particular the case in the limit of weak interactions. The close relationship of the many-body problem to the quantum Hall liquid then helps to explain the vortex localization and the similarity of vortex formation in boson and fermion systems. The many-body energy spectrum, although experimentally yet inaccessible, provides a wealth of information on the localization of vortices and their mutual interactions. The energy spectrum should also allow an approximation of the partition function and thus evaluation of temperature effects in future studies (Dean and Papenbrock, 2002).

The exact diagonalization is limited to systems with only a few particles. Mean-field and density-functional methods are necessary for capturing basic features of vortices in larger systems. In general, the density-functional methods describe the vortex structures in excellent qualitative agreement with the exact diagonalization results. In most density-functional approaches, the particles move in an effective field which allows internal symmetry breaking, making the observation of vortices more transparent than in the exact diagonalization method. However, the present state-of-the-art density-functional approaches fail to describe properly the highly correlated regime at small filling fractions where vortices start to attach to particles, forming composites.

Experimentally, clear signatures of vortices in small electron droplets are still waiting to be observed. Imaging methods of electron densities in quantum dots may provide direct evidence of vortex formation in the future (Pioda *et al.*, 2004; Fallahi *et al.*, 2005; Dial *et al.*, 2007). The predicted localization of vortices in asymmetric confinements and in the presence of pinning impurities open a possible way to direct detection of vortices by means of measurements of the charge density of the electron droplet. Scanning probe imaging techniques have been developed to visualize the subsurface charge accumulation (Tessmer *et al.*, 1998), localized electron states (Zhitenev *et al.*, 2000), and charge flow (Topinka *et al.*, 2003) of a quantum Hall liquid. Similar methods could also turn out to be useful in probing electron density of two-dimensional electron droplets in quantum dots.

In rotating traps the present observation techniques are based on releasing the atoms from the trap and are limited to large atom numbers. Naturally, the experimental goal has been the study of large condensates. Optical lattices, with a small number of atoms in each lattice site, could in the future provide information of vortex formation in the few-body limit.

Despite experimental and theoretical advances in studies of rotating finite-size systems this review can provide only glimpses of this rich field of physics where vorticity plays a central role. Many important theoretical results presented here remain unverified in experiments. Theoretical challenges remain as well, especially in the regime of rapid rotation (Baym, 2005) where strong correlations may lead to emergence of exotic states. Vortex localization and ordering in the transition regime to a quantum Hall liquid, as well as the breakdown of this liquid state into a crystalline one, are still lively discussed themes in the field.

ACKNOWLEDGMENTS

S.M.R. and M.M. thank Georgios Kavoulakis and Ben Mottelson for many helpful discussions and advice and for their collaboration on part of the subjects presented here. We are also indebted to S. Bargi, M. Borgh, K. Capelle, J. Christensson Cremon, K. Kärkkäinen, M. Koskinen, R. Nieminen, E. Räsänen, S. Viefers, and others for their collaboration. We thank J. Jain, C. Pethick, D. Pfannkuche, and V. Zelevinsky, as well as many others, for discussions. We also thank F. Malet for a careful reading of the paper. Our work was financially supported by the Swedish Research Council, the Swedish Foundation for Strategic Research, the Academy of Finland, and the Magnus Ehrnrooth Foundation. This article is the result of a collaboration within the NordForsk Nordic Network on "Coherent Quantum Gases: From Cold Atoms to Condensed Matter."

REFERENCES

Abo-Shaeer, J. R., C. Raman, J. M. Vogels, and W. Ketterle, 2001, Science **292**, 476.

Abrikosov, A. A., 1957, Zh. Eksp. Teor. Fiz. **32**, 1442 [Sov. Phys. JETP **5**, 1174 (1957)].

Aifer, E., B. Goldberg, and D. Broido, 1996, Phys. Rev. Lett. **76**, 680.

Al Khawaja, U., and H. Stoof, 2001a, Nature (London) **411**, 918.

Al Khawaja, U., and H. T. C. Stoof, 2001b, Phys. Rev. A **64**, 043612.

Al Khawaja, U., and H. T. C. Stoof, 2001c, Phys. Rev. A **65**, 013605.

Andersen, A., T. Bohr, B. Stenum, J. J. Rasmussen, and B. Lautrup, 2003, Phys. Rev. Lett. **91**, 104502.

Anderson, M., J. Ensher, M. Matthews, C. Wieman, and S. Cornell, 1995, Science **269**, 198.

Anderson, P., and G. Toulouse, 1977, Phys. Rev. Lett. **38**, 508.

Andrei, E. Y., S. Yücel, and L. Menna, 1991, Phys. Rev. Lett. **67**, 3704.

Anisimovas, E., M. B. Tavernier, and F. M. Peeters, 2008, Phys. Rev. B **77**, 045327.

Ashoori, R., 1996, Nature (London) **379**, 413.

Attaccalite, C., S. Moroni, P. Gori-Giorgi, and G. Bachelet, 2002, Phys. Rev. Lett. **88**, 256601.

Attaccalite, C., S. Moroni, P. Gori-Giorgi, and G. Bachelet, 2003, Phys. Rev. Lett. **91**, 109902.

Austing, D. G., S. Sasaki, S. Tarucha, S. M. Reimann, M. Koskinen, and M. Manninen, 1999, Phys. Rev. B **60**, 11514.

Austing, G., Y. Tokura, T. Honda, S. Tarucha, M. Danoesastro, J. Janssen, T. Oosterkamp, and L. Kouwenhoven, 1999, Jpn. J. Appl. Phys., Part 1 **38**, 372.

Avogadro, P., F. Barranco, R. A. Broglia, and E. Vigezzi, 2007, Phys. Rev. C **75**, 012805(R).

Baelus, B. J., L. R. E. Cabral, and F. M. Peeters, 2004, Phys. Rev. B **69**, 064506.

Baelus, B. J., and F. M. Peeters, 2002, Phys. Rev. B **65**, 104515.

Baelus, B. J., F. M. Peeters, and V. A. Schweigert, 2001, Phys. Rev. B **63**, 144517.

Barberán, N., M. Lewenstein, K. Osterloh, and D. Dagnino, 2006, Phys. Rev. A **73**, 063623.

Bårdsen, G., E. Tölö, and A. Harju, 2009, Phys. Rev. B **80**, 205308.

Bargi, S., J. Christensson, G. M. Kavoulakis, and S. M. Reimann, 2007, Phys. Rev. Lett. **98**, 130403.

Bargi, S., J. Christensson, H. Saarikoski, A. Harju, G. Kavoulakis, M. Manninen, and S. M. Reimann, 2010, Physica E **42**, 411.

Bargi, S., K. Karkkainen, J. Christensson, G. Kavoulakis, M. Manninen, and S. Reimann, 2008, AIP Conf. Proc. **995**, 25.

Barranco, M., R. Guardiola, S. Hernández, R. Mayol, J. Navarro, and M. Pi, 2006, J. Low Temp. Phys. **142**, 1.

Barrett, M., J. Sauer, and M. Chapman, 2001, Phys. Rev. Lett. **87**, 010404.

Barrett, S., G. Dabbagh, L. Pfeiffer, K. West, and R. Tycko, 1995, Phys. Rev. Lett. **74**, 5112.

Baym, G., 2001, J. Phys. B **34**, 4541.

Baym, G., 2003, Phys. Rev. Lett. **91**, 110402.

Baym, G., 2004, Phys. Rev. A **69**, 043618.

Baym, G., 2005, J. Low Temp. Phys. **138**, 601.

Baym, G., and C. Pethick, 1996, Phys. Rev. Lett. **76**, 6.

Baym, G., and C. Pethick, 2004, Phys. Rev. A **69**, 043619.

Baym, G., C. Pethick, and D. Pines, 1969, Nature (London) **224**, 673.

Bedanov, V. M., and F. M. Peeters, 1994, Phys. Rev. B **49**, 2667.

Bertsch, G. F., and T. Papenbrock, 1999, Phys. Rev. Lett. **83**, 5412.

Blaauwgeers, R., V. B. Eltsov, M. Krusius, J. J. Ruohio, R. Schanen, and G. E. Volovik, 2000, Nature (London) **404**, 471.

Blanc, X., and N. Rougerie, 2008, Phys. Rev. A **77**, 053615.

Blatter, G., and B. Ivlev, 1993, Phys. Rev. Lett. **70**, 2621.

Bloch, I., J. Dalibard, and W. Zwerger, 2008, Rev. Mod. Phys. **80**, 885.

Bloch, I., M. Greiner, O. Mandel, T. Hänsch, and T. Esslinger, 2001, Phys. Rev. A **64**, 021402.

Bohr, A., and B. R. Mottelson, 1975, *Nuclear Structure: Volume I and II* (World Scientific, Singapore).

Bolton, F., and U. Rössler, 1993, Superlattices Microstruct. **13**, 139.

Borgh, M., M. Koskinen, J. Christensson, M. Manninen, and S. Reimann, 2008, Phys. Rev. A **77**, 033615.

Borgh, M., M. Koskinen, M. Manninen, S. Åberg, and S. Reimann, 2005, Int. J. Quantum Chem. **105**, 817.

Bose, S., 1924, Z. Phys. **26**, 178.

Braaten, E., and A. Nieto, 1997, Phys. Rev. B **56**, 14745.

Brink, D. M., and R. A. Broglia, 2005, *Nuclear Superfluidity* (Cambridge University Press, Cambridge).

Bruce, N. A., and P. A. Maksym, 2000, Phys. Rev. B **61**, 4718.

Burgess, C. P., and B. P. Dolan, 2001, Phys. Rev. B **63**, 155309.

Burke, J., J. Bohn, B. Esry, and C. Greene, 1998, Phys. Rev. Lett. **80**, 2097.

Butts, D. A., and D. S.Rokhsar, 1999, Nature (London) **397**, 327.

Capelle, K., 2006, Braz. J. Phys. **36**, 1318.

Capelle, K., 2008, unpublished.

Capelle, K., and E. K. U. Gross, 1997, Phys. Rev. Lett. **78**, 1872.

Castin, Y., and R. Dum, 1999, Eur. Phys. J D **7**, 399.

Cazalilla, M., N. Barberán, and N. Cooper, 2005, Phys. Rev. B **71**, 121303.

Cerletti, V., O. Gywat, and D. Loss, 2005, Phys. Rev. B **72**, 115316.

Chakraborty, T., and F. C. Zhang, 1984, Phys. Rev. **29**, 7032.

Chamon, C., and X. Wen, 1994, Phys. Rev. B **49**, 8227.

Chevy, F., K. W. Madison, and J. Dalibard, 2000, Phys. Rev. Lett. **85**, 2223.

Chin, J., D. Miller, Y. Liu, C. Stan, W. Setiawan, C. Sanner, K. Xu, and W. Ketterle, 2006, Nature (London) **443**, 961.

Chin, S., and E. Krotscheck, 2005, Phys. Rev. E **72**, 036705.

Christensson, J., S. Bargi, K. Karkkainen, Y. Yu, G. Kavoulakis, M. Manninen, and S. Reimann, 2008, New J. Phys. **10**, 033029.

Christensson, J., M. Borgh, M. Koskinen, G. Kavoulakis, M. Manninen, and S. M. Reimann, 2008, Few-Body Syst. **43**, 161.

Chui, S., V. Ryzhov, and E. Tarayeva, 2001, Phys. Rev. A **63**, 023605.

Coddington, I., P. Engels, V. Schweikhard, and E. Cornell, 2003, Phys. Rev. Lett. **91**, 100402.

Coddington, I., P. C. Haljan, P. Engels, V. Schweikhard, S. Tung, and E. A. Cornell, 2004, Phys. Rev. A **70**, 063607.

Coish, W., and D. Loss, 2007, Phys. Rev. B **75**, 161302.

Condon, E. U., 1930, Phys. Rev. **36**, 1121.

Cooper, N. R., 2008, Adv. Phys. **57**, 539.

Cooper, N. R., and N. K. Wilkin, 1999, Phys. Rev. B **60**, R16279.

Cooper, N. R., N. K. Wilkin, and J. M. F. Gunn, 2001, Phys. Rev. Lett. **87**, 120405.
Cornell, E., and C. Wieman, 2002, Rev. Mod. Phys. **74**, 875.
Dagnino, D., N. Barberán, and M. Lewenstein, 2009, Phys. Rev. A **80**, 053611.
Dagnino, D., N. Barberán, M. Lewenstein, and J. Dalibard, 2009, Nat. Phys. **5**, 431.
Dagnino, D., N. Barberán, K. Osterloh, A. Riera, and M. Lewenstein, 2007, Phys. Rev. A **76**, 013625.
Dai, Z., J.-L. Zhu, N. Yang, and Y. Wang, 2007, Phys. Rev. B **76**, 085308.
Dalfovo, F., S. Giorgini, L. P. Pitaevskii, and S. Stringari, 1999, Rev. Mod. Phys. **71**, 463.
Darwin, C., 1931, Proc. Cambridge Philos. Soc. **27**, 86.
Davis, K. B., M. O. Mewes, M. R. Andrews, N. J. Vandruten, D. S. Durfee, D. M. Kurn, and W. Ketterle, 1995, Phys. Rev. Lett. **75**, 3969.
Davis, K. B., M. O. Mewes, M. Joffe, M. Andrews, and W. Ketterle, 1995, Phys. Rev. Lett. **74**, 5202.
Dean, D., and T. Papenbrock, 2002, Phys. Rev. A **65**, 043603.
Dial, O., R. Ashoori, L. Pfeiffer, and K. West, 2007, Nature (London) **448**, 176.
Donnelly, R., 1991, *Quantized Vortices in Helium II* (Cambridge University Press, Cambridge, England).
Dreizler, R. M., and E. K. U. Gross, 1990, *Density Functional Theory* (Springer, Berlin).
Egger, R., W. Häusler, C. H. Mak, and H. Grabert, 1999, Phys. Rev. Lett. **82**, 3320.
Einstein, A., 1924, Sitzungsber. K. Preuss. Akad. Wiss. 261.
Einstein, A., 1925, Sitzungsber. K. Preuss. Akad. Wiss. 3.
Emperador, A., 2006, Phys. Rev. B **73**, 155438.
Emperador, A., E. Lipparini, and F. Pederiva, 2005, Phys. Rev. B **72**, 033306.
Engels, P., I. Coddington, P. C. Haljan, and E. A. Cornell, 2002, Phys. Rev. Lett. **89**, 100403.
Engels, P., I. Coddington, P. Haljan, V. Schweikhard, and E. Cornell, 2003, Phys. Rev. Lett. **90**, 170405.
Ensher, J. R., D. S. Jin, M. R. Matthews, C. E. Wieman, and E. A. Cornell, 1996, Phys. Rev. Lett. **77**, 4984.
Esry, B., and C. Greene, 1999, Phys. Rev. A **60**, 1451.
Ezawa, Z. F., 2000, *Quantum Hall Effects*, 2nd ed. (World Scientific, Singapore).
Ezra, G. S., and R. S. Berry, 1983, Phys. Rev. A **28**, 1974.
Fallahi, P., A. C. Bleszynski, R. M. Westervelt, J. Huang, J. D. Walls, E. J. Heller, M. Hanson, and A. C. Gossard, 2005, Nano Lett. **5**, 223.
Feder, D. L., C. W. Clark, and B. I. Schneider, 1999a, Phys. Rev. A **61**, 011601.
Feder, D. L., C. W. Clark, and B. I. Schneider, 1999b, Phys. Rev. Lett. **82**, 4956.
Fetter, A., 2001, Phys. Rev. A **64**, 063608.
Fetter, A., 2009, Rev. Mod. Phys. **81**, 647.
Fetter, A., B. Jackson, and S. Stringari, 2005, Phys. Rev. A **71**, 013605.
Feynman, R. P., 1955, Prog. Low Temp. Phys. **1**, 17.
Filinov, A. V., M. Bonitz, and Y. E. Lozovik, 2001, Phys. Rev. Lett. **86**, 3851.
Fischer, U., and G. Baym, 2003, Phys. Rev. Lett. **90**, 140402.
Fock, V., 1928, Z. Phys. **47**, 446.
Fowler, G., S. Raha, and R. Weiner, 1985, Phys. Rev. C **31**, 1515.
Fu, H., and E. Zaremba, 2006, Phys. Rev. A **73**, 013614.
García-Ripoll, J. J., and V. M. Pérez-García, 1999, Phys. Rev. A **60**, 4864.
Ghosal, A., A. H. Güçlü, C. J. Umrigar, D. Ullmo, and H. U. Baranger, 2006, Nat. Phys. **2**, 336.
Ginzburg, V., and L. Landau, 1950, Zh. Eksp. Teor. Fiz. **20**, 1064.
Giorgini, S., L. P. Pitaevskii, and S. Stringari, 2008, Rev. Mod. Phys. **80**, 1215.
Girvin, S. M., 1996, Science **274**, 524.
Girvin, S. M., and T. Jach, 1983, Phys. Rev. B **28**, 4506.
Girvin, S. M., and T. Jach, 1984, Phys. Rev. B **29**, 5617.
Goldmann, E., and S. R. Renn, 1999, Phys. Rev. B **60**, 16611.
Graham, K. L., S. S. Mandal, and J. K. Jain, 2003, Phys. Rev. B **67**, 235302.
Greiner, M., C. Regal, and D. Jin, 2003, Nature (London) **426**, 537.
Griffin, A., 1995, Can. J. Phys. **73**, 755.
Grigorieva, I. V., W. Escoffier, J. Richardson, L. Y. Vinnikov, S. Dubonos, and V. Oboznov, 2006, Phys. Rev. Lett. **96**, 077005.
Grisenti, R., and J. Toennies, 2003, Phys. Rev. Lett. **90**, 234501.
Gross, E. P., 1961, Nuovo Cimento **20**, 454.
Grover, J., 1967, Phys. Rev. **157**, 832.
Güçlü, A. D., A. Ghosal, C. J. Umrigar, and H. U. Baranger, 2008, Phys. Rev. B **77**, 041301(R).
Güçlü, A. D., G. S. Jeon, C. J. Umrigar, and J. K. Jain, 2005, Phys. Rev. B **72**, 205327.
Gunnarsson, O., and B. I. Lundqvist, 1976, Phys. Rev. B **13**, 4274.
Guttman, L., and J. Arnold, 1953, Phys. Rev. **92**, 547.
Haljan, P., I. Coddington, P. Engels, and E. Cornell, 2001, Phys. Rev. Lett. **87**, 210403.
Hall, D., M. Matthews, J. Ensher, C. Wieman, and E. Cornell, 1998, Phys. Rev. Lett. **81**, 1539.
Hall, D., M. Matthews, C. Wieman, and E. Cornell, 1998, Phys. Rev. Lett. **81**, 1543.
Halperin, B. I., 1983, Helv. Phys. Acta **56**, 75.
Hanson, R., L. Kouwenhoven, J. Petta, S. Tarucha, and L. Vandersypen, 2007, Rev. Mod. Phys. **79**, 1217.
Harju, A., 2005, J. Low Temp. Phys. **140**, 181.
Harju, A., E. Räsänen, H. Saarikoski, M. J. Puska, R. M. Nieminen, and K. Niemelä, 2004, Phys. Rev. B **69**, 153101.
Harju, A., H. Saarikoski, and E. Räsänen, 2006, Phys. Rev. Lett. **96**, 126805.
Harju, A., S. Siljamäki, and R. M. Nieminen, 2002, Phys. Rev. B **65**, 075309.
Harju, A., V. A. Sverdlov, R. M. Nieminen, and V. Halonen, 1999, Phys. Rev. B **59**, 5622.
Heinonen, O., J. M. Kinaret, and M. D. Johnson, 1999, Phys. Rev. B **59**, 8073.
Helle, M., A. Harju, and R. M. Nieminen, 2005, Phys. Rev. B **72**, 205329.
Hess, H. F., R. B. Robinson, R. C. Dynes, J. M. Valles, and J. V. Waszczak, 1989, Phys. Rev. Lett. **62**, 214.
Hill, R., and L. Eaves, 2008, Phys. Rev. Lett. **101**, 234501.
Ho, T. L., 1998, Phys. Rev. Lett. **81**, 742.
Ho, T. L., 2001, Phys. Rev. Lett. **87**, 060403.
Ho, T. L., and V. Shenoy, 1996, Phys. Rev. Lett. **77**, 3276.
Hohenberg, P., and W. Kohn, 1964, Phys. Rev. **136**, B864.
Homer, 8th century B.C., *The Odyssey*, translated by E. V. Rieu (Penguin Books, London, 2003).
Huang, K., 1963, *Statistical Mechanics* (Wiley, New York).
Hunter, G., 2004, Int. J. Quantum Chem. **29**, 197.
Hussein, M., and O. Vorov, 2002, Phys. Rev. A **65**, 035603.

Hylleraas, E., 1928, Z. Phys. **48**, 469.
Inguscio, M., S. Stringari, and C. Wieman, 1999, *Bose-Einstein Condensation in Atomic Gases* (IOS, Amsterdam).
Isoshima, T., and K. Machida, 2002, Phys. Rev. A **66**, 023602.
Isoshima, T., K. Machida, and T. Ohmi, 2001, J. Phys. Soc. Jpn. **70**, 1604.
Jackson, A., and G. Kavoulakis, 2004, Phys. Rev. A **70**, 023601.
Jackson, A., G. Kavoulakis, and M. Magiropoulos, 2008, Phys. Rev. A **78**, 063623.
Jackson, A., G. Kavoulakis, B. Mottelson, and S. Reimann, 2001, Phys. Rev. Lett. **86**, 945.
Jackson, A. D., and G. M. Kavoulakis, 2000, Phys. Rev. Lett. **85**, 2854.
Jackson, A. D., G. M. Kavoulakis, and E. Lundh, 2004, Phys. Rev. A **69**, 053619.
Jain, J. K., 1989, Phys. Rev. Lett. **63**, 199.
Jain, J. K., 2007, *Composite Fermions* (Cambridge University Press, Cambridge, England).
Jauregui, K., W. Häusler, and B. Kramer, 1993, Europhys. Lett. **24**, 581.
Jeon, G. S., C. Chang, and J. K. Jain, 2007, Eur. Phys. J. B **55**, 271.
Jeon, G. S., C.-C. Chang, and J. K. Jain, 2004, Phys. Rev. B **69**, 241304R.
Jeon, G. S., A. D. Güçlü, C. J. Umrigar, and J. K. Jain, 2005, Phys. Rev. B **72**, 245312.
Jezek, D., and P. Capuzzi, 2005, J. Phys. B **38**, 4389.
Jezek, D., P. Capuzzi, and H. Cataldo, 2001, Phys. Rev. A **64**, 023605.
Jochim, S., M. Bartenstein, A. Altmeyer, G. Hendl, S. Riedl, C. Chin, J. H. Denschlag, and R. Grimm, 2003, Science **302**, 2101.
Julienne, P., F. Mies, E. Tiesinga, and C. Williams, 1997, Phys. Rev. Lett. **78**, 1880.
Kalliakos, S., M. Rontani, V. Pellegrini, C. P. Garcí, A. Pinczuk, G. Goldoni, E. Molinari, L. N. Pfeiffer, and K. W. West, 2008, Nat. Phys. **4**, 467.
Kasamatsu, K., and M. Tsubota, 2009, Phys. Rev. A **79**, 023606.
Kasamatsu, K., M. Tsubota, and M. Ueda, 2002, Phys. Rev. A **66**, 053606.
Kasamatsu, K., M. Tsubota, and M. Ueda, 2003, Phys. Rev. Lett. **91**, 150406.
Kasamatsu, K., M. Tsubota, and M. Ueda, 2005a, Int. J. Mod. Phys. B **19**, 1835.
Kasamatsu, K., M. Tsubota, and M. Ueda, 2005b, Phys. Rev. A **71**, 043611.
Kavoulakis, G., and G. Baym, 2003, New J. Phys. **5**, 51.
Kavoulakis, G., B. Mottelson, and C. Pethick, 2000, Phys. Rev. A **62**, 063605.
Kavoulakis, G. M., S. M. Reimann, and B. R. Mottelson, 2002, Phys. Rev. Lett. **89**, 079403.
Ketterle, W., 2002, Rev. Mod. Phys. **74**, 1131.
Khalatnikov, I., 1957, Sov. Phys. JETP **5**, 542.
Kim, Y. E., and A. L. Zubarev, 2003, Phys. Rev. A **67**, 015602.
Kinaret, J. M., Y. Meir, N. S. Wingreen, P. A. Lee, and X.-G. Wen, 1992, Phys. Rev. B **46**, 4681.
Kita, T., T. Mizushima, and K. Machida, 2002, Phys. Rev. A **66**, 061601(R).
Kohn, W., 1999, Rev. Mod. Phys. **71**, 1253.
Kohn, W., and L. Sham, 1965, Phys. Rev. **140**, A1133.
Kolomeisky, E., and J. Straley, 1996, Rev. Mod. Phys. **68**, 175.
Koskinen, M., M. Manninen, B. Mottelson, and S. Reimann, 2001, Phys. Rev. B **63**, 205323.
Koskinen, M., M. Manninen, and S. M. Reimann, 1997, Phys. Rev. Lett. **79**, 1389.
Koskinen, M., S. M. Reimann, J.-P. Nikkarila, and M. Manninen, 2007, J. Phys.: Condens. Matter **19**, 076211.
Kouwenhoven, L., D. Austing, and S. Tarucha, 2001, Rep. Prog. Phys. **64**, 701.
Lam, P. K., and S. M. Girvin, 1984, Phys. Rev. B **30**, 473.
Landau, L., and E. Lifshitz, 1951, *Statisticheskai Fizika* (Fizmatgiz, Moscow) (in Russian).
Laughlin, R. B., 1983, Phys. Rev. Lett. **50**, 1395.
Law, C., H. Pu, and N. Bigelow, 1998, Phys. Rev. Lett. **81**, 5257.
Leadley, D. R., R. J. Nicholas, D. K. Maude, A. N. Utjuzh, J. C. Portal, J. J. Harris, and C. T. Foxon, 1997, Phys. Rev. Lett. **79**, 4246.
Leanhardt, A., Y. Shin, D. K. D, D. Pritchard, and W. Ketterle, 2003, Phys. Rev. Lett. **90**, 140403.
Lee, D., and C. Kane, 1990, Phys. Rev. Lett. **64**, 1313.
Leggett, A., 1975, Rev. Mod. Phys. **47**, 331.
Leggett, A. J., 2001, Rev. Mod. Phys. **73**, 307.
Leggett, A. J., 2006, *Quantum Liquids: Bose Condensation and Cooper Pairing in Condensed-Matter Systems* (Oxford University Press, Oxford).
Lehmann, K., and R. Schmied, 2003, Phys. Rev. B **68**, 224520.
Lehoucq, R., D. Sorensen, and Y. Yang, 1997, *ARPACK Users Guide: Solution to Large Scale Eigenvalue Problems with Implicitly Restarted Arnoldi Methods* (FORTRAN code http://www.caam.rice.edu/software/ARPACK).
Li, Y., C. Yannouleas, and U. Landman, 2006, Phys. Rev. B **73**, 075301.
Lin, Y.-L., R. Compton, K. Jiménes-Garcia, J. Porto, and I. Spielman, 2009, Nature (London) **462**, 628.
Lindemann, F., 1910, Phys. Z. **11**, 609.
Link, B., 2003, Phys. Rev. Lett. **91**, 101101.
Linn, M., M. Niemeyer, and A. Fetter, 2001, Phys. Rev. A **64**, 023602.
London, F., 1954, *Superfluids: Microscopic Theory of Superfluid Helium* (Dover, New York), Vol. II.
Löwdin, P.-O., 1955, Phys. Rev. **97**, 1474.
Lundh, E., 2002, Phys. Rev. A **65**, 043604.
MacDonald, A. H., S.-R. E. Yang, and M. D. Johnson, 1993, Aust. J. Phys. **46**, 345.
Madison, K., F. Chevy, V. Bretin, and J. Dalibard, 2001, Phys. Rev. Lett. **86**, 4443.
Madison, K., F. Chevy, W. Wohlleben, and J. Dalibard, 2000, Phys. Rev. Lett. **84**, 806.
Maksym, P. A., 1996, Phys. Rev. B **53**, 10871.
Maksym, P. A., H. Imamura, G. Mallon, and H. Aoki, 2000, J. Phys.: Condens. Matter **12**, R299.
Manninen, M., M. Koskinen, S. Reimann, and B. Mottelson, 2001, Eur. Phys. J. D **16**, 381.
Manninen, M., M. Koskinen, Y. Yu, and S. Reimann, 2006, Phys. Scr. T **125**, 31.
Manninen, M., S. M. Reimann, M. Koskinen, Y. Yu, and M. Toreblad, 2005, Phys. Rev. Lett. **94**, 106405.
Manninen, M., S. Viefers, M. Koskinen, and S. M. Reimann, 2001, Phys. Rev. B **64**, 245322.
Martikainen, J., A. Collin, and K. Suominen, 2002, Phys. Rev. A **66**, 053604.
Matagne, P., J. P. Leburton, D. G. Austing, and S. Tarucha, 2002, Phys. Rev. B **65**, 085325.
Matthews, M., D. Hall, J. Ensher, C. Wieman, and E. Cornell, 1998, Phys. Rev. Lett. **81**, 243.
Matthews, M. R., B. Anderson, P. Haljan, D. Hall, C. Wieman,

and E. Cornell, 1999, Phys. Rev. Lett. **83**, 2498.
Mayol, R., M. Pi, M. Barranco, and F. Dalfovo, 2001, Phys. Rev. Lett. **87**, 145301.
Mermin, N., and T. Ho, 1976, Phys. Rev. Lett. **36**, 594.
Miesner, H., D. Stamper-Kurn, J. Stenger, S. Inouye, A. Chikkatur, and W. Ketterle, 1999, Phys. Rev. Lett. **82**, 2228.
Milošević, M., and F. Peeters, 2003, Phys. Rev. B **68**, 024509.
Mizushima, T., K. Machida, and T. Kita, 2002a, Phys. Rev. A **66**, 053610.
Mizushima, T., K. Machida, and T. Kita, 2002b, Phys. Rev. Lett. **89**, 030401.
Modugno, G., M. Modugno, F. Riboli, G. Roati, and M. Inguscio, 2002, Phys. Rev. Lett. **89**, 190404.
Mottelson, B., 1999, Phys. Rev. Lett. **83**, 2695.
Mottelson, B., 2001, Nucl. Phys. A **690**, 201.
Möttönen, M., T. Mizushima, T. Isoshima, M. M. Salomaa, and K. Machida, 2003, Phys. Rev. A **68**, 023611.
Mueller, E. J., 2004, Phys. Rev. A **69**, 033606.
Mueller, E. J., and T.-L. Ho, 2002, Phys. Rev. Lett. **88**, 180403.
Mueller, E. J., T.-L. Ho, M. Ueda, and G. Baym, 2006, Phys. Rev. A **74**, 033612.
Myatt, C., E. Burt, R. Ghrist, E. A. Cornell, and C. Wieman, 1997, Phys. Rev. Lett. **78**, 586.
Nikkarila, J.-P., and M. Manninen, 2007a, Phys. Rev. A **76**, 013622.
Nikkarila, J.-P., and M. Manninen, 2007b, Solid State Commun. **141**, 209.
Nishi, Y., P. A. Maksym, D. G. Austing, T. Hatano, L. P. Kouwenhoven, H. Aoki, and S. Tarucha, 2006, Phys. Rev. B **74**, 033306.
Nunes, G. S., 1999, J. Phys. B **32**, 4293.
Nunnenkamp, A., A. M. Rey, and K. Burnett, 2010, Proc. R. Soc. London, Ser. A **466**, 1247.
Oaknin, J. H., L. Martín-Moreno, J. J. Palacios, and C. Tejedor, 1995, Phys. Rev. Lett. **74**, 5120.
Oaknin, J. H., L. Martín-Moreno, and C. Tejedor, 1996, Phys. Rev. B **54**, 16850.
Ohmi, T., and K. Machida, 1998, J. Phys. Soc. Jpn. **67**, 1822.
Onsager, L., 1949, Nuovo Cimento **6**, 279.
Oosterkamp, T. H., J. W. Janssen, L. P. Kouwenhoven, D. G. Austing, T. Honda, and S. Tarucha, 1999, Phys. Rev. Lett. **82**, 2931.
Pan, W., H. L. Stormer, D. C. Tsui, L. N. Pfeiffer, K. W. Baldwin, and K. D. West, 2002, Phys. Rev. Lett. **88**, 176802.
Papenbrock, T., and G. F. Bertsch, 2001, Phys. Rev. A **63**, 023616.
Parke, M., N. Wilkin, J. Gunn, and A. Bourne, 2008, Phys. Rev. Lett. **101**, 110401.
Parr, R. G., and W. Yang, 1989, *Density-Functional Theory of Atoms and Molecules* (Oxford University Press, Oxford).
Penrose, O., 1951, Philos. Mag. **42**, 1373.
Penrose, O., and L. Onsager, 1956, Phys. Rev. **104**, 576.
Pethick, C. J., and H. Smith, 2002, *Bose-Einstein Condensation in Dilute Gases* (Cambridge University Press, Cambridge, England).
Petković, A., and M. V. Milovanović, 2007, Phys. Rev. Lett. **98**, 066808.
Pioda, A., S. Kičin, T. Ihn, M. Sigrist, A. Fuhrer, K. Ensslin, A. Weichselbaum, S. E. Ulloa, M. Reinwald, and W. Wegscheider, 2004, Phys. Rev. Lett. **93**, 216801.
Pitaevskii, L., and S. Stringari, 2003, *Bose-Einstein Condensation* (Oxford University Press, Oxford).
Pitaevskii, L. P., 1961, Zh. Eksp. Teor. Fiz. **40**, 646 [Sov. Phys. JETP **13**, 451 (1961)].
Pitaevskii, L. P., and A. Rosch, 1997, Phys. Rev. A **55**, R853.
Pu, H., C. K. Law, J. H. Eberly, and N. P. Bigelow, 1999, Phys. Rev. A **59**, 1533.
Pudalov, V. M., M. D'Iorio, S. V. Kravchenko, and J. W. Campbell, 1993, Phys. Rev. Lett. **70**, 1866.
Rajagopal, K. K., 2007, Phys. Rev. B **76**, 054519.
Raman, C., J. R. Abo-Shaeer, J. M. Vogels, K. Xu, and W. Ketterle, 2001, Phys. Rev. Lett. **87**, 210402.
Räsänen, E., A. Castro, J. Werschnik, A. Rubio, and E. K. U. Gross, 2007, Phys. Rev. Lett. **98**, 157404.
Räsänen, E., H. Saarikoski, Y. Yu, A. Harju, M. J. Puska, and S. M. Reimann, 2006, Phys. Rev. B **73**, 235324.
Rasolt, M., and F. Perrot, 1992, Phys. Rev. Lett. **69**, 2563.
Read, N., and E. Rezayi, 1999, Phys. Rev. B **59**, 8084.
Regal, C., M. Greiner, and D. Jin, 2004, Phys. Rev. Lett. **92**, 040403.
Regnault, N., and T. Jolicoeur, 2003, Phys. Rev. Lett. **91**, 030402.
Regnault, N., and T. Jolicoeur, 2004, Phys. Rev. B **69**, 235309.
Reijnders, J., F. van Lankvelt, K. Schoutens, and N. Read, 2004, Phys. Rev. A **69**, 023612.
Reimann, S. M., M. Koskinen, and M. Manninen, 2000, Phys. Rev. B **62**, 8108.
Reimann, S. M., M. Koskinen, M. Manninen, and B. R. Mottelson, 1999, Phys. Rev. Lett. **83**, 3270.
Reimann, S. M., M. Koskinen, Y. Yu, and M. Manninen, 2006a, New J. Phys. **8**, 59.
Reimann, S. M., M. Koskinen, Y. Yu, and M. Manninen, 2006b, Phys. Rev. A **74**, 043603.
Reimann, S. M., and M. Manninen, 2002, Rev. Mod. Phys. **74**, 1283.
Rokhsar, D. S., 1997, Phys. Rev. Lett. **79**, 2164.
Romanovsky, I., C. Yannouleas, and U. Landman, 2008, Phys. Rev. A **78**, 011606.
Rousseau, E., D. Ponarin, L. Hristakos, O. Avenel, E. Varoquaux, and Y. Mukharsky, 2009, Phys. Rev. B **79**, 045406.
Rozhkov, A., and D. Stroud, 1996, Phys. Rev. B **54**, R12697.
Ruuska, V., and M. Manninen, 2005, Phys. Rev. B **72**, 153309.
Saarikoski, H., and A. Harju, 2005, Phys. Rev. Lett. **94**, 246803.
Saarikoski, H., A. Harju, J. Cremon, S. Bargi, M. Manninen, and S. M. Reimann, 2010, Europhys. Lett. **91**, 30006.
Saarikoski, H., A. Harju, M. J. Puska, and R. M. Nieminen, 2004, Phys. Rev. Lett. **93**, 116802.
Saarikoski, H., A. Harju, M. J. Puska, and R. M. Nieminen, 2005, Physica E (Amsterdam) **26**, 317.
Saarikoski, H., S. M. Reimann, E. Räsänen, A. Harju, and M. J. Puska, 2005, Phys. Rev. B **71**, 035421.
Saarikoski, H., E. Tölö, A. Harju, and E. Räsänen, 2008, Phys. Rev. B **78**, 195321.
Salis, G., Y. Kato, K. Ensslin, D. C. Driscoll, A. C. Gossard, and D. D. Awschalom, 2001, Nature (London) **414**, 619.
Salomaa, M., and G. Volovik, 1987, Rev. Mod. Phys. **59**, 533.
Schmidt, J., N. Shenvi, and J. Tully, 2008, J. Chem. Phys. **129**, 114110.
Schwarz, M. P., D. Grundler, M. Wilde, C. Heyn, and D. Heitmann, 2002, J. Appl. Phys. **91**, 6875.
Schweikhard, V., I. Coddington, P. Engels, V. P. Mogendorff, and E. A. Cornell, 2004, Phys. Rev. Lett. **92**, 040404.
Shahar, D., D. Tsui, M. Shayegan, E. Shimshoni, and S. L. Sondhi, 1996, Science **274**, 589.
Shin, Y., M. Saba, M. Vengalattore, T. A. Pasquini, C. Sanner, A. E. Leanhardt, M. Prentiss, D. E. Pritchard, and W. Ket-

terle, 2004, Phys. Rev. Lett. **93**, 160406.
Siljamäki, S., A. Harju, R. M. Nieminen, V. A. Sverdlov, and P. Hyvönen, 2002, Phys. Rev. B **65**, 121306.
Sinova, J., C. B. Hanna, and A. H. MacDonald, 2002, Phys. Rev. Lett. **89**, 030403.
Skyrme, T. H. R., 1961, Proc. R. Soc. London, Ser. A **260**, 127.
Skyrme, T. H. R., 1962, Nucl. Phys. **31**, 556.
Slater, J. C., 1929, Phys. Rev. **34**, 1293.
Slater, J. C., 1931, Phys. Rev. **38**, 1109.
Smith, R., and N. Wilkin, 2000, Phys. Rev. A **62**, 061602.
Sola, E., J. Casulleras, and J. Boronat, 2007, Phys. Rev. B **76**, 052507.
Sondhi, S., A. Karlhede, S. Kivelson, and E. Rezayi, 1993, Phys. Rev. B **47**, 16419.
Stamper-Kurn, D., M. Andrews, A. Chikkatur, S. Inouye, H. Miesner, J. Stenger, and W. Ketterle, 1998, Phys. Rev. Lett. **80**, 2027.
Stenger, J., S. Inouye, D. Stamper-Kurn, H. Miesner, A. Chikkatur, and W. Ketterle, 1998, Nature (London) **396**, 345.
Stoof, H. T. C., E. Vliegen, and U. Al Khawaja, 2001, Phys. Rev. Lett. **87**, 120407.
Stopa, T., B. Szafran, M. B. Tavernier, and F. M. Peeters, 2006, Phys. Rev. B **73**, 075315.
Suorsa, J., 2006, Master's thesis (Helsinki University of Technology).
Svidzinsky, A. A., and A. L. Fetter, 2000, Phys. Rev. Lett. **84**, 5919.
Szabo, A., and N. Ostlund, 1996, *Modern Quantum Chemistry* (Dover, New York).
Tanatar, B., and D. M. Ceperley, 1989, Phys. Rev. B **39**, 5005.
Tarucha, S., D. G. Austing, T. Honda, R. J. van der Hage, and L. P. Kouwenhoven, 1996, Phys. Rev. Lett. **77**, 3613.
Tavernier, M. B., E. Anisimovas, and F. M. Peeters, 2004, Phys. Rev. B **70**, 155321.
Tavernier, M. B., E. Anisimovas, and F. M. Peeters, 2006, Phys. Rev. B **74**, 125305.
Tessmer, S. H., P. I. Glicofridis, R. C. Ashoori, L. S. Levitov, and M. R. Melloch, 1998, Nature (London) **392**, 51.
Tinkham, M., 1964, *Group Theory and Quantum Mechanics* (McGraw-Hill, New York).
Tinkham, M., 2004, *Introduction to Superconductivity* (Dover, New York).
Tölö, E., and A. Harju, 2009, Phys. Rev. B **79**, 075301.
Topinka, M. A., R. M. Westervelt, and E. J. Heller, 2003, Phys. Today **56** (12), 47.
Toreblad, M., M. Borgh, M. Koskinen, M. Manninen, and S. M. Reimann, 2004, Phys. Rev. Lett. **93**, 090407.
Toreblad, M., Y. Yu, S. M. Reimann, M. Koskinen, and M. Manninen, 2006, J. Phys. B **39**, 2721.
Trauzettel, B., D. Bulaev, D. Loss, and G. Burkhard, 2007, Nat. Phys. **3**, 192.
Trugman, S., and S. Kivelson, 1985, Phys. Rev. B **31**, 5280.
Ueda, M., and T. Nakajima, 2006, Phys. Rev. A **73**, 043603.
van der Wiel, W., S. de Franceschi, J. Elzerman, T. Fujisawa, S. Tarucha, and L. Kouwenhoven, 2003, Rev. Mod. Phys. **75**, 1.
Viefers, S., 2008, J. Phys.: Condens. Matter **20**, 123202.
Viefers, S., T. H. Hansson, and S. M. Reimann, 2000, Phys. Rev. A **62**, 053604.
Viefers, S., P. Koskinen, P. S. Deo, and M. Manninen, 2004, Physica E **21**, 1.
Vignale, G., and M. Rasolt, 1987, Phys. Rev. Lett. **59**, 2360.
Vignale, G., and M. Rasolt, 1988, Phys. Rev. B **37**, 10685.
von Barth, U., 1979, Phys. Rev. A **20**, 1693.
Vorov, O., M. Hussein, and P. V. Isacker, 2003, Phys. Rev. Lett. **90**, 200402.
Weisbuch, C., and C. Hermann, 1977, Phys. Rev. B **15**, 816.
Wigner, E. P., 1934, Phys. Rev. **46**, 1002.
Wilkin, N. K., and J. M. F. Gunn, 2000, Phys. Rev. Lett. **84**, 6.
Wilkin, N. K., J. M. F. Gunn, and R. A. Smith, 1998, Phys. Rev. Lett. **80**, 2265.
Williams, G., and R. Packard, 1974, Phys. Rev. Lett. **33**, 280.
Williams, J. E., and M. J. Holland, 1999, Nature (London) **401**, 568.
Wunsch, B., T. Stauber, and F. Guinea, 2008, Phys. Rev. B **77**, 035316.
Xie, X. C., Y. Guo, and F. C. Zhang, 1989, Phys. Rev. B **40**, 3487.
Yang, C., 1962, Rev. Mod. Phys. **34**, 694.
Yang, S.-J., S.-N. Z. Q.-S. Wu, and S. Feng, 2008, Phys. Rev. A **77**, 033621.
Yang, S.-R. E., and A. H. MacDonald, 2002, Phys. Rev. B **66**, 041304(R).
Yannouleas, C., and U. Landman, 1999, Phys. Rev. Lett. **82**, 5325.
Yannouleas, C., and U. Landman, 2000, Phys. Rev. B **61**, 15895.
Yannouleas, C., and U. Landman, 2002, Phys. Rev. B **66**, 115315.
Yannouleas, C., and U. Landman, 2003, Phys. Rev. B **68**, 035326.
Yannouleas, C., and U. Landman, 2007, Rep. Prog. Phys. **70**, 2067.
Yannouleas, C., and U. Landman, 2009, e-print arXiv:0902.3421.
Yarmchuk, E., M. Gordon, and R. Packard, 1979, Phys. Rev. Lett. **43**, 214.
Yarmchuk, E., and R. Packard, 1982, J. Low Temp. Phys. **46**, 479.
Yip, S. K., 1999, Phys. Rev. Lett. **83**, 4677.
Zhitenev, N. B., T. A. Fulton, A. Yacoby, H. F. Hess, I. N. Pfeiffer, and K. W. West, 2000, Nature (London) **404**, 473.
Zwierlein, M., J. Abo-Shaeer, A. Schirotzek, C. Schunck, and W. Ketterle, 2005, Nature (London) **435**, 1047.
Zwierlein, M., C. Stan, C. Schunck, S. Raupach, A. Kerman, and W. Ketterle, 2004, Phys. Rev. Lett. **92**, 120403.